291

GUIDELINES FOR METEOROLOGICAL ICING MODELS, STATISTICAL METHODS AND TOPOGRAPHICAL EFFECTS

Working Group
B2.16

Task Force 03

April 2006

GUIDELINES FOR METEOROLOGICAL ICING MODELS, STATISTICAL METHODS AND TOPOGRAPHICAL EFFECTS

Task Force B2.16.03

Task Force Members:

André Leblond – Canada (TF Leader)
Svein M. Fikke – Norway (WG Convenor)
Brian Wareing – United Kingdom (WG Secretary)
Sergey Chereshnyuk – Russia
Árni Jón Elíasson – Iceland
Masoud Farzaneh – Canada
Angel Gallego – Spain
Asim Haldar – Canada
Claude Hardy – Canada
Henry Hawes – Australia
Magdi Ishac – Canada
Samy Krishnasamy – Canada
Marc Le-Du – France
Yukichi Sakamoto – Japan
Konstantin Savadjiev – Canada
Vladimir Shkaptsov – Russia
Naohiko Sudo – Japan
Sergey Turbin – Ukraine

Other Working Group Members:

Anand P. Goel – Canada
Franc Jakl – Slovenia
Leon Kempner – Canada
Ruy Carlos Ramos de Menezes – Brasil
Tihomir Popovic – Serbia
Jan Rogier – Belgium
Dario Ronzio – Italy
Tapani Seppa – USA
Noriyoshi Sugawara – Japan

TABLE OF CONTENTS

1. EXECUTIVE SUMMARY

1.1 Introduction

Atmospheric icing is a complex phenomenon involving many basic processes affected by large variations over time and space and influenced by topography. It results either from precipitation icing such as freezing rain and wet snow accretion or from in-cloud icing where suspended, supercooled droplets freeze immediately upon impact on an object exposed to the airflow.

Important atmospheric icing events have been reported in many countries with catastrophic consequences on overhead line networks. On account of the variability in global climate, including possible increased frequencies and magnitudes of ice storms in certain regions, such events could be more threatening to the electrical networks. Hence, it is important to assess ice loads on overhead lines at the design stage in order to ensure that they will not overtake the overhead line strength.

Over the last twenty years, there has been considerable effort in the study of ice accretion on overhead lines. Meteorological models and statistical methods for assessing ice loads are required for design purposes since atmospheric icing is generally not measured at meteorological stations and sufficient information is often not available in existing building codes and standards. While a good engineering judgment based on past experience is obviously very useful, it is generally not sufficient to define proper design criteria.

This Brochure, resulting from the work of Task Force B2.16.03, aims at providing guidelines to overhead line designers as regards use of icing models and statistical methods including topographical effects. These guidelines are generally provided from a meteorological point of view with relevant background material. The intentional guidance perspective of this Brochure is to underline the uncertainties associated with the icing phenomenon, but also the new achievements that certainly will emerge from ongoing research and development within all fields, such as remote monitoring, physical modelling and local scale weather forecasting. The Brochure has been prepared in such a way as to allow the different sections to be read easily whilst improving the understanding of the whole subject of atmospheric icing. Numerous references and appendices are included for more detailed information.

1.2 Icing Models

As underlined above, ice accretion of various types may occur on transmission lines. These are classified as glaze, rime (soft and hard), snow (wet and dry) and hoar frost. Ice accretion may also be a mixture of two or more ice types due to variations in the meteorological parameters during the icing event. The different types of ice accretion are described in the Brochure.

Electricity utilities rely on estimates of extreme ice loadings to design new lines and to upgrade existing lines. The use of icing models to provide such estimates is obviously attractive. They yield an estimation of ice loads for given conductors but they are often restricted to one particular type of icing. Ice load on overhead conductors can be assessed locally in terms of line height above ground and conductor size. The application of these models depends strongly on the availability of such input meteorological parameters as wind speed, air temperature, relative humidity, etc. The intent of the Brochure is not to provide an exhaustive review of all the existing icing models since their number is quite large. However, some models that have already been compared with field experience are described in more details in order to give a useful indication of their accuracy. This is done either for glaze icing, in-cloud icing or wet-snow accretion.

Torsionally stiff conductors can generate non-circular ice shapes that have a significant influence on the modelled ice loads. Semi-empirical expressions are given to express ice mass per unit length as a function of conductor diameter. In the same context, differential ice accretion loads on ground wires, single and bundled phase conductors are of interest to transmission line engineers. Some empirical ratios are provided in the Brochure to enable a transfer function modelling from single conductors to ground wires and bundled conductors.

Ice loads on independent structures can be assessed by modelling the structure shape (e.g. round poles) or the structure components (e.g. tower steelwork).

Wind-on-ice statistics should ideally be used to generate the combined wind and ice loadings corresponding to the selected reliability level. However, such statistics are usually not available and it is generally acceptable to deduce them from the yearly wind statistics by applying a reduction factor.

There is a current general scientific consensus that the global climate has changed more rapidly over the last 20-50 years than previously as shown in historical records. Global climate studies indicate a continued and enhanced development in similar directions. As a result, electric utilities from many countries question the future consequences of atmospheric icing on their infrastructures. The variability and projected changes in climate may affect the icing conditions, probably most in northern latitudes. Although the variability pattern is expected to be relatively complex, it is likely that the frequency of wet snow may decrease in coastal lowlands and increase in inland (continental) areas. Rime icing may decrease in lower mountain areas and increase in higher altitudes. It is not obvious how freezing rain may be affected.

1.3 Statistical Methods

Traditionally, atmospheric icing has been taken as a phenomenon belonging to the northernmost regions of the Earth, such as Canada, Japan, Russia, the Nordic countries and central Europe. However, there are many reports of icing in southern France, United Kingdom, Spain, Algeria, South Africa and Latin America as well. For most of these latter countries, wet snow and rime icing are the most common icing types. The frequencies and intensities of such icing depend strongly on the geographical location with respect to the oceans as well as on the local topography.

Extreme value analysis for design purposes should be carried out only on the basis of statistical analysis of reliable data from a sufficiently long time series (number of years of observation). The Brochure reviews current statistical methods related to annual maxima of icing and compares the convergence of some actual distributions. A great majority of initial distributions of ice radial thickness (or ice unit weight) are of the exponential type – Weibull, exponential, gamma, lognormal, and more rarely Gumbel and normal. The Brochure shows that the distribution of annual maxima taken from all these distributions converges more or less rapidly toward the Gumbel distribution.

Generally, the Gumbel distribution is used for wet snow accretion load. However, in some areas where there is almost no accretion in a normal year, large snow accretion could occur in very rare cases, and the use of Gumbel laws, or more generally Generalized Extreme Value distributions (GEV), is not satisfactory either for theoretical and practical reasons. In contrast, the use of Peak Over Threshold (POT) methods is suitable for such irregular events, in which the selected extremes are not the yearly maxima (as for the Gumbel distribution) but the values exceeding a threshold on which a Generalized Pareto Distribution is fitted.

One aspect of extreme value analysis involves usually the prediction of the long-term maximum ice load along a proposed line route. Typically, ice loads are measured by a number of punctual measurement stations and the maximum ice load along this line route can be estimated from past experience and available climatological data from the stations. Guidelines to achieve such a transfer function modeling for glaze icing, rime icing and wet snow accretion are provided in the Brochure.

1.4 Topographical Effects

The influence of the topography on icing is addressed in the Brochure. Topography modifies the vertical motions of the air masses, which, in turn, modify the cloud structure, precipitation intensity and, by these, the icing conditions. The influence of terrain is generally different for in-cloud icing and for precipitation icing. In general, topography is the basis for defining icing zones that enable line design and components to be specified and used according to the environment. For instance, a typical topographical description

might include the distance from the coast, elevation above sea level, presence of plains and valleys, high mountains situated on high level areas, etc.

In complex terrain, there may be large spatial variations in ice accretion. Studies have shown that mountains may favour icing upstream by increasing precipitation, creating a low level inversion and a barrier wind.

In some countries, wind/icing maps exist for overhead lines which split the country up into specific areas according to their wind and snow/ice susceptibilities. Such maps depict the difference in load with geographical position and land height above mean sea level.

1.5 Application of Atmospheric Boundary Layer Models

Modern meteorology and weather forecasts are based on mathematical models that describe the dynamical and physical processes in the atmosphere. However, before the models can run they need a detailed description of the state of the atmosphere at the starting point for the model. For this purpose, observations are made of air temperature, air pressure, wind, humidity, clouds, precipitation, etc. at fixed hours worldwide. These measurements are made both on the ground by manned or automatic weather stations, and vertically by radiosondes fixed to balloons that may reach throughout 80 – 90% of the atmosphere. Satellites and radars provide now important supplementary information, especially over areas where there is little conventional information (oceans, polar regions, uninhabited areas, etc.).

A weather forecasting system consists of two main parts, a data assimilation system and a forecasting model. The purpose of the data assimilation is to combine observations and forecasts in an optimal way in order to produce initial values for the unknown parameters in the 3D computer model of the atmosphere. The output of a weather forecasting model consists of variables in the equations, for example horizontal and vertical winds, temperature, pressure and humidity, as well as output from parameterization of other variables, for example evaporation and condensation of water, surface fluxes of heat and momentum and components of radiation.

Model nesting has been used for a number of years and the experience with the performance of fine scale models, in the 0.1–1 km range, is continuously improving. Unfortunately such models cannot be used directly for extreme value calculations. However, it may often be useful to compare one site with another, and hence have better foundations for assessing differences in wind, ice or combined wind and ice loadings. Also, certain case studies could be important for failure analyses for certain events in either remote areas or in areas with particular topographical characteristics. Some examples of atmospheric boundary layer models are presented in the Brochure and some important features of model nesting are listed leading to more accurate spatial variation of meteorological parameters.

Icing models depend on many other types of data that may not be directly available in the resolution required. In particular, knowledge of the water cycle in the atmosphere has to be improved in order to be sufficient for describing all types of icing phenomena. However, there are great ongoing international efforts to improve the descriptions of processes involving water and therefore it is important to check current status whenever meteorological models are to be used for icing purposes.

1.6 Conclusion

Ice load modeling is still in the development stage. All icing models should have been calibrated for the specific icing types, structures, climatological conditions and topographic locations of their intended use. It is important to appreciate that the accuracy of the ice load predictions depends upon the quality of climatological data used as input into the models. The reliability of the prediction increases as the length of the climatological data records and the frequency of icing events increase.

It is important to monitor ice accretions and ice loads for power utilities in all countries where damage cost due to ice loads is high. Such time series of observations may be long, costly and difficult to obtain but are of great value for obtaining statistically reliable distributions of ice loads. Generally, the Gumbel

distribution is adopted for extreme value distribution of ice loads. However, Peak Over Threshold (POT) methods are more suitable for irregular events like wet snow accretion in mild climate areas, for which Generalized Extreme Value (GEV) distributions are inadequate. It is highly recommended to keep the initial distributions, including date and time, as a reference for future analyses in the study of loads on structures. More research is needed in this field.

However, care should be taken when correlating data from meteorological stations to the actual line route because of the influence of the topography, as appropriate transfer models normally need to be applied. The estimated ice load values should be adjusted appropriately to account for height differences, unusual terrain changes and other unique features associated with the line route, such as valleys, hills, etc. In general, topography is the basis for defining ice load maps which split the country up into specific areas according to their wind and snow/ice susceptibilities.

The science of meteorology has developed significantly during the last decades. In particular, the combination (nesting) of operational forecasting models with turbulence models of smaller scales, e.g. down to 100–300 m grid size, has already provided results that make them interesting for overhead line applications.

Finally, it is relevant to underline the importance of careful awareness regarding ice accretions in the future, especially in the light of a varying climate. Increased temperatures of the atmosphere will consequently lead to higher atmospheric humidity. The frequencies and intensities of such icing depend strongly on the geographical location with respect to the seas as well as on the local topography. Each country or region is recommended to evaluate their own risks depending on these factors.

2. INTRODUCTION

Atmospheric icing is a complex phenomenon involving many basic processes affected by large variations over time and space and influenced by topography. It results either from precipitation icing such as freezing rain and wet snow accretion or from in-cloud icing where suspended, supercooled droplets freeze immediately upon impact on an object exposed to the airflow.

There are several motives for assessing ice loads on overhead lines at the design stage. One of the most obvious reasons is to ensure that the maximum anticipated ice loading does not overtake the overhead line strength. Meteorological models and statistical methods for assessing ice loads are required for design purpose since atmospheric icing is generally not measured at meteorological stations and sufficient information is often not available in existing building codes and standards. While a good engineering judgment based on past experience is obviously very useful, it is generally not sufficient to define proper design criteria.

Atmospheric icing may occur in any country where precipitation or fog occurs together with air temperatures near the freezing point. Important freezing rain events have been reported in countries where cold air can be trapped or forced over lowlands such as in Canada, USA and many central European countries, wet snow accretion usually occurs in countries where significant precipitation rates occur during wintertime such as France, United Kingdom, Alaska in the USA, Norway, Iceland and Japan. Rime ice occurs in mountainous regions exposed to humid maritime air, over the cloud base. The latter is important for overhead lines in countries like Japan, Canada, USA, Iceland, Norway, Czech Republic, Hungary, Croatia, Rumania and countries connected to the Pyrenees, Alps and Carpathian mountains. The many adverse and wide-spread impacts of such events on electrical systems combined with the variability in global climate, including possible increased frequencies of high wind and icing incidents, are a major concern for many electric utilities in Northern countries.

Over the last twenty years, there has been considerable effort in the study of ice accretion on overhead lines since the resulting ice load, coupled with wind-on-ice load, may lead to catastrophic consequences such as the failure and cascading collapse of towers. Structural damages may also result from wind-induced conductor motions such as galloping, a low frequency, high-amplitude conductor motion associated with aerodynamically unstable ice profiles, that generates high dynamic loads into the structures. Severe Aeolian vibrations of the enlarged-diameter, ice-covered conductor may also lead to fatigue failures of conductor wires at suspension clamps.

This report aims at providing guidelines for icing models, meteorological models, statistical methods and topographical effects with respect to icing events and ice loads on overhead lines. These guidelines are generally provided from a meteorological point of view with relevant background material in order to act as a bridge between meteorological sciences and engineering practices. Some suggested sources of information can be found in references [1-6]. It should be noted that this report does not deal with the impacts themselves or any other technical consequences for the lines.

3. MODELS FOR ATMOSPHERIC ICING

3.1 Ice Accretion Processes

3.1.1 Classification of Icing [5]

Icing is classified into the following two types. Each type is sub-grouped as follows:

a) Precipitation Icing

- Glaze due to freezing rain
- Wet snow accretion
- Dry snow accretion

b) In-Cloud Icing

- Glaze due to super cooled cloud/fog droplet
- Hard rime
- Soft rime

It is important to notice that an ice accretion may be a mixture of two or more ice types, for instance soft rime, hard rime and wet snow, due to variations in the meteorological parameters during the icing event. Various shapes, densities, adhesion strengths, etc. result accordingly. A brief description of the different types of accretion is given in Section 3.1.2.

3.1.2 Types of Accretion

Various types of ice accretion may occur on transmission lines. These are classified as glaze, rime (soft and hard), snow (wet and dry) and hoar frost. Table 1 shows a summary of the different types of ice accretion with typical density ranges as defined by CIGRÉ TB 179 [5].

Table 1: Classification of ice types with typical density ranges – Reference [5]

Ice and snow type	Density (kg/m^3)	Description
Glaze ice	700-900	Pure solid ice, sometimes icicles underneath the wires. The density may vary with the content of air bubbles. Very strong adhesion and difficult to knock off.
Hard rime	300-700	Homogenous structure with inclusions of air bubbles. Pennant shaped against the wind on stiff objects, more or less circular on flexible cables. Strong adhesion and more or less difficult to knock off, even with a hammer.
Soft rime	150-300	Granular structure, “feather-like” or “cauliflower-like”. Pennant shaped also on flexible wires. Can be removed by hand.
Wet snow	100-850	Various shapes and structures are possible, mainly dependent on wind speed and torsional stiffness of conductor. When the temperature is close to zero it may have a high content of liquid water, slide to bottom side of the object and slip off easily. If the temperature drops after the accretion, the adhesion strength may be very strong.
Dry snow	50-100	Very light pack of regular snow. Various shapes and structures are possible, very easy to remove by shaking of wires.
Hoar frost	<100	Crystal structure (needle like). Low adhesion, can be blown off.

3.1.2.1 Glaze Ice

Glaze ice occurs in a temperature inversion situation in valleys on calm warm fronts. Raindrops in the warm (above 0ºC) air region can fall through a few hundred meters of sub-zero air to ground level. The raindrops are then super-cooled, i.e. still in the liquid phase but at sub-zero temperatures e.g.-1 to -5ºC. Glaze icing may also result from in-cloud icing when the in-flux of cloud water is very high [16].

On contact with a physical object, which may be an overhead line or tower structure, the raindrops freeze rapidly with virtually no trapped air within the accretion. Glaze icing produces the densest form of icing – a typical density being 900 kg/m^3 – and high ice loads are reached within hours. Icicles are often seen below the conductors as the raindrops freeze as they run off the lines (Fig. 1). The widely reported Canadian ice storm of January 1998 was due to glaze icing.

Figure 1: Typical glaze ice sample

3.1.2.2 Rime Ice

Rime ice accretion occurs when small, super cooled water droplets (~10 μm) travel along with the wind flow in temperatures typically below –5°C, freeze spontaneously on contact with a physical body. The accretion formed is often strongly asymmetric with leading vanes into the wind direction (Fig. 2). This type of icing is often referred to as “in-cloud” icing and is common in hilly areas over the cloud base. The density of rime varies depending on the size and speed with which the water droplets freeze. Hard rime ranges in density from 300 to 700 kg/m^3 while soft rime has densities of 150-300 kg/m^3. Figure 3 depicts the dependency of droplet diameter on temperature for various types of accretion. Ice loads take days or even weeks to reach damaging levels. Rime ice often accretes more rapidly on small conductors or sharp edges.

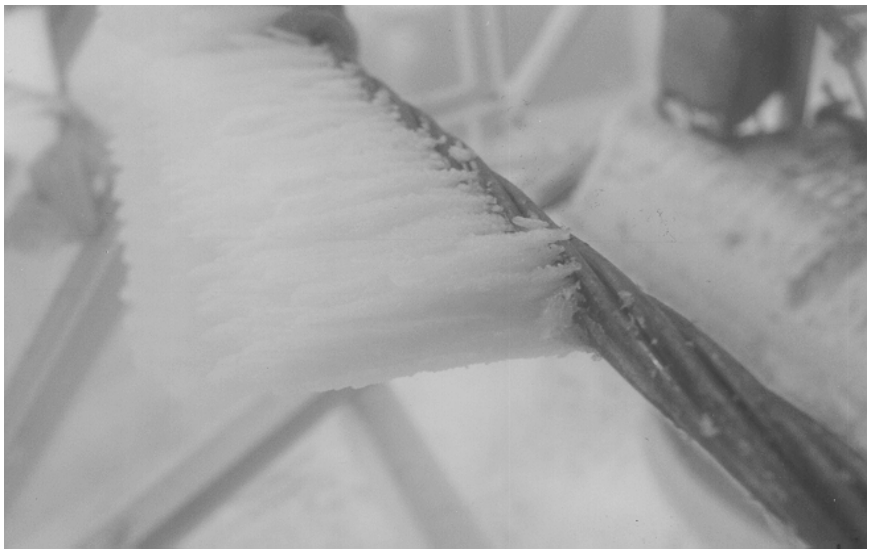

Figure 2: Rime icing vane – Reference [57]

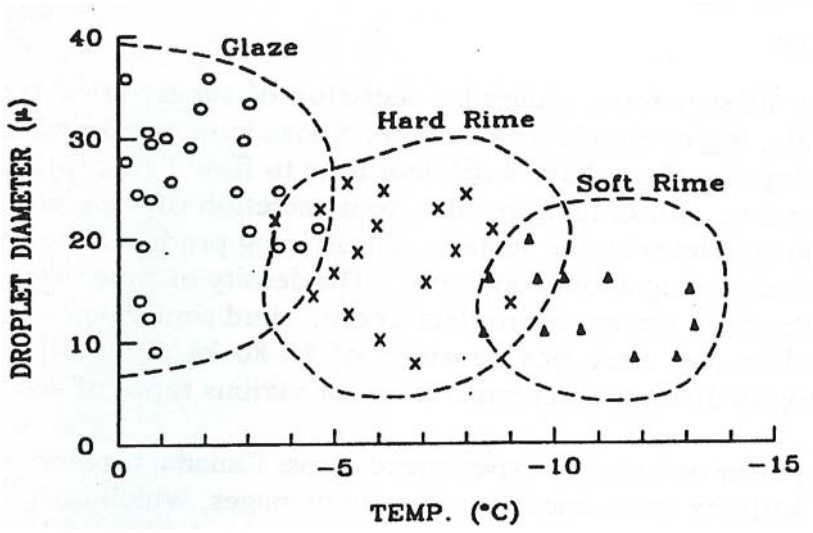

Figure 3: Ice accretion type as a function of air temperature and droplet size – Reference [63]

3.1.2.3 Wet Snow

Wet snowflakes occur as ice crystals suspended in a liquid water matrix at temperatures just above the freezing point, usually between 0,5 and 2ºC. At liquid water contents (LWC) between 15 and 40% the flakes adhere readily to objects. They can reach a terminal velocity which is less than the local wind speeds. At LWC levels below 15% the snow often fails to accrete on structures and lines but can penetrate into motors or other components. At LWC levels above 20% the accretion often falls off objects.

The force of the wind compresses the snow on the surface and the accretion will become more compacted over time, meaning the porosity will decrease and density value as high as 850 kg/m^3 may be reached within the deposit. This phenomenon does not increase the overall snow load on the conductor

but will affect only its density. A process of circular accretion can lead to very high loads being reached in a matter of hours (Fig. 4). The physical process of wet-snow adhesion is still not well understood.

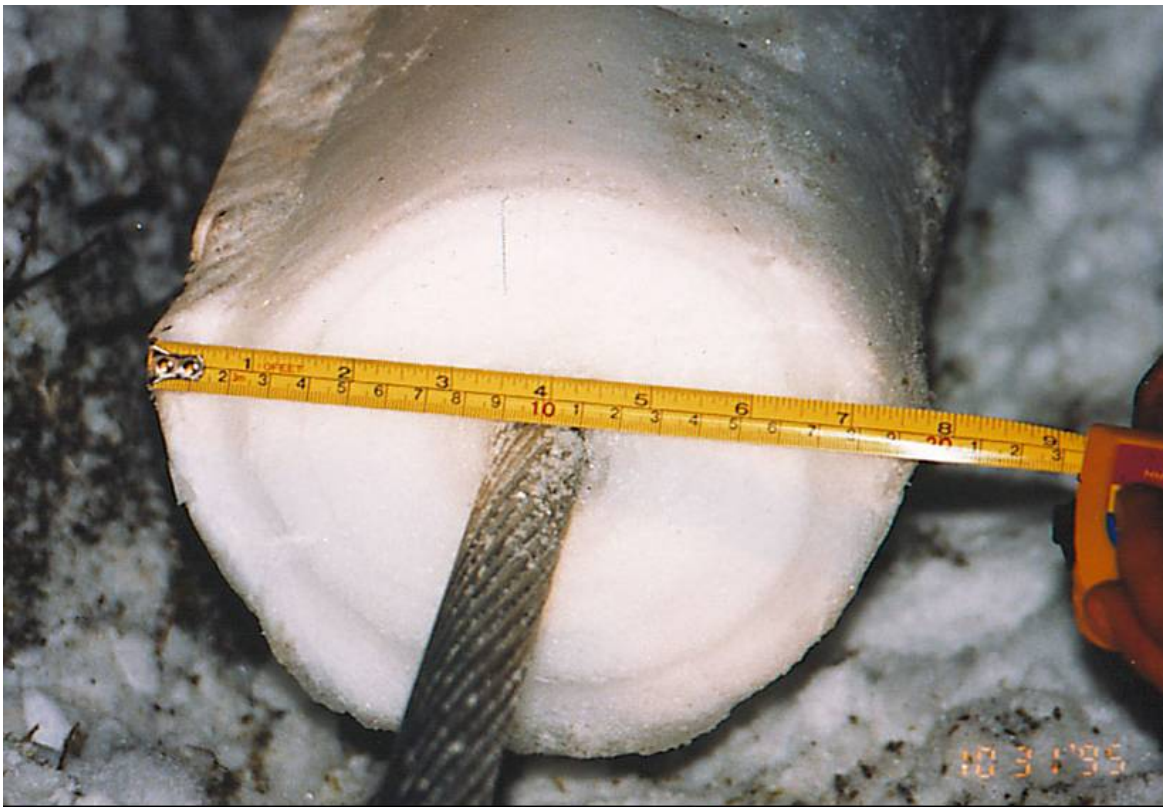

Figure 4: Wet snow accretion on overhead conductor

3.1.2.4 Dry Snow

Dry snowflakes may accrete at temperatures significantly below freezing and can - under very low wind speed conditions - accumulate on objects to form a dry snow accretion (Fig. 5).

3.1.2.5 Hoar Frost

Hoar frost is the deposit of ice crystals from the freezing condensation of the vapor in air. The density is low and the coating generally thin (Fig. 6). It has a low adhesion and can be easily blown off. It will not be discussed further since it does not have a significant effect on ice load. However, it may lead to severe Aeolian vibrations of the enlarged-diameter cable that could result to fatigue damage of the cable itself and/or fittings.

Figure 5: Dry snow accretion on overhead conductors

Figure 6: Hoar frost accretion on a Chaînette Tower

3.1.3 Fundamental Meteorological Parameters Involved in Icing

Many meteorological parameters are significant in relation to icing accretions. Table 2 shows the meteorological parameters associated with each icing type with those having the greatest influence denoted "■" and those with some influence denoted "□".

Some of these parameters are contained and recorded in the general observed parameters, and others are not. The parameters generally observed are the weather, air temperature, relative humidity, precipitation (precipitation intensity), wind speed, and wind direction. Moreover, some cases may include cloud type, cloud amount, cloud base and visibility. On the other hand, among the parameters which are not generally observed, the super cooled liquid-water content of air, distribution of the volume diameter (particularly mean volume diameter) of super cooled fog/cloud droplets, liquid-water content of snowflakes, etc. have a significant influence on the icing phenomena.

In order to estimate ice loads, several physical and empirical models have been developed for glaze due to freezing rain, including icicle growth, in-cloud icing and for snow accretion. Their application depends strongly on the availability of the meteorological parameters required as an input to the models.

Table 2: Meteorological parameter associated with each icing type. Those that have greatest influence are denoted "■", those with less influence "□".

Type of icing	Precipitation icing			In-cloud icing		
	Glaze due to freezing rain	Wet snow accretion	Dry snow accretion	Glaze due to super cooled cloud/fog droplets	Hard rime	Soft rime
Wind speed	■	■	□	■	■	■
Air temperature	■	■	□	■	■	■
Precipitation	■	■	■			
Liquid water content of air	■				■	■
Water droplet size	■			■	■	■
Relative humidity	■	□		■	■	■
Liquid-water content of snowflake		■				
Snow flake size		■	■			

For example, the methods transforming the observed data from meteorological stations into values associated with the transmission line route remain the most important problem. Particularly for wet snow

accretion, the density and accretion rate strongly depend on the liquid-water content of snowflakes. This water content is greatly influenced by the stratification conditions of the atmosphere in the upper layer, not only by surface air temperature. This will also cause difficulty in estimating air temperature along the transmission line route from the observed data.

When parameters not contained in general weather data are needed as input for a model, i.e. for in-cloud icing, it is necessary to develop a method to estimate the key parameters based on parameters which are generally available.

3.2 Icing Models

There are two approaches to modeling ice accretion: the empirical one and the physical. Empirical or semi-empirical models relate one or more parameters, such as amount of precipitation, precipitation rate or temperature, to amount of ice accretion. These parameters are determined from laboratory experiments or field observations. Physical models, on the other hand, attempt to simulate the physical processes involved in ice accretion. All physical models and semi-empirical models try to model the dynamics of the fluid flow around the ice accretion surface in order to calculate the collection efficiency and use meteorological data to simulate droplet size distribution and liquid water content in the air.

The use of icing models to provide ice load data is obviously attractive. They give an estimation of ice loads for defined conductors and are often restricted to a particular type of icing.

Initial attempts to model ice loads from meteorological data had to rely on transferred data of the standard meteorological parameters. Except from glaze on the ground, icing was never reported at weather stations, and precipitation often only as the amount over a day or longer period and not a "precipitation rate" as the wet snow or glaze ice models require. Precipitation itself is extremely difficult to measure when in the form of snow or when temperatures are below 0 °C.

Icing storms can often supply useful data for validating ice models, although significant ice dimensions and density data are often difficult to obtain at the time of, or just after, the incident. A major database has been developed in Iceland [56], where linesmen carry specific equipment to measure ice loads and take samples for density measurements. One problem with storm event data is that the icing levels are normally high and so of little use to modelling the lower levels of ice accretion that occur more frequently.

Estimating ice loads from models based on atmospheric data is a complex process sequence involving:

a) Source of moisture (maritime air)
b) Cloud formation
c) Precipitation (for precipitation icing)
d) Terrain effects
e) Collision of drops or droplets with the ice surface
f) Accretion rate
g) Torsional rigidity effects
h) Change in accreting surface characteristics (size, roughness, shape)
i) Ice shedding
j) Local temperature/wind effects.

The selection of icing models is dependent upon icing processes as described in Section 3.1. Some icing models use relatively simple approaches and are restricted to a particular type of icing, while others start from more fundamental equations and can address a range of icing types. Icing models may be used both to estimate ice loads for defined conditions and to compute icing statistics from a historical database of meteorological conditions. In most cases, essential input parameters such as LWC and droplet sizes

are, in general, not available from a climate database and must be estimated from the available meteorological parameters.

The intent of this section is not to provide an exhaustive review of all the existing icing models since their number is quite large. However, some models that have already been compared with field experience are described in more details in order to give a useful indication of their accuracy. This is done either for glaze icing, in-cloud icing or wet-snow accretion since they are the most common accretion types.

3.2.1 Glaze-Icing Models

3.2.1.1 Background

During the late 60's design ice load on transmission lines in Canada was primarily obtained following standard CSA C22.3 and information gathered through the Climatological Branch of Environment Canada. This involved running a specific empirical ice accretion model (Chaîné and Skeates Model [8] for freezing precipitation only) with the hourly meteorological data obtained from an airport.

A considerable amount of work has been done during the past thirty years with regard to development of various ice accretion models but validation of these models with regard to field data has been very limited so far. Advantage of using a specific model or models provides guidelines with regard to long term forecasting although uncertainties associated with these predictions could be high due to lack of validation of these models by actual field measurement or observed data from line failures.

In recent years Canadian Electricity Association (CEA) in collaboration with three utilities in Canada undertook a major research project where three specific ice accretion models were validated with measured field data (for various meteorological and load parameters) obtained by monitoring three full-scale test and/or energized lines (CEA Report [55]). Each site was well equipped with various sensors to collect this information.

3.2.1.2 Model Review

There are a number of models available to predict the ice load and thickness on a cylindrical object such as a transmission line conductor, due to freezing rain precipitation. A review of a number of models carried out by the Canadian Climate Centre in 1984 [69] indicated that the following features were considered important in a model based on the review of physical ice accretion process.

- Flexibility with regard to handle various sources of icing phenomenon such as freezing precipitation, in-cloud rime, wet snow etc.
- Ability to handle wet or dry growth conditions.
- Time dependent characteristics.
- Ability - to handle rotational characteristics of cables.
- Ability - to predict the shape of icing as the time progresses
- Consideration of run-back under wet growth thus providing the information on icicle formation.
- Ability to include the variation of ice density.
- To include the direction of wind angle directly in the model.
- Ability to handle the melting of accreted ice if above freezing conditions are met.

Table 3 provides the list of ice accretion models that have been developed up until 1991 and reviewed by Mitten and Makkonen in their report [64]. CRREL (Jones [60, 61]) has also developed two models for freezing precipitation and at the time of CEA study these models were not available.

Table 3: Candidate ice accretion models by accretion type – Reference [64]

Freezing Precipitation	In-Cloud Icing	Wet Snow Accretion
Chaîné and Skeates, 1974 [8]	Imai, 1953 [74]	Sakamoto, 1984 [77]†
Goodwin *et al.*, 1983 [70]	Leavengood, 1972 [75]	Makkonen, 1990 [71]
Makkonen, 1990 [71]	McComber, 1983 [76]	MRI, 1977 [52]
MRI, 1977 [52]	Makkonen, 1984 [12]	MEP, 1984 [72]
MEP, 1984 [72]	Makkonen, 1990 [71]	Finstad, 1988 [73]
Finstad, 1988 [73]	MRI, 1977 [52]	Admirat *et al.*, 1984-85 [101,102]‡
CRREL, 1996 [60, 61]	MEP, 1984 [72]	
	Finstad, 1988 [73]	

†: An earlier model was reviewed by Mitten and Makkonen in their report [64].
‡: These models were not included as such at the time of the CEA study.

3.2.1.2.1 Chaîné and Skeates Model

Chaîné and Skeates' Model [8] is based on observations of ice build up on vertical and horizontal surfaces. The horizontal and vertical components of ice accretion thickness are first computed based on the rainfall rate, and the results are converted (via an empirical expression) to a representative equivalent radial ice thickness. Certain assumptions are made. One is that the conductor is a non-rotating cylinder. Normally, ice accretion is elliptical in shape on the windward side of the cylinder. Thus, a radial distribution of accreted ice -- applicable to a rotating conductor -- that is equivalent in volume to the elliptical ice formation is calculated. Thus, an equivalent estimate of the radial ice thickness can be generated.

The Chaîné and Skeates model assumed that 100% of the precipitation on a flat surface accretes as ice to give a horizontal ice thickness A_h from:

$$A_h = P_r \cdot \Delta\tau \tag{1}$$

where P_r = precipitation rate (cm/h)
$\Delta\tau$ = duration (h)

The model assumes that the vertical ice accretion thickness is proportional to precipitation rate and wind speed based on the work of McKay and Thompson [67] and is expressed as:

$$A_v = 0.195 \cdot V \cdot P_r^{0.88} \cdot \Delta\tau \tag{2}$$

where V is the wind speed in m/s.

In the Chaîné model, it is assumed that all impinging water freezes and the accretion process occurs only for temperatures near or below freezing. Chaîné and Skeates [8] recommended to combine the horizontal and vertical accretion to a combined equivalent radial ice thickness based on the work of Stallabrass and Hearty [66]. Equivalent radial ice thickness is computed as follows:

$$A_r = \sqrt{\frac{K \cdot r}{2}(A_h^2 + A_v^2)^{0.5} + r^2} - r \tag{3}$$

where r is the initial conductor radius and K is a correction factor. Figure 7 depicts the variation of K as a function of ambient temperature and diameter of conductor.

Yip [65] has carried out the sensitivity of Chaîné model with respect to change in temperature, conductor size, precipitation rate and wind speed. Figure 8 depicts results from the model output and shows that predicted ice load is least sensitive to the changes in air temperature while most sensitive to changes in wind speed and precipitation rate. Model output is moderately sensitive to change in conductor diameter.

In a recent study for developing wind and ice loads for a 230 kV transmission line on the west coast of Newfoundland, this model was used and Fig. 9 depicts the result of a sensitivity study which is in line with the observation made by Yip [65].

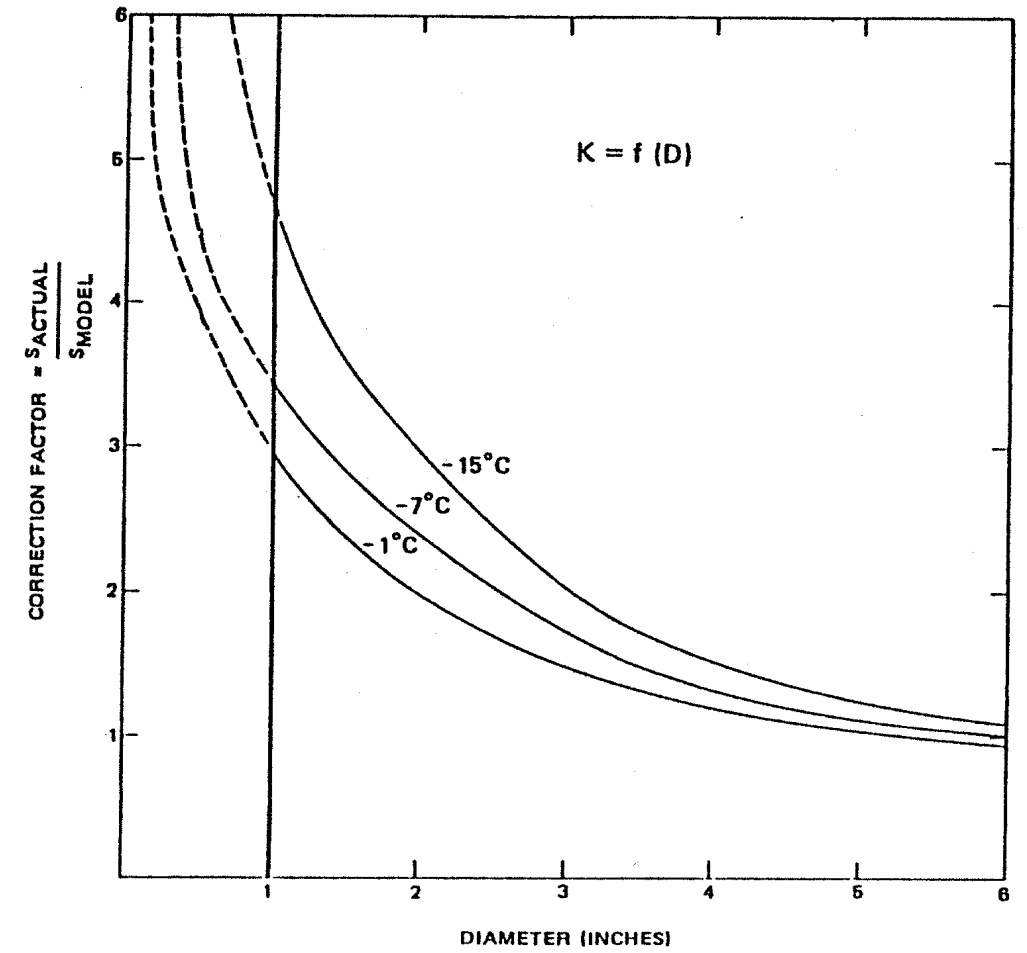

Figure 7: Correction factor, *K* – Reference [8]

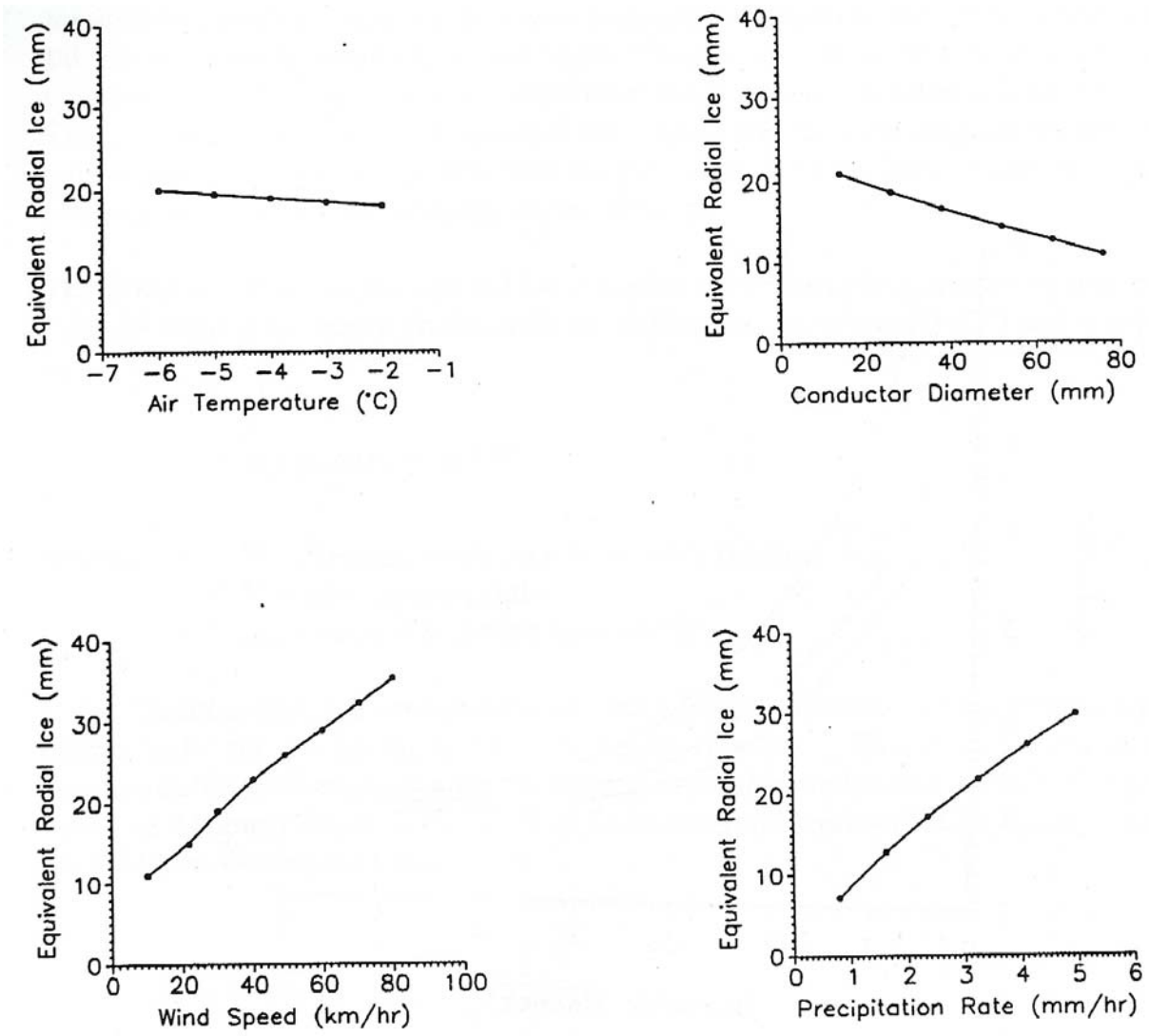

Figure 8: Sensitivity of Chaîné Model with respect to various input parameters (Yip [65])

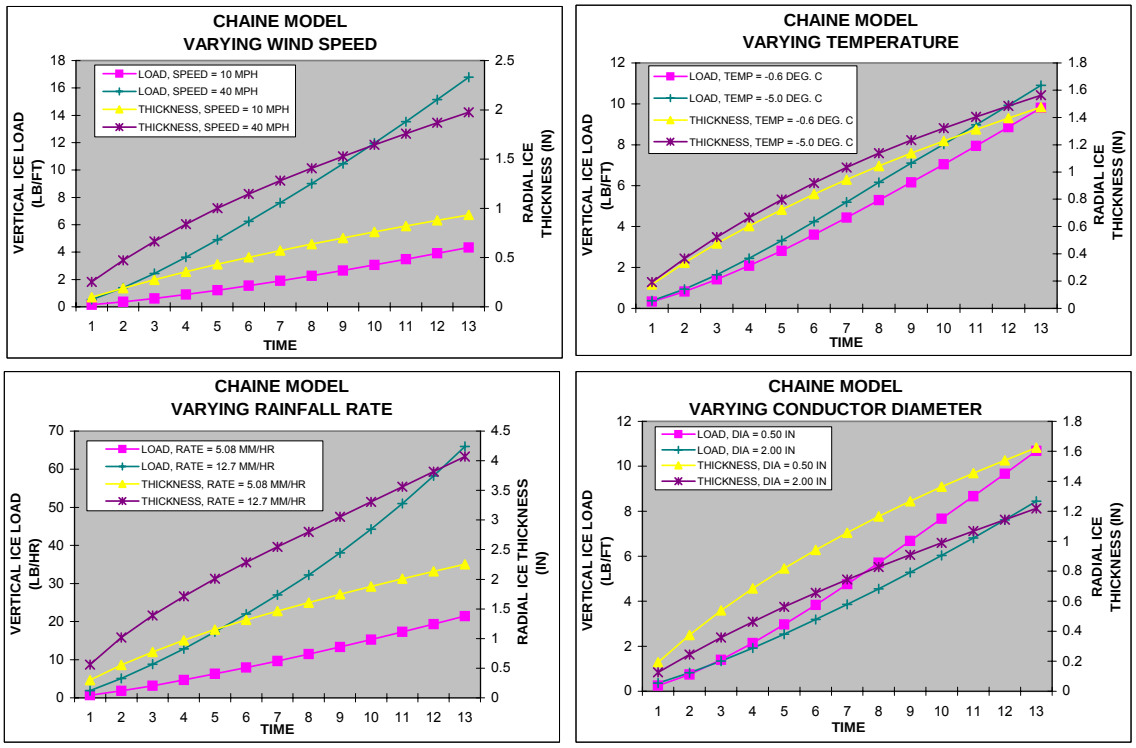

Figure 9: Sensitivity study using Chaîné and Skeates Model (NLH study)

3.2.1.2.2 Makkonen Model [12]

This model was originally developed as a time dependent in-cloud icing model, which incorporates both wet and dry growth conditions. Icing intensity is determined on the portion of the surface area of the ice deposit that faces the wind. On a circular cylinder, the icing intensity is dependent on: E (the collection efficiency), n (the freezing fraction), V (the wind speed), and W (the liquid water content). The ice deposit is assumed to maintain a circular form during the icing process because of rotation. Furthermore, the rotation is assumed to be slow enough, so there is no icing on the leeward side. During dry growth $n = 1$, while for wet growth, $n < 1$, run-off water is assumed to be shed. The model calculations are made in an iterative manner. However the model was later updated to account for both freezing rain as well as wet snow conditions by using the appropriate parameters to calculate the growth.

The obvious advantage of using the Makkonen model [12] is that it accommodates: i) time dependencies, ii) changes from wet to dry growth conditions (or vice versa) during the ice accretion process, iii) variations in the ice density and iv) the relative angle between the direction of the wind and the conductor (Haldar, Mitten and Makkonen [68]).

Makkonen model estimates the ice on a circular cylinder over time by computing an incremental deposition of ice in terms of the icing intensity, I, or growth rate of ice mass, $dM/d\tau$, per unit area and given as

$$I = \frac{(dM / d\tau)}{A} \qquad (4)$$

where A is the surface area of the windward face.

The water mass flux, or the rate at which water droplets in the air are deposited on a collection surface, $dM_w/d\tau$, depends on droplet speed, V_d, liquid water content, W, collection efficiency of the surface, E, (i.e.: the ratio of the mass flow of the impinging water droplets to the mass flow that would be experienced by the collecting surface if the droplets were not deflected in the air stream), the diameter, D_c, and the length, L, of the cylindrical surface. Hence,

$$\frac{dM_w}{d\tau} = E \cdot W \cdot V_d \cdot D_c \cdot L \tag{5}$$

The freezing fraction, n, controls the dry and wet growth process and is defined as the ratio of the icing intensity to the mass flow of the impinging droplets. Wet growth is considered when n<1, i.e., there is some water run-off from the ice deposit as a whole.

Dry growth is said to occur when the freezing rate is greater than the impingement rate and there is no run-off. In this case, the value of n is equal to 1. Introducing the parameter, n, in Eq. (5),

$$\frac{dM_w}{dt} = E \cdot n \cdot W \cdot V_d \cdot D_c \cdot L \tag{6}$$

The surface area of one half of a circular cylinder is given by

$$A = \frac{\pi}{2} \cdot D_c \cdot L \tag{7}$$

Combining the above Eqs. (4), (6) and (7), the following expression for icing intensity per unit length of conductor (g/cm^2/h) is obtained as

$$I = \frac{2}{\pi} \cdot E \cdot n \cdot V_d \cdot W \tag{8}$$

If the liquid water content W, is not directly input in the model, then it must be calculated based on the following expression:

$$W = 0.72 \cdot R^{0.88} \tag{9}$$

where R is the rainfall rate.

During the ice accretion process, the diameter of the conductor changes as the ice deposit increases. Therefore, the collection efficiency (for dry growth) and the freezing fraction (for wet growth), which are dependent upon conductor diameter, also change over time. Variations in meteorological conditions during an icing storm also affect these and other parameters associated with the ice accretion process.

Assuming the atmospheric conditions remain unchanged, the ice mass m_i per unit length of the conductor at time τ_i is obtained from Eqs. (4), (7) and (8) as

$$m_i = V_d \cdot W \int_0^{\tau_i} E(\tau_i) n(\tau_i) \cdot D_c(\tau_i)\, d\tau \tag{10}$$

Model calculations are performed in a stepwise manner to reflect the change in geometry and environmental conditions. The model uses the hourly meteorological and visibility for each hour of an icing event to calculate the collection efficiency, freezing fraction, effective wind speed, and liquid water

content using the empirical and/or theoretical relationships between the above parameters. Figure 10 illustrates the flow diagram of the Makkonen model.

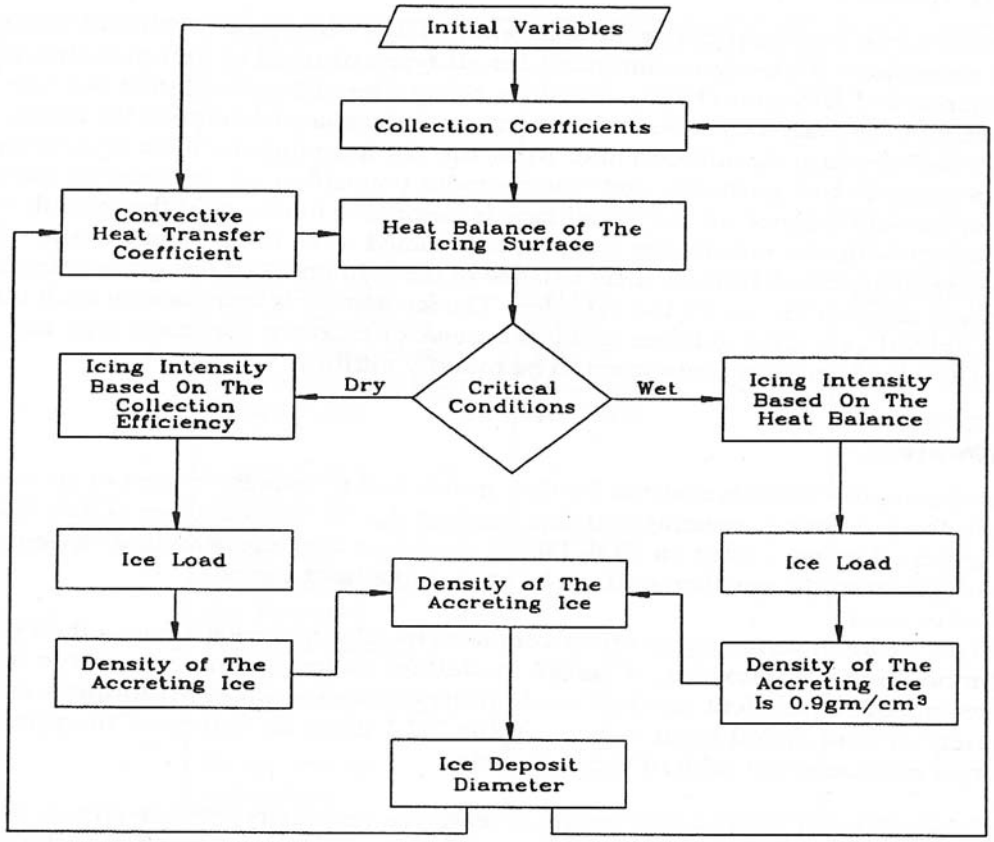

Figure 10: Flow diagram for Makkonen Model [12]

The basic steps, which are used in the model, are as follows:

- A simulation of an icing event begins with an ice-free conductor of specified diameter and orientation.
- Hourly meteorological data for the event are input to the model until the duration of the event has been established. The relevant parameters are converted to units compatible with the model input requirements.
- For each hour of the event, the median volume droplet diameter, liquid water content, effective wind speed, and droplet impact speed are calculated, as applicable to the type of ice accretion.
- For each time step of each hour, icing intensities based on the collection efficiency for dry growth and the heat balance of the icing surface (see Section 3.2.2.3.4) are calculated. The critical and surface temperatures are derived as a result and used to determine the type of growth conditions and the icing intensity. If the process is wet growth, the freezing fraction is also determined. The mass of the ice for the current time step is computed, and the associated ice density, diameter of the iced conductor, and radial thickness of the ice deposit follow. This new diameter is then used as the initial condition for the next time step.
- After the last hour of the event, the total ice accretion thickness and load are output and, if applicable, the model continues to predict the next icing event in the series.

Based on the above model formulation, Newfoundland and Labrador Hydro (NLH) used the meteorological data from seven weather stations to assess the reliability of two parallel 230 kV existing transmission lines on the east coast of Newfoundland. The results of this study were published by Haldar, Mitten and Makkonen in [68] and are summarized below in Tables 4 and 5 respectively.

Table 4: Maximum wind speed (km/h) for selected return period values – Reference [68]. Elevations are in meters.

Stations	Elevation(s)	Return Periods 10-yr (km/h)	25-yr (km/h)	50 yr (km/h)	Maximum Hourly Wind (km/h)	99.9 Confidence Limit on 50-Yr Rtn Period Values (km/h)	Max Gust For 50 yr Return Period (km/h)
St. John's-Torbay	140	110	122	130	136	±31	160
Gander	151	99	108	115	117	±26	157
Argentia	14	104	114	122	111	±31	152
Bonavista	25	115	124	132	126	±31	162
St. Lawrence	49	126	141	152	144	±67	184
St. Alban's	13	80	90	96	98	±48	135
Arnold's Cove	16	91	99	104	93	±39	142

Table 5: Glaze ice thickness (in mm) for selected return period values – Reference [68]. Elevations are in meters.

Stations	Elevation(s)	Return Periods 10-yr (mm)	25-yr (mm)	50 yr (mm)	99.9 Confidence Limit on 50-Yr Rtn Values (mm)	Max Glaze Ice Thickness Period (mm)
St. John's-Torbay	140	28	35	41	±21	59
Bonavista	25	18	22	25	±12	28
Gander	151	16	21	24	±13	27
Argentia	14	15	19	22	±14	21
St. Lawrence	49	13	16	19	±14	18
St. Alban's	13	6	7	8	±9	7

3.2.1.2.3 MRI model [52]

The mass of freezing precipitation is determined from the equation with the modification that the collection efficiency is computed for all types of icing by interpolating the results of Langmur and Blodgett [53]. Besides being time dependent, they also considered the interaction between the process of heat and mass transfer to determine the nature and amount of ice deposit on a transmission line. Mass transfer from impingement of freezing rain, cloud droplets and snow particles, and water vapor deposition are considered, simultaneously. Then the heat balance on the ice surface is computed to decide if the growth is wet or dry. In wet growth, the non-frozen fraction is assumed to be shed. The amount of wafer to be frozen is determined from the heat balance of the cylinder. For wet growth situations, excess water is assumed to run off the cylinder. The ice density is computed at each time step from a weighted averaging scheme using the mass of each ice accretion type and an assumed density. Ice accretion is assumed to be uniform radially. Figure 11 depicts the result of a sensitivity study using the MRI model.

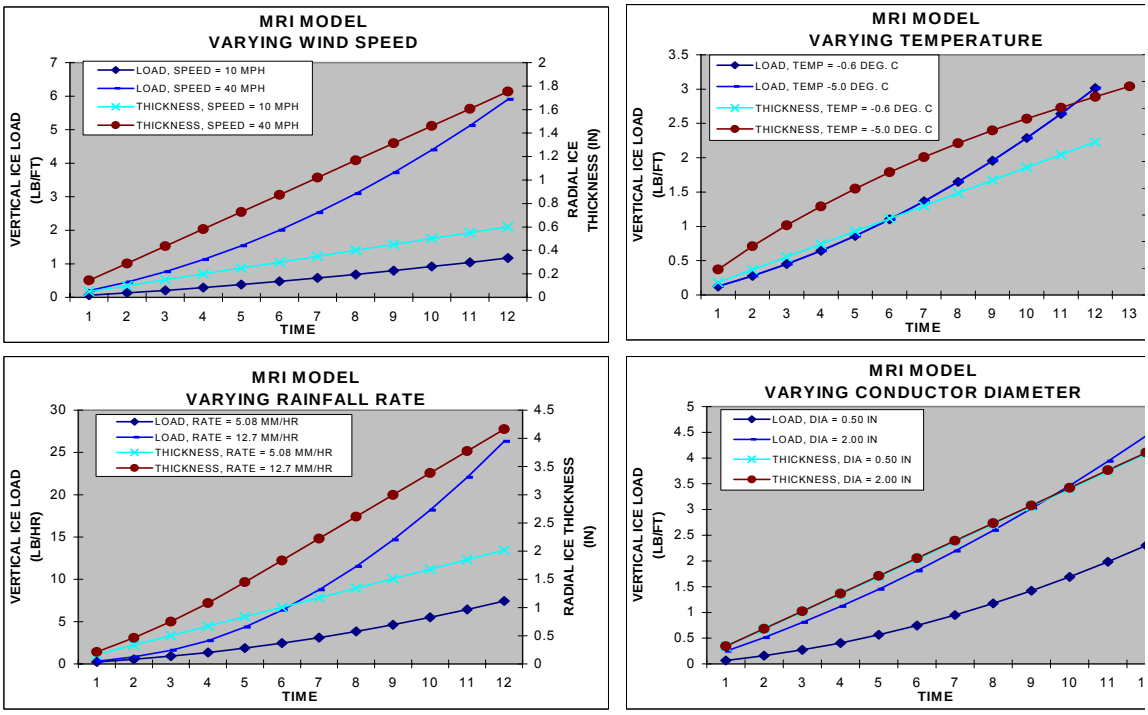

Figure 11: Sensitivity Study Using MRI Model (NLH Study)

3.2.1.3 Model Parameters – Input and Output

Table 6 summarizes the input and output parameters for each of the three previous models.

Table 6: Input and output parameters for the three models – Reference [55]

Model	Input	Accretion Type	Output
Chaîné and Skeates	• Wind Speed • Air Temperature • Precipitation Rate	Glaze	• Equivalent Ice Thickness-Horizontal and Vertical; • Maximum Transverse and Vertical Loads
Makkonen	• Wind Speed • Air Temperature • Precipitation Rate • Air Pressure • Liquid Water Content • Drop Size • Relative Humidity • Visibility	• Glaze • Rime	• Equivalent Ice Thickness; • Maximum Transverse and Vertical Loads; • Time Histories of these Parameters
MRI	• Wind Speed • Air Temperature • Precipitation Rate • Air Pressure • Liquid Water Content • Drop Size • Relative Humidity • Visibility	• Glaze • Rime	• Equivalent Ice Thickness; • Maximum Transverse and Vertical Loads; • Time Histories of these Parameters

3.2.1.4 Model Validation Using Field Data – Freezing Rain

The purpose of this section is to provide guidelines for users to verify the accuracy of icing models for estimating ice loads on overhead lines.

Canadian Electricity Association initiated a project [55] to validate three ice accretion models for freezing rain precipitation using the field data. Three Canadian utilities participated in this project and committed the resources to collect the field data for model validation process. Figure 12 shows one typical test site which was developed by Newfoundland and Labrador Hydro (NLH).

Two other utilities Ontario Hydro and Hydro-Québec also monitored the wind and ice loads on energized lines for three years as part of this study. NLH test site was specifically designed to serve as an instrumented monitoring station to continuously record: wind speed, wind direction, temperature, precipitation, ice accretion rate using ice detector, horizontal and vertical loads at the insulator attachment point, swing angles in both directions, end tension in the cable strains in selected members at the foundation level, and the loads in the guy wires. The site is located approximately 35 km west of the St. John's international airport. The site is also equipped with a Remote Ice Growth Detector (RIGD) which is situated 1.5 m above the ground level and is made of 25.4 mm diameter aluminum hollow pipe, one meter long and uses three strain gages to monitor the ice load on line. Figure 13 depicts the beam and shows the ice accretion data collected in 1997. Details of the test site and other associated information can be found in the CEA report [55].

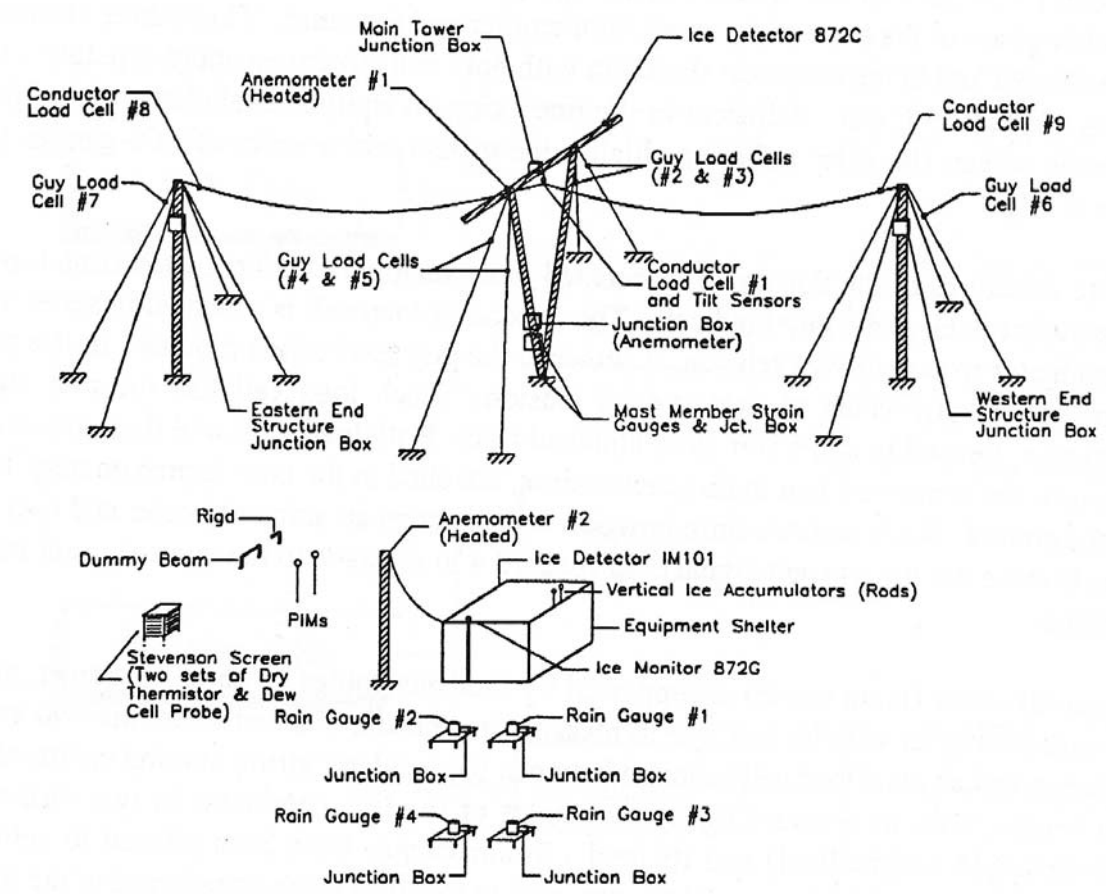

Figure 12: Hawke Hill test site – Reference [55]

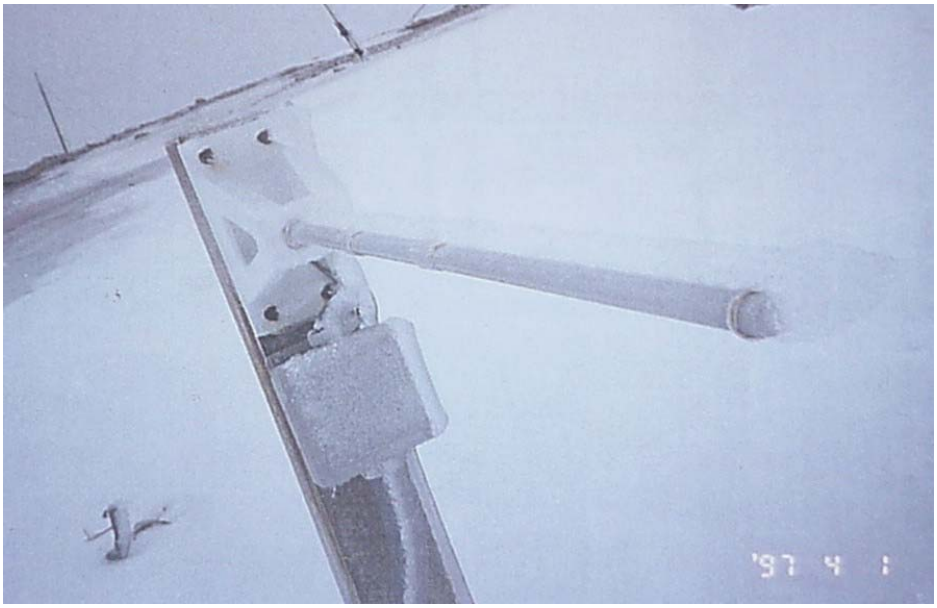

Figure 13: Ice load measurement using rigid rod (NLH,1997)

3.2.1.5 Discussion

A total number of 22 storms were tracked by the three utilities as part of the CEA Study [55]. However many of these storms did not produce a significant amount of load on the conductor. Figure 14 compares the results for those storms which produced more than 5.0 N/m load on the line. A regression analysis was done to correlate the data i.e predicted versus measured loads. Data correlation was good. This figure shows Chaîné model overestimated the load by 71% while Makkonen model overestimated the same by 33% for a measured load of 30 N/m. The MRI model underpredicted the same by 15%. This comparison was state of the art at the time of this study. Since then NLH and Hydro-Québec are still operating these sites but Ontario Hydro has closed the site near Ottawa. During the past six years (1998-2004) NLH site has recorded few more storms. However these data need to be analyzed further and will be reported in the future.

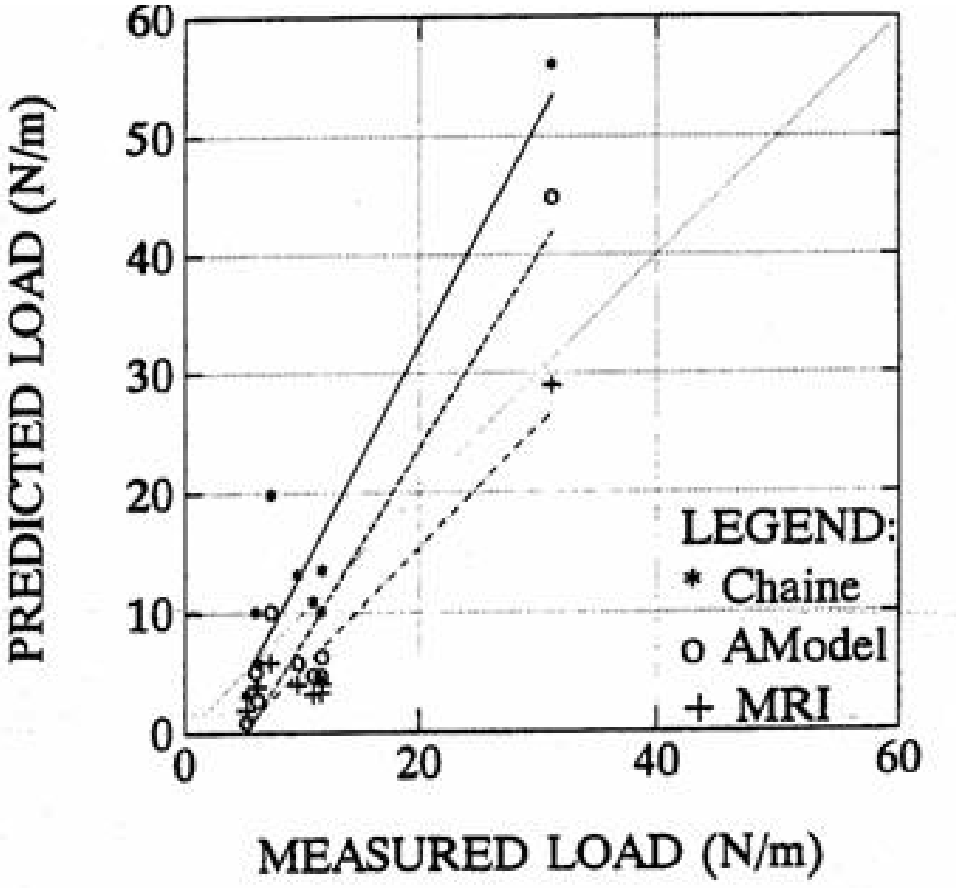

Figure 14: Comparison of measured ice load with model runs – Reference [55]

3.2.1.6 Effect of Ice Accretion Shape

McComber [15] used the meteorological data of the Canadian January 1998 storm to illustrate the effect of accretion shape on an ice load evaluation. Basically, two models were chosen – one based on drop trajectories to produce an ice shape (Poots [16]) and the other based on a simple assumed accretion shape (Chaîné and Castonguay [14]) that was semi-elliptical and based on wind tunnel data. McComber uses four basic models to estimate ice loads:

a) Existing circular accretion model (C)

b) Rigid conductor model (R)

c) Oblique plate model (0)

d) Chaîné Model (E)

All the models showed more sensitivity to wind speed than to precipitation. In a specific study, the meteorological data of the January 1998, ice storm was fed into each model. Figure 15 shows the equivalent radial thickness with time of each of the models.

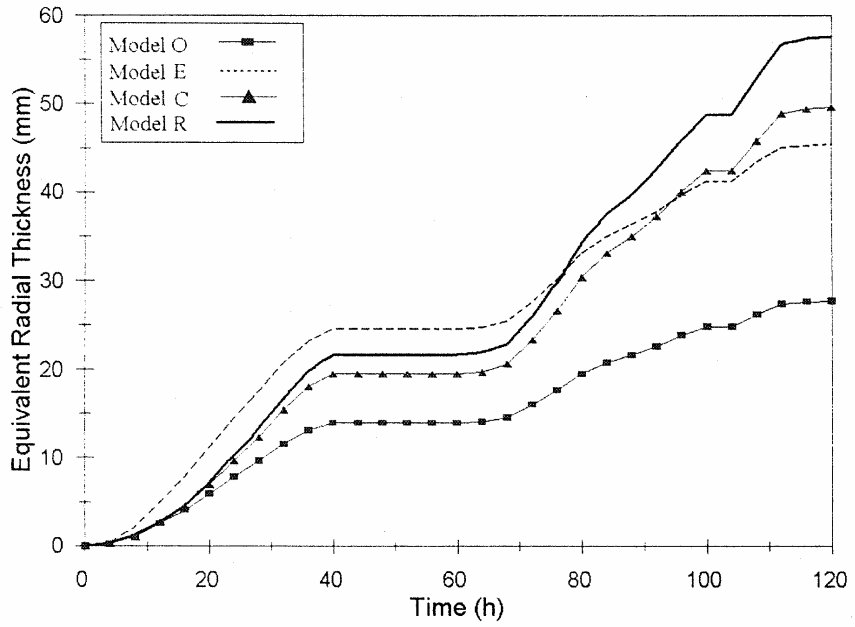

Figure 15: Radial thickness for January 1998 Ice Storm with normal wind direction – Reference [15]

Over time, the rigid model, R, gave the highest loads by over 16%. The Chaîné model, E, initially gives higher loads but eventually gives a lower load, even then the circular accretion model, C. The oblique plate model gave substantially low ice loads throughout.

3.2.2 Rime-Icing Models

3.2.2.1 Meteorological Parameter Input and Model Output

Rime ice models can require a collection efficiency (the proportion of water droplets intercepted by the accreting ice envelope) which is a function of droplet size, wind speed and accretion size. A proportion of those droplets which strike the accretion envelope will actually freeze – known as the freezing efficiency. This is calculated in some models by the various heat exchange mechanisms (conduction, convection, radiation and latent heat). At low temperatures, the freezing efficiency can be assumed to be unity and the accretion is classed as “dry” and so dependent only on the collection efficiency. This will change as both the accretion envelope and weather condition change.

The input data to this type of model [12] is:

a) Wind speed normal to line

b) Air temperature
c) Cloud base, cover and type
d) LWC
e) Water droplet size
f) Relative humidity

The model will then give an output of:

a) Mass of accreted ice
b) Density of accreted ice
c) Dimensions of accreted ice envelope (assuming characteristics of accreting object)

The actual accretion level will depend significantly on the torsional stiffness of the conductor [109]. The resistance to rotation is extremely high close to conductor supports but falls of within a few meters for small conductors as observed [19] and calculated [16]. Additional input data is then required:

a) Conductor torsional stiffness
b) Conductor span length

but the model then gives the additional output:

a) Ice load along the span
b) Rotational state at a point
c) Accretional envelope at a point

These models can therefore produce the necessary ice load on the total conductor span which is then applied to the support structure. Finally, models are available, generally semi-empirical, which can relate these ice loads on single conductors to twin and quad bundled conductors.

3.2.2.2 Field Test Validation

Previously, most model validation was in simulated laboratory experiments or wind tunnels. As the data required is to determine the actual ice loads on real electricity supply networks, the model output of Section 3.2.2.1 to give ice loads on real spans is the most useful parameter. It is therefore very important that the output of such models be tested against real field data taken at the same time and place as the meteorological input parameters. Most past field verification [54,55] has wind, temperature and precipitation input data, whereas laboratory studies have provided droplet size distribution and LWC.

Previous field evaluation tests [50] have also used input data and rime ice load measured data that were not at the same location and this has been one reason for discrepancies between modelled and measured data.

3.2.2.3 Fundamentals of Ice Modelling

3.2.2.3.1 Rime Ice Accretion Process

This section concentrates on rime or ‘in-cloud’ issues, although some aspects are common to other icing types. Rime ice is associated with water droplets in cloud (normally hill-cloud or fog) and not with raindrops. The droplet size is important, as the smaller particles can travel with the airflow, whereas larger droplets can collide with objects instead of diverting round them with the airflow (Fig. 16). These particles can give significant ice loads and the maximum icing rate per unit area is determined by their flux density, F. This is a product of the mass concentration of particles in the air, w, and velocity, v, of the droplets relative to the target surface. Makkonen [58] gives a rate of icing of:

$$\frac{dm}{dt} = \alpha_1 \cdot \alpha_2 \cdot \alpha_3 \cdot w \cdot v \cdot D_c \qquad (11)$$

where D_c is the external diameter of the object and α_1, α_2 and α_3 are collision, collection and accretion efficiencies.

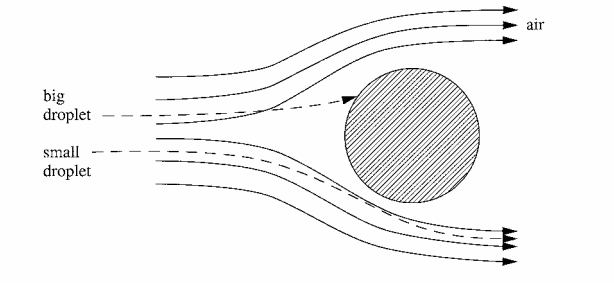

Figure 16: Streamline flow and droplet trajectories around a conductor – Reference [12]

The *collision efficiency*, α_1, is the ratio of the flux density of particles that hit the object to the maximum flux density. The collision efficiency is reduced from one because small particles tend to follow the streamlines and may be deflected from their path towards the object, as illustrated in Fig. 16.

The sticking efficiency, α_2, is the ratio of the flux of particles that stick to the object to the flux of particles that hit the object. The sticking efficiency is reduced from one when particles bounce from the surface (Fig. 17). This is mostly the case with wet snow.

The efficiency of accretion, α_3, is the ratio of the rate of icing to the flux density of the particles that stick to the surface. The accretion efficiency is reduced from one when the heat flux from the accretion is too small to cause sufficient freezing to incorporate all sticking particles into the accretion. In this case a part of the accreted mass is lost from the water surface by run-off (Fig. 18). This situation is most frequent for freezing rain. A critical point is where the ice accretion is dry ($\alpha_3 = 1$) or wet ($\alpha_3 < 1$).

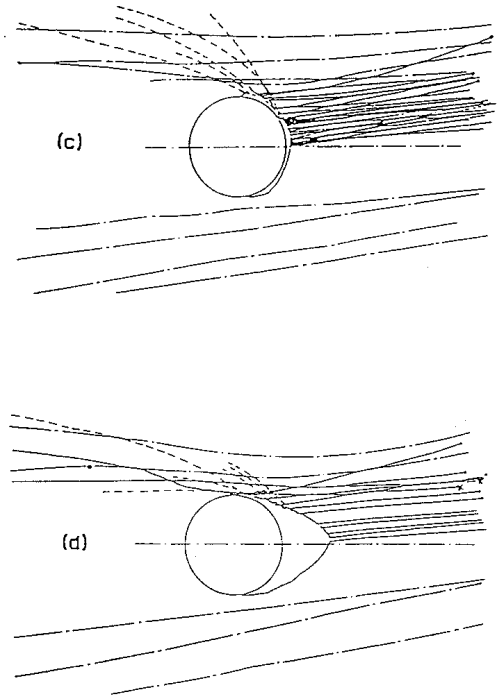

Figure 17: Simulated wet snow accretion after [12]. Solid line: snowflake collided and adhered, dashed line: snowflake collided and reflected, solid line + x: no impaction, and dash-dotted line: other snowflakes.

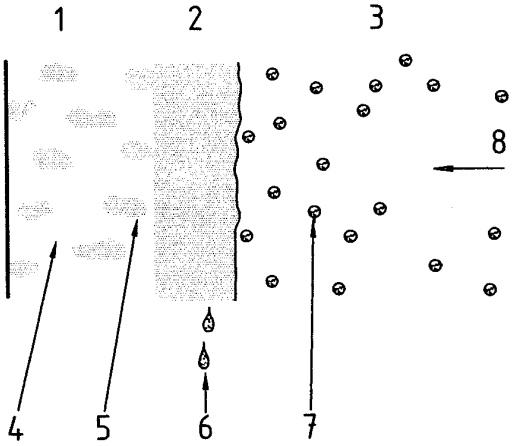

Figure 18: Growth of glaze after [12] (wet growth). 1 – ice, 2 – water film, 3 – cold air, 4 – ice, 5 – liquid water, 6 – runoff-water, 7 – droplets, 8 – wind direction

3.2.2.3.2 Icing Rate

A simple version of Eq. (11) is when $\alpha_2 = \alpha_3 = 1$. In this case, the factor $\alpha_1 \cdot D_c$ can be put equal to a constant value and the icing rate is essentially dependent on wind velocity and the presence of water droplets and sub-zero temperatures. To obtain a more realistic value for α_1, the drag of the water droplets in the air stream needs to be considered and a simplified calculation can be made for a round conductor of circular cross-section [12,13]. The collision efficiency α_1 can be determined [56] from 2 dimensionless parameters:

$$k = \rho_w \cdot d^2 \cdot v / 9 \cdot \mu \cdot D_c \tag{12}$$

and

$$\phi = R_e^2 / k \tag{13}$$

where

$$R_e = \rho_a \cdot d \cdot v / \mu \tag{14}$$

where R_e is the droplet Reynolds number
d is the droplet diameter
D_c is the external diameter of the object
ρ_w is the water density
μ is the absolute viscosity of air
ρ_a is the air density

An empirical fit to obtain α_1 from these 2 parameters, k and ϕ, has been developed [57]:

$$\alpha_1 = A - 0.028 - C \cdot (B - 0.0454) \tag{15}$$

where:

$$A = 1.066 \cdot k^{-0.00616} \cdot \exp(-1.103 \cdot k^{-0.688}) \tag{16}$$

$$B = 3.641 \cdot k^{-0.478} \cdot \exp(-1.497 \cdot k^{-0.694}) \tag{17}$$

$$C = 0.00637 \cdot (\phi - 100)^{0.381} \tag{18}$$

A further simplification allows the use of a median value (MVD) for the volume diameter of the droplets (d in Eqs. (12) and (14)) so that a droplet size range need not be identified. The calculation for α_1 is absolutely necessary for in-cloud icing. For glaze icing and wet snow accretion, α_1 is often set equal to unity as the individual particles are heavy enough not to be diverted by the air flow.

3.2.2.3.3 Stickiness

In terms of collection efficiency, α_2, water droplets tend to spread on the surface and, if the heat exchange is sufficient, freeze quickly enough for there to be no loss due to bouncing or run-off, i.e. $\alpha_2 \approx 1$. For snow at < 15% LWC, α_2 can be zero as there is virtually no 'stickiness'. This factor can, however, reach unity for higher LWC, low wind speeds and temperatures around 1° to 1.5 °C.

3.2.2.3.4 Accretion

In dry growth situations (typical for rime ice at temperatures < -3°C) the accretion rate, α_3, will be virtually unity. The process depends on the efficiency in which the latent heat from the droplets freezing can be taken away by convective ventilation, evaporation and radiation. The equation of the heat balance is given by [58]:

$$\Delta Q_c + \Delta Q_s + \Delta Q_e = \Delta Q_f \tag{19}$$

Where Q_c, Q_s and Q_e are the heat losses due to convection, radiation and evaporation respectively, and Q_f is the latent heat released during freezing and is given by:

$$Q_f = I \cdot L_f \tag{20}$$

where I is the icing intensity (see Eq. (8))
L_f is the latent heat of fusion.

The convective heat loss, Q_c, from the iced surface is defined [58] as:

$$Q_c = I \cdot C_w \cdot (t_s - t_a) \tag{21}$$

where C_w is the specific heat of water
t_s is the temperature of the ice surface
t_a is the air temperature.

Strictly speaking, it is the droplet temperature that is important, but for in-cloud icing, this is likely to be very close to the air temperature and so this is used instead.

There is also some radiation loss from the surface, Q_s, which is evaluated using the Stefan-Boltzmann constant, σ, and a radiation linearisation constant, a, which is used to allow the simplified expression (Eq. (22) below) to be used instead of using a fourth power expression:

$$Q_s = \sigma a \cdot (t_s - t_a) \tag{22}$$

where $\sigma = 5.67 \cdot 10^{-8}$ [$W \cdot m^{-2} \cdot K^{-4}$]
$a = 8.1 \cdot 10^{7}$ [K^3]

The units of σ are Watt per meter squared per Kelvin to the fourth. Equation (20) is an approximation, but since t_s and t_a are both low (in radiation terms) and fairly close, the error will be quite small.

A final requirement is to calculate the evaporative heat transfer coefficient. The evaporative heat transfer, Q_e, is obtained from the latent heat of evaporation (or sublimation), L_e, the saturation vapour pressure over ice surface, e_s, and the ambient water vapour pressure in the airflow, e_a. Thus:

$$Q_e = h \cdot \varepsilon \cdot L_e \cdot (e_s - e_a)/(C_p \cdot P) \tag{23}$$

where h is the convective heat exchange coefficient
ε is the ratio of the molecular weights of dry air and water vapour
C_p is the specific heat of air with constant pressure
P is the air pressure

Measurements on rime ice accretion in China (Wu *et al*. [59]) allowed the influence of various factors such as height above ground, height above mean sea level, electric field, wind and conductor diameter to be determined. Local topographical effects were found to be very significant.

3.2.3 Wet-Snow Models

3.2.3.1 Background for Snow Accretion

Snow accretion on overhead wires forms from adhesive forces between the surface of the wire and the snow accumulation, and between snowflakes themselves. The origins of the adhesive forces are as follows:

a) Freezing (including pressure melting)
b) Bonding through freezing of supercooled water droplets existing on the surface of snowflakes [108]
c) Sintering (process of minimizing the surface area to volume ratio, similar to recrystallization)
d) Condensation and freezing of vapor in the air
e) Mechanical interwinding of snowflakes
f) Capillary action due to liquid water included
g) Coherent force between ice particles formed through metamorphosis of snowflakes

Sintering is also known as a method for bonding and consolidating ceramic and metal particles at the microscopic level, below the melting point. Sintering is used to make metal and ceramic parts in a high-production process and also can be used to make unique metal alloys and ceramic systems. One common example of sintering is ice cubes that stick together in the freezer. In fact, while ice cubes are in the freezer, sintering processes are at work below the melting point of water, causing the cubes to stick together.

As a result, snow accretion occurs under relatively broad meteorological conditions. But the snow accretion which exerts the largest load is based on accretion of wet snowflakes at temperatures above freezing which originates from capillary action and coherent force between ice particles formed through metamorphosis of snowflakes.

It was reported that Electric utilities experienced severe damage to their power lines, including many tower collapses.

Since France and Japan experienced severe damage, both countries conducted collaborated studies, and developed empirical models. The following is a brief outline.

3.2.3.2 Japanese Cylindrical-Sleeve Model [77]

Snow accretion depends on the amount of snow passing around the wire with the speed of the vector sum of wind speed and falling speed of snowflakes. Among them, some keep accretion and some don't contribute to snow accretion. Snow accretion efficiency is defined as α_s. Assuming that snow accretion always develops in a cylindrical shape, the mass of snow accreted per unit length of wire is

$$m = \frac{\overline{\alpha}_s^2 + \overline{P}_n^2 \cdot \Delta\tau^2}{\pi \cdot \overline{\rho}_s} + D_0 \cdot \overline{\alpha}_s \cdot \overline{P}_n \cdot \Delta\tau \qquad (24)$$

where $\Delta\tau$ is the duration time of accretion development, D_0 is the diameter of the bare wire, ρ_s is the density of accreted snow and P_n is the snow precipitation intensity. The bar denotes average value of quantities taken over a time interval of accretion. When wind action is taken into account, the value of the snow precipitation intensity P_n is approximated by:

$$P_n = P\sqrt{1 + \left(\frac{V \sin\theta}{V_s}\right)^2} \qquad (25)$$

where P is the intensity of precipitation observed on ground surface (g/cm^2·s), V is the wind speed (cm/s), V_s is the falling speed of snowflake (cm/s), and θ is the angle between the axes of wire and wind direction.

Although this equation is based on the use of mean values of α_s, P_n and ρ_s, it is possible to divide one event of accretion into sub-sequences and calculate the mass of snow for each sub-sequence using representative mean values, especially when they change significantly with time.

In this equation, the quantities P_n and $\Delta\tau$ are known or can be estimated if synoptic meteorological parameters are available and, of course, the diameter of the wire D_0 is known. However, the quantities ρ_s and α_s are unknown and have to be estimated from available data.

Based on the above idea, joint research of France and Japan [103] was conducted in an attempt to seek a method to estimate density of accreted snow and snow accretion efficiency from meteorological parameters which are generally available. The study was comprised of wind tunnel experiments and field data collection using indoor facilities to keep a controlled environment conditions.

As a result of wind tunnel experiments, density of snow accretion shows the strongest dependence with the wind speed. Snow accretion efficiency became the largest at a certain temperature, and small on either side of it. Although these tendencies are qualitatively correct, but from an investigation performed at the same time on the relationship between liquid-water content of snowflake and temperature of the laboratory, they are different from the relationship in natural conditions. In conclusion, the relationship derived from the experiments cannot be used to estimate snow accretion.

Consequently, from the limited observation results, those having the data used for deriving an empirical model, were selected and analyzed, but uncertainty of the data is large, and it is difficult to obtain reliable results. Therefore Sakamoto [77] linked qualitative tendencies obtained from the wind tunnel experiment with the equation proposed by Finstad [73] on snow accretion efficiency, calibrated them according to the limited observation results of natural snow and provisionally proposed the following equation for determining the mass of accreted snow per unit length of wire :

$$m = 4.5 \cdot \frac{exp\left[-6 \cdot \{(T_a / T_d) - 0.32\}^2\right]}{V_n^{0.2}} P_n \cdot \Delta\tau \qquad (26)$$

where T_a is air temperature (°C), V_n is the mean value of the normal components of the wind speed to the line (m/sec) and the equation for T_d is as follows:

$$T_d = 2.31 - 0.101 \cdot ln(H) \qquad (27)$$

where H is the sea level (m).

Thus, a wet snow accretion model was determined for qualitative dependence by wind tunnel experiments and natural snow accretion data, but more natural snow accretion data is required for quantitative dependence. For that purpose, more observations are needed.

3.2.3.3 French Cylindrical-Sleeve Model [20, 83, 104, 105, 106]

The model developed in France is based on the work of Admirat *et al.* [20, 83, 104, 105, 106] performed in the 1980's, partly in collaboration with Japan. The general formulation of increase of mass accretion m versus time t is given by Eq. (11).

In the case of wet snow, the inertia of particles is important (big particles) and therefore the *collision efficiency* α_1 = 1.

If snowflakes are dry (low temperatures), they do not adhere and the *sticking efficiency* α_2 tends to 0. In the case of wet snow, α_2 depends on wind speeds, air temperature and humidity. Based on experimental results and the main influence of wind, the model consider α_2=1/V, where V is the wind velocity (m/s).

The accretion efficiency α_3 is determined by the thermal equation, balancing the energy due to the fusion of particles, the convection and conduction in the airflow, the evaporation of water and the Joule effect. This balance gives the condition for the beginning of accretion, and for each step of time the proportion α_3 of snow that actually melts, and thus the liquid content. If the liquid content is too high, the sleeve begins to break up. In operation, this balance is used to check for the condition of accretion, and the model considers a conservative value of α_3=1.

The product of the mass *w* and velocity *v* in Eq. (11) may be replaced by the flux density *F*. The following form is assumed for *F*:

$$F = P_r \cdot \sqrt{1 + \frac{V^2}{V_s^2}} \tag{28}$$

where P_r is the precipitation rate (equivalent in water on ground in mm/s), V is the wind velocity and V_s the vertical velocity of snowflakes fall. In operation, V_s is assumed to be 1 m/s.

The general equation (11) can thus be written:

$$\frac{dm}{d\tau} = \frac{1}{V} \cdot P_r \cdot \sqrt{1 + \frac{V^2}{V_s^2}} \cdot D_\tau \tag{29}$$

where D_τ is the diameter of the sleeve at time τ.

We can also express the increase of mass accretion as a function of increase of diameter and of the density ρ of accretion:

$$\frac{dM}{d\tau} = \frac{\pi}{2} \cdot \rho \cdot D_\tau \cdot \frac{dD_\tau}{d\tau} \tag{30}$$

From these two equations, we get the increase of diameter of sleeve between time τ_k and time τ_{k+1}:

$$\Delta D_{\tau_k}^{\tau_{k+1}} = D_{\tau_{k+1}} - D_{\tau_k} = \frac{2 \cdot P_r(\tau) \cdot \sqrt{1 + V^2 / V_s^2}}{\pi \cdot \rho \cdot V} \cdot (\tau_{k+1} - \tau_k) \tag{31}$$

At time τ_0 = 0, D_0 is the diameter of the bare cable.

The increase of mass is deduced:

$$\Delta m_{\tau_k}^{\tau_{k+1}} = \frac{\pi \cdot \rho}{4} \left(D_{\tau_{k+1}}^2 - D_{\tau_k}^2 \right) \tag{32}$$

The density ρ (kg/m^3) is assumed to depend on wind velocity V (m/s) according to the relation:

$$\rho = 100 + 20 \cdot V \tag{33}$$

The model developed implies an iterative computation of the mass of snow accreted versus time. For operational use of this model, an important data is the precipitation $P_r(\tau)$ versus time. Depending on the location, this distribution might not be known, the only data available being the total amount of precipitation and an estimate of the times for the beginning and the end of the event. In this case,

following several observations in France, the model distributes the precipitation $P_r(\tau)$ as a "bell curve" with a maximum in the middle of the event.

3.2.4 Discussion

Electric utilities rely on estimates of extreme ice loadings to design new lines and upgrade existing lines. The use of icing models to provide such estimates is obviously attractive. The models presented in Sections 3.2.1, 3.2.2 and 3.2.3 for glaze icing, rime icing and wet-snow accretion respectively are also very useful to compute statistics from a historical database of meteorological conditions. Theoretical icing data are generated from the meteorological data, using the relevant icing models. The influence of terrain is obviously very important as described in Chapter 5. Hence, the resulting icing data need to be transferred from sites of origin to the site of the overhead line (see Section 4.2). The final icing data can then be statistically processed (see Section 4.1) to give the design data on ice load. In addition, together with the wind data, the wind force on iced conductors is obtained and can be statistically processed (see Section 3.3.4).

However, some precautions [84] may be taken when using icing models to assess ice loads on overhead lines. For instance, local variations in wind speed and air temperature and variations among the wires and conductors themselves may be significant. Structures at sites that are typically windier than the measurement sites may accrete more ice. A proper transfer function modelling may sometimes be difficult to assess. Furthermore, since wind speed typically increases with height above ground, more ice is expected to accrete on higher wires of the same line. Also, Joule heating from the current in conductors may have a significant effect on the amount of ice that accretes.

The air temperature may vary at any location during an icing event and across the region affected by the event. For near-freezing temperatures, even small variations in temperature can have a significant effect on the fraction of the impinging precipitation that freezes to a structure and on the rate of freezing, which controls the shape of the accretion. At relatively high temperatures, icicles may account for a significant portion of the accreted ice. At lower temperatures, on the other hand, the impinging precipitation may freeze where it hits, accumulating in an eccentric accretion that would tend to rotate torsionally flexible wires (such as ground wires), with the ice eventually forming a cylindrical sleeve around the wire. The shape of the accretion affects both the further accretion of ice and also the rate of ice shedding when the icing event ends.

On the other hand, on wires of spans that are parallel to the wind direction, the ice thickness may be less than the model estimates. One has to be aware of such limitations before using any icing models. More research is needed in this field.

3.3 Ice Load Assessment on Overhead Lines

Ice loads on structures can be assessed in several ways:

1. By the use of historical data on icing incidents
2. By the use of historical weather data combined with an icing model
3. By the use of load cell data on test spans on the route
4. By conversion of ice load or weather data away from the line route using a simple transfer model
5. By the use of rigid rods

Ice loads on overhead line conductors can be assessed locally in terms of line height above ground (effect of wind shear) and conductor size.

Ice loads on independent structures can be assessed by modelling the structure shape (e.g. round pole) or the structure components (e.g. tower steelwork).

Wind-on-ice loads can be determined from a modelled version of the accretion envelope and the type of airflow assumed. In a simple version the projected area of the accretion in the wind direction is used to determine wind pressure.

Ice loads on structures attached to overhead lines can be assessed by a vector sum of all the forces involved on the structures from the phase and earth conductors taking into account crossarm dimensions. These loads must then be combined with the ice load on the structure itself.

Section 3.3 covers several distinct areas:

a) Load on independent structures
b) Transfer modelling of weather/load rate data from remote sites
c) Types of icing models used to assess loads
d) Assessing loads on structures with overhead lines
e) Data needed for ice load assessment

The term "ice load" is assumed to cover all types of ice and snow accretion. In some areas the ice load may be all of one type, e.g. rime ice in mountainous areas. However, in some areas (e.g. coastal or valleys) the accretion within a single incident may change from glaze to rime icing and rime ice to snow or other combinations. Predicting ice loads under these conditions is extremely difficult. Definition of snow types can vary between countries and so the definitions given in IEC 61774 [2] are used here.

3.3.1 Accretion on Lattice Structures

3.3.1.1 General

Ice accretion rates vary with the type of ice and the size, shape and orientation of the structure component. The most severe loads occur when the component has a small cross-sectional area with the narrow dimension pointing into the wind. It is for this reason that lattice towers can suffer severe icing loads, far in excess of similar size solid structures.

3.3.1.2 Ice Class

The publication ISO 12494 [3] described the concept of an ice class to enable the designers to assess the severity of icing at any particular location. Measurements (direct or transferred) together with modelling studies are usually necessary to determine the ice class. The model can use meteorological data with an accretion scenario. It may be calibrated against local measurements of ice load. In general terms, accretion due to glaze ice is treated separately from rime ice (including wet snow) but in both cases the ice mass per unit length is determined by the total ice cross-section times the ice density.

3.3.1.2.1 Ice Class – Glaze Icing

Table 7 lists the ice classes (IC) for glaze icing severity (ICG). The ice density is taken as 900 kg/m^3. The table relates the ice thickness as shown in Fig. 19 to a reference ice collection.

The ice thickness, *t*, is always measured normal to the object surface.

3.3.1.2.2 Ice Class – Rime Icing

Table 8 shows the ice classes, ICR, for icing severity related to a reference ice collector, which is a horizontal rotating cylinder (diameter = 30 mm) used with different rime ice densities. Figure 20 shows the typical ice accretion scenarios for various object shapes, A to F.

Specific ice mass values for the objects A to F in Fig. 20 are given for an ice density of 500 kg/m^3 in ISO 12494 [3]. Large objects of type A and C with W > 300 mm tend to exhibit accretion envelopes that are a mix of different types. Load calculations for these large flat or round objects according to the dimensions in Fig. 21 are given in ISO 12494 [3].

Table 7: Ice classes, ICG for glaze icing – Reference [30]

Ice Class ICG	Ice Thickness *t* (mm)	Glaze Ice Mass (kg/m) Cylinder Diameter (mm)			
		10	30	100	300
G1	10	0.6	1.1	3.1	8.8
G2	20	1.7	2.8	6.8	18.1
G3	30	3.4	5.1	11.0	28.0
G4	40	5.7	7.9	15.8	38.5
G5	50	8.5	11.3	21.2	49.5

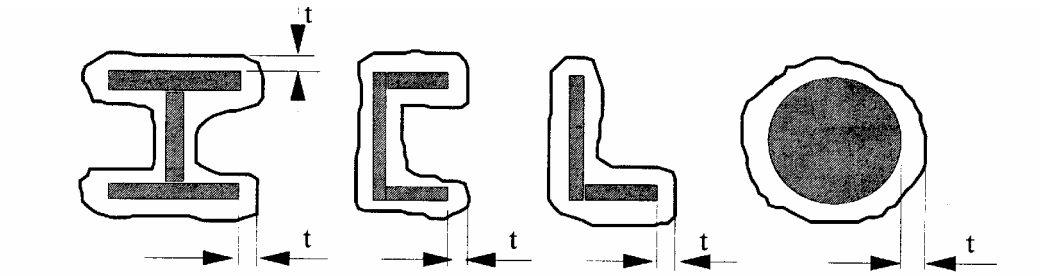

Figure 19: Ice accretion models for glaze icing – Reference [30]

Table 8: Ice Classes, ICR, for rime icing – Reference [30]

Ice Class ICR	Ice Mass kg/m	Rime ice diameter for 30mm diameter object Density of ice in kg/m^3			
		300	500	700	900
R1	0.5	55	47	43	40
R2	0.9	69	56	50	47
R3	1.6	88	71	62	56
R4	2.8	113	90	77	70
R5	5.0	149	117	100	89
R6	8.9	197	154	131	116
R7	16.0	262	204	173	153
R8	28.0	346	269	228	201
R9	50.0	462	358	303	268

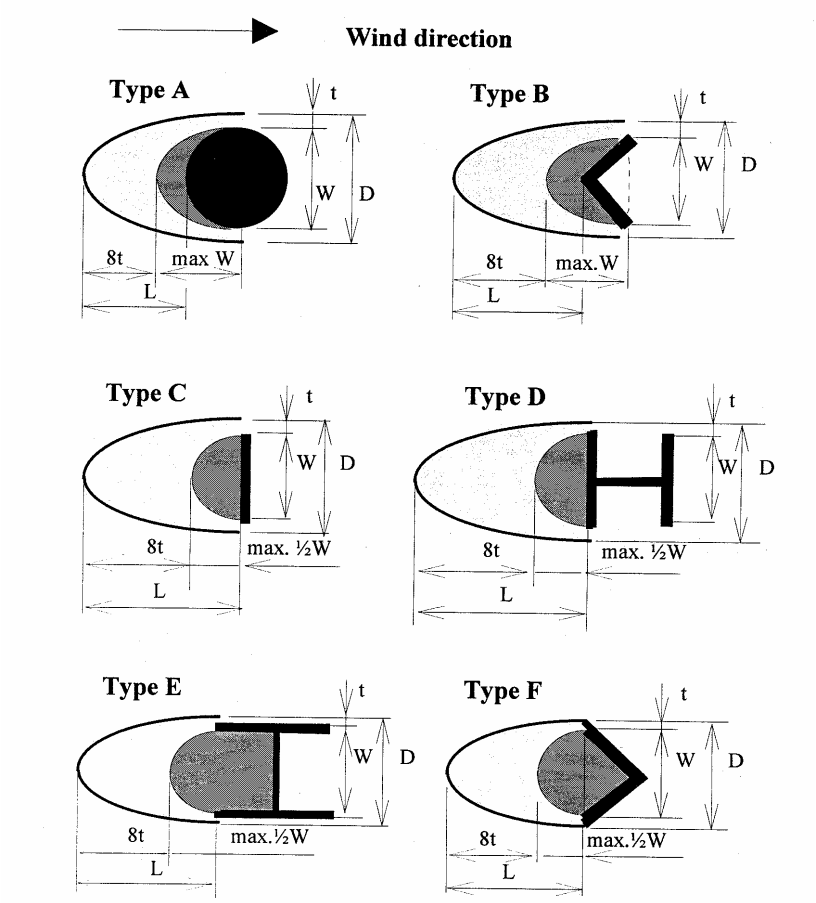

Figure 20: Ice accretion models for rime icing – Reference [30]

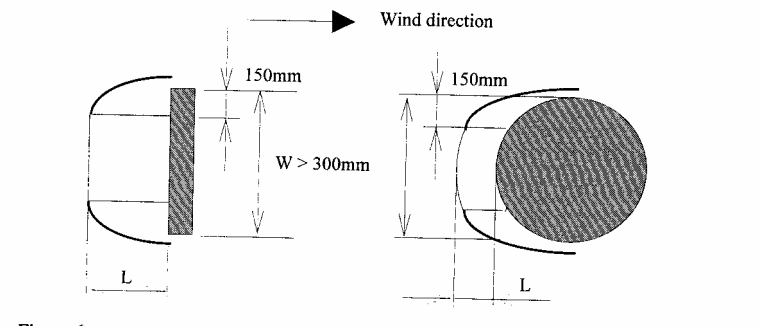

Figure 21: Ice accretion model (big objects) – Reference [30]

For lattice structures, the overall ice load can be calculated from the sum of the ice load on all the component sections. The ice load envelope is dependent on wind direction and when dealing with ice vanes, these should be considered for each particular wind direction for the structures as a whole. This means that different calculations must be made for each specified wind direction.

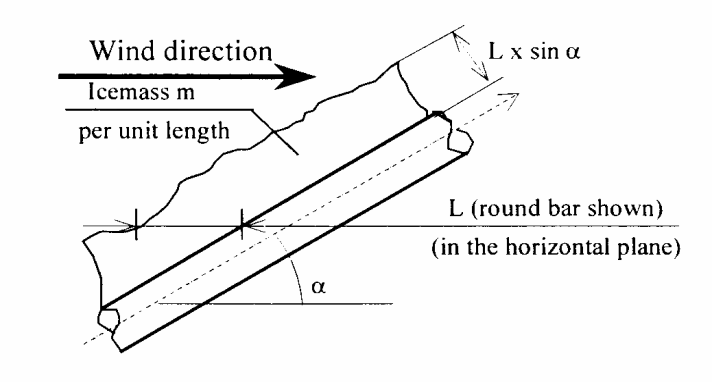

Figure 22: Inclined plane accretion – Reference [30]

In terms of wind vanes, as these always grow into the wind direction, allowance must be made for inclined surfaces according to the angle, α, of the surface to the wind direction (Fig. 22). The new ice mass is thus $m \sin \alpha$. The loads must be calculated for all angles, α, down to a minimum of 10º. Below this level, the load is calculated at α = 10º so that there will always be some accreted load on surfaces parallel to the wind direction.

3.3.2 Ice Accretion Loads on other Structures

Schaub [7] focused on estimating glaze and rime ice loads on flat plates and wires to provide maximum expected ice thickness for engineering design of structures. The values are determined by extreme value analysis of several years of recorded data, the uses of the models of Chaîné and Skeates [8] and McComber and Govani [9].

Measurements of ice load were made on Mount Washington by McComber and Govani. Meteorological data was also logged and an experimental growth model determined:

$$m = m_o \cdot e^{k\tau} \tag{34}$$

where m = ice mass per unit length (kg/m) at time τ (h)
m_o = initial ice mass per unit length (kg/m)

and k is given by:

$$k = [0.04 \cdot (E \cdot W \cdot V_n)]/\rho \cdot D_o \tag{35}$$

where E = collection efficiency
W = liquid water content (g/cm^3)
V_n = average wind speed (m/s)
ρ = ice accretion density (g/cm^3)
D_o= diameter of the bare conductor (cm)

From the above equations, the ice accretion diameter, D_c, is given by:

$$D_c = (12.7 \cdot m/\rho)^{0.5} \tag{36}$$

This was validated by the measured data.

Schaub [10] also attempts to relate meteorological data from stations away from the accretion site by assuming an achaibatic lapse rate of 1ºC for 200 m land height. Thom [11] uses a wind speed calibration of:

$$V_2 = V_1 \cdot [z_2/z_1]^{0.14} \quad (37)$$

where V_2 = wind speed at accretion site (m/s)
V_1 = wind speed at observing station (m/s)
z_2 = elevation of accretion site (m)
z_1 = elevation of observing station (m)

In order to evaluate k, Makkonen [12] assumed an average collection efficiency of 0.1. An average LWC of 0.8 g/m^3 is assumed for glaze ice and 0.4 g/m^3 for rime ice. These figures are a compromise of Makkonen [13] in fog and the data from McComber and Govani.

In-cloud rime icing load calculations are dependent on knowledge of the cloud ceiling in relation to the accretion area. The periods of low cloud at times when the calculated temperature is above 0ºC or less than -10ºC are removed. For calculated temperatures in the range 0 to -3ºC glaze icing is assumed and for temperatures in the range –4 to –10ºC rime ice is assumed with respective densities of 0.8 and 0.3 g/cm^3 respectively. The various time periods of in-cloud icing can thus be used to obtain the estimated ice loads.

For a flat plate, Chaîné and Castonguay [14] determined a relationship between the horizontal ice thickness A_h and equivalent radial ice thickness t:

$$A_h = 4.47 \cdot t / V_n \quad (38)$$

3.3.3 Ice Loads on Circular Conductors

3.3.3.1 Glaze Icing on Torsionally Stiff Conductors

A description of glaze icing models was presented in section 3.2.1. However, many models use a circular (or equivalent circular) accretion shape to evaluate ice loads. Torsionally stiff conductors can generate non-circular ice shapes that have a significant effect on modelled ice loads.

Figure 23 shows a field observed ice accretion shape and the equivalent circular cross-section. The field ice diameter varies from 0.8 to 1.5 times the equivalent cross-section diameter. An eccentric ice shape creates a torque which is balanced by the conductor torsional stiffness. Assuming a torsional rigidity factor, f, which is between 0 (for flexible conductors) and 1 (for rigid conductors), the equivalent radial thickness, t^m, for a conductor of known rigidity can be found from a weighted average of the flexible situation, t^f, and the rigid situation t^r.

$$t^m = f \cdot t^r + (1 - f) \cdot t^f \quad (39)$$

Hardy *et al*. [109] demonstrated by means of a dedicated numerical model that the propensity of cables to icing is bracketed within two limits translating accretion on a fixed rigid cylinder on the low side and a freely rotating cylinder on the high side, with actual cases standing in between according to decreasing torsional stiffness. It was also shown accordingly that spacered conductor bundles are much less prone to severe icing than similar single conductors.

A simple non-circular accretion can be derived from certain characteristics of the glaze icing process:

a) Drop impinging direction

b) Spread of water on drop impact

c) Water run-back before freezing

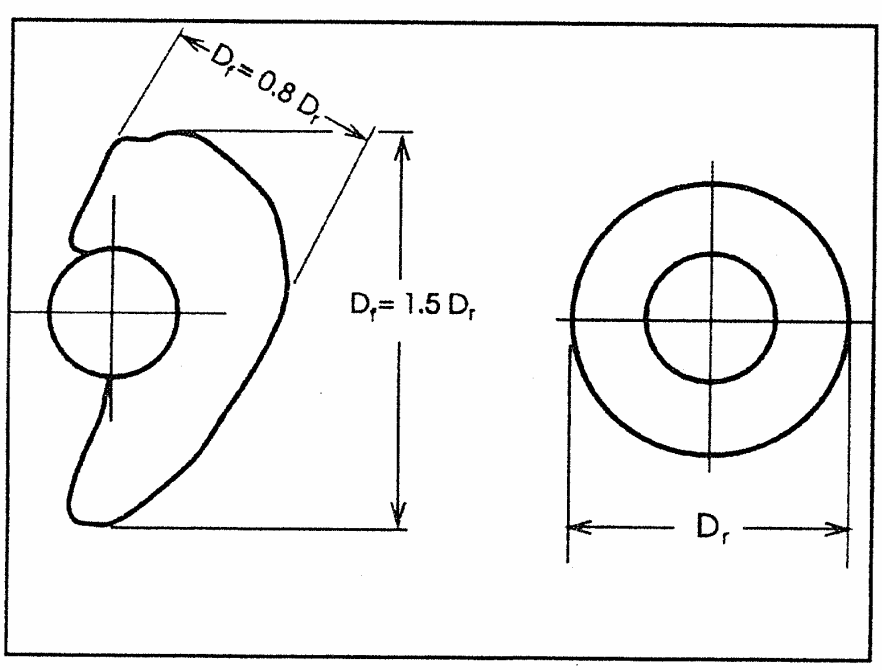

Figure 23: Observed ice accretion shape and circular accretion – Reference [15]

3.3.3.2 Modelling Ice Loads Including Ice-Shedding and Motion

A stochastic model based on droplet trajectory and random walk was used by Chen *et al.* [17] to estimate ice loads and include freezing probabilities, shedding and motion. The trajectory model determines the location of the impacting droplets whilst the random walk model predicts their motion along the surface.

For freezing rain, the terminal velocity V_T (in m/s) is obtained from Atlas *et al*. as:

$$V_T = 9.65 - 10.3 \cdot E^{-0.6d} \qquad (40)$$

where d is the droplet diameter in mm. This is obtained from the precipitation rate, P_r (mm/h) from Mason [18]:

$$d = P_r^{0.23} \qquad (41)$$

3.3.3.3 Ice Loads According to Conductor Diameter

Wareing [19] compared the Poots model and Admirat [20] data with field data from the EA Technology test site at Deadwater Fell. A semi-empirical expression was presented by Wareing to fit conductors from 5 to 40 mm diameter. The following expressions give ice mass per unit length, m, in terms of conductor diameter, D, (mm) as:

Poots $m = (0.243 + 1.792 \cdot D + 0.034 \cdot D^2) \cdot 10^{-3}$ [kg/m]

Wareing $m = 16.79 - 0.65 \cdot D + 0.055 \cdot D^2 - 0.007 \cdot D^3$

The Wareing expression is normalised for 10 mm radial ice and gave higher loads than Admirat for large conductors but consistently lower loads than Poots. Admirat includes an accretion efficiency factor, S, for wet snow adhesion to overhead line conductors.

$$S = \frac{0.038 \cdot T_a}{2 \cdot V \cdot D} \tag{42}$$

where T_a is the ambient temperature (°C) and V, the wind speed ($5 \leq V \leq 15$ m/s)

This expression implies increased accretion efficiency for small conductors.

3.3.3.4 Probabilistic Wind/Ice Loads

Savadjiev and Farzaneh [21] used a probabilistic model to deal with the joint occurrence of wind and ice loads on overhead line conductors. The wind speed associated with ice events $V(T)$ is given by:

$$V(T) = \kappa_{rw} \cdot V_{max}(T) \tag{43}$$

where V_{max} is the maximum annual wind speed for a given return period, T, and κ_{rw} is a reduction factor. Similarly, the ice thickness for combined wind/ice loads, $t(T)$, is given by:

$$t(T) = \kappa_{ri} \cdot t_{max}(T) \tag{44}$$

where t_{max} is the maximum annual ice thickness for a given return period, T and κ_{ri} is a reduction factor. In simulated experiments, this factor was found to be close to 1, no matter what time period was chosen. However, κ_{rw} was found to vary between 0.4 and 0.6 for a coefficient of variations of 0.7 to 1.3. For instance, the values of κ_{rw} for 20 and 500 year return periods are shown in Fig. 24.

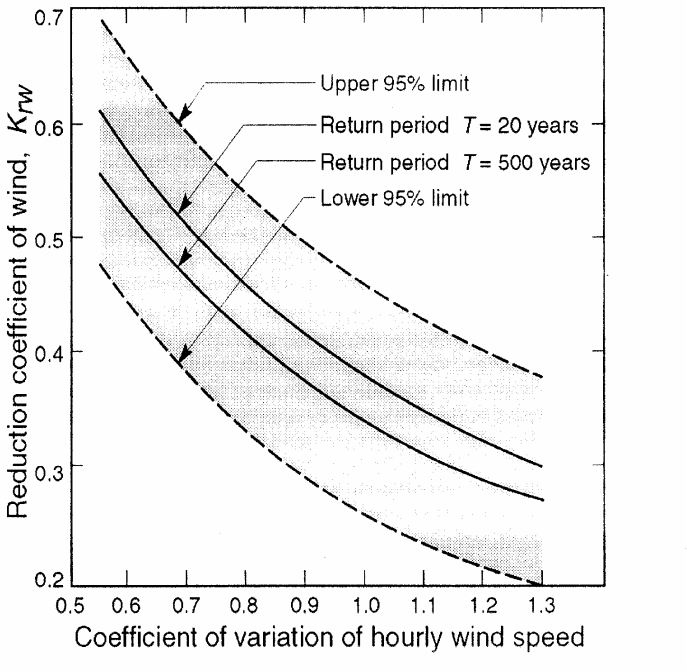

Figure 24: Reduction factor κ_{rw}

3.3.4 Wind Actions on Iced Conductors

3.3.4.1 General

Wind loads are usually calculated on a wind direction and projected surface area basis. However, the major differences between wind loads on bare and covered conductors are the envelope shape and the drag coefficient. These coefficients also vary with icing types which are here revealed according to the terminology of each of the following reference document.

3.3.4.2 Glaze Ice

Glaze ice is considered as a uniform deposit which tends to "smooth out" the surface of the iced object. IEC 60826 (Table 8) gives an effective drag coefficient of 1.0. For circular cross-sections up to 300 mm diameter, ISO 12494 (Tables 11-15) gives several values of coefficients with (C_i) and without (C_o) ice for various ice severities. These vary from an increase in drag for small coefficient values to a reduction in drag for large values of C_o. For large objects, the difference between C_o and C_i is reduced.

3.3.4.3 Rime Ice

IEC 60826 (Table 8) gives an effective drag coefficient of 1.2 for soft rime and 1.1 for hard rime. ISO 12494 relates rime ice drag coefficients to ice load (kg/m) and gives values for large and small objects (Tables 17-25). They follow a similar pattern to that for glaze icing. Objects which were initially smooth (circular rods or supports) would have a low C_o but the coefficient would increase when iced. For objects which were already rough to varying degrees (eg stranded conductors, fibre-wrapped conductors) the un-iced value of C_o would be high and icing actually **reduces** the drag coefficient.

3.3.4.4 Wet Snow

IEC 60826 (Table 8) gives an effective drag coefficient of 1.0 for wet snow accretion having a density of 600 kg/m^3.

3.3.4.5 Wind Direction

The above coefficients all assume a wind direction normal to the long axis of the object (e.g. normal to an overhead line conductor). If the wind is at angle, θ, to the line (θ = 90° for direction normal to the line) then the wind force:

$$F_N(\theta) = F_W(90°)\cdot\sin^2\theta \qquad (45)$$

3.3.5 Combined Wind and Ice Loads

3.3.5.1 IEC 60826

Statistics of wind during ice presence on conductors should ideally be used to generate the combined wind and ice loadings corresponding to the selected reliability level. However, such wind data is not usually available and it is generally accepted to deduce it from the yearly wind statistics. The yearly reference wind velocity is multiplied by a reduction factor as proposed by IEC 60826 as varying from 0.60 to 0.85. This range is assumed to correspond to the reference wind during icing persistence on conductors and takes into account the relative rarity of extreme wind during icing periods.

When combined data are available, statistical methods can be used to estimate values for combined variables corresponding to a selected return period or to the average of yearly extreme winds.

As an example of wind measurement in wet snow conditions, Fig. 25 shows the histogram of wind velocities (10-min average) during wet snow conditions in France, measured by Meteo-France [99] on 121 meteorological stations from 1984 to 2001. The data is divided in two categories, the wind velocities corresponding to low or high wet snow accretion risk, mainly depending on the precipitation level.

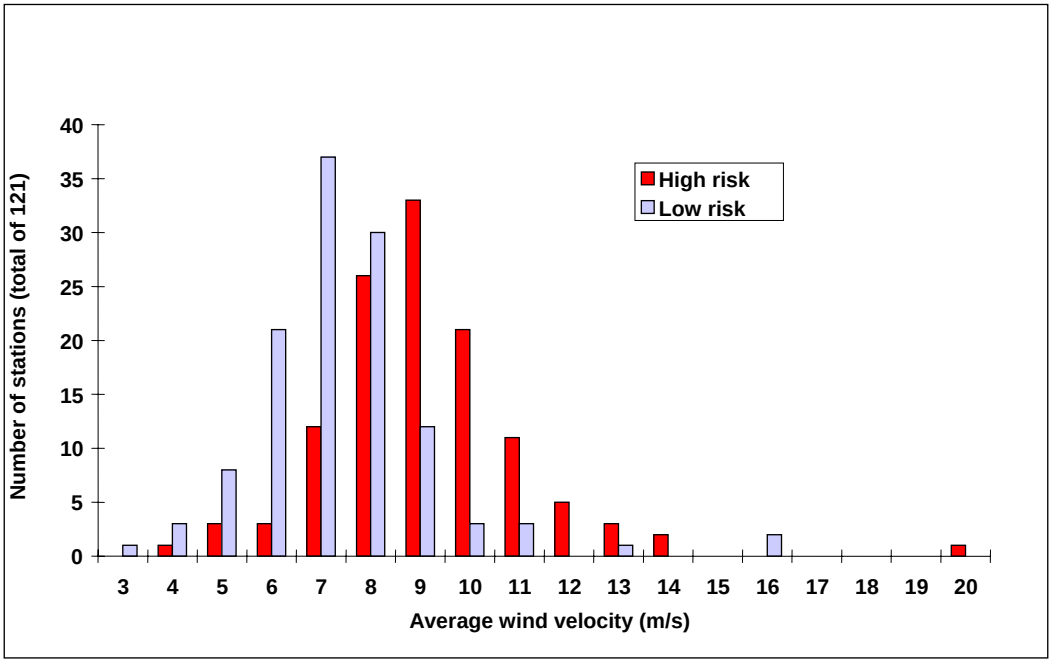

Figure 25: Average wind velocities corresponding to high or low wet snow risks (121 meteorological stations from 1984 to 2001)

The wind velocities corresponding to high wet snow accretion risks are slightly higher than those corresponding to low accretion risks. The observations and the results of the research program on wet snow accretion, jointly with Japan, show that the higher wet snow loads occur for wind velocities in the range 7-9 m/s. This value is a bit lower than the mean value of velocities measured in high risk conditions. The final choice was made to combine the maximum load (due to 7-9 m/s wind velocities) with wind pressures due to higher velocities, around 11-12 m/s (10% probability of being exceeded in wet snow conditions). This value is about 50% of the yearly reference wind velocity, which makes it a bit lower than the one recommended by IEC 60826 (60% to 85%).

3.3.5.2 ISO 12494

The wind at the time of accretion is often different from that after the accretion incident. It is therefore likely that wind-on-ice loads will increase after an icing event. The effect of this depends on the type of accretion. Historically, heavy ice accretion is often followed by high winds, whereas light icing is not. The opposite is the case for glaze icing, where melting often occurs before high winds become present. Wind force factors on glaze ice loads are therefore shown by ISO 12494 as varying from 0.4 to 0.6 for interstices from G1 to G5 (see Table 7 in this report) and 0.4 to 1.0 for R1 to R9 (see Table 8).

3.3.5.3 Peabody & Jones [22]

Peabody and Jones [22] developed a method of determining ice loads from glaze ice incidents with wind direction variations. Freezing rain striking a cylinder is assumed to accrete as ice with 100% efficiency.

The LWC and the velocity of the rain normal to the conductor surface are used to generate a uniform ice thickness value on a cylinder, *t*, as:

$$t = \frac{1}{\pi \cdot \rho} \sum_{i=1}^{N} W_i \cdot V_{d\,i} \cdot \Delta\tau_i \qquad (46)$$

where t is the uniform ice thickness
W is the LWC in g/m^3
$\Delta\tau$ is the time period
ρ is the ice density
V_d is the velocity of the rain normal to the conductor (m/s)
N is the number of time periods.

For a circular conductor normal to the wind, the factor $V_{d\,i}$ is replaced by $\sqrt{V_{fi}^2 + V_i^2}$ where V_f is the raindrop velocity and V the wind velocity. The LWC can be included as a simple expression from Best [23] where:

$$W = 0.067 \cdot P_r^{0.846} \qquad (47)$$

where P_r = precipitation rate in mm/h, and so:

$$V_f = 4.15 \cdot P_r^{0.154} \qquad (48)$$

The model allows for wind speed variation above local ground level by:

$$V = V_a \cdot (H_w / H_a)^{0.14} \qquad (49)$$

where V_a = wind speed at anemometer
H_w = wind height considered
H_a = height of anemometer

Peabody and Jones provide a Cartesian coordinate graphical representation to demonstrate how wind direction is incorporated (Fig. 26).

The raindrop velocity vector, *V*, is given by:

$$V = V_x + V_y - V_f\kappa \qquad (50)$$

$$V = -V_w \cdot \sin\theta - V_w \cdot \cos\theta - V_f\kappa \qquad (51)$$

where θ = wind direction
V_x = x component of wind speed
V_y = y component of wind speed

The paper gives example calculations for ice thickness against height above ground (Fig. 27) on a cylinder normal and parallel to the wind. The data used is:

Wind at 0 m	0 m/s
Wind at 10 m	5 m/s
Wind at 275 m	8 m/s
Precipitation	2 mm/h
Storm duration	24 h
Fall speed	4.6 m/s

LWC	0.12 g/m^3

At 10 m the radial ice thickness was:

horizontal normal	25 mm
horizontal parallel	17 mm
vertical	18 mm

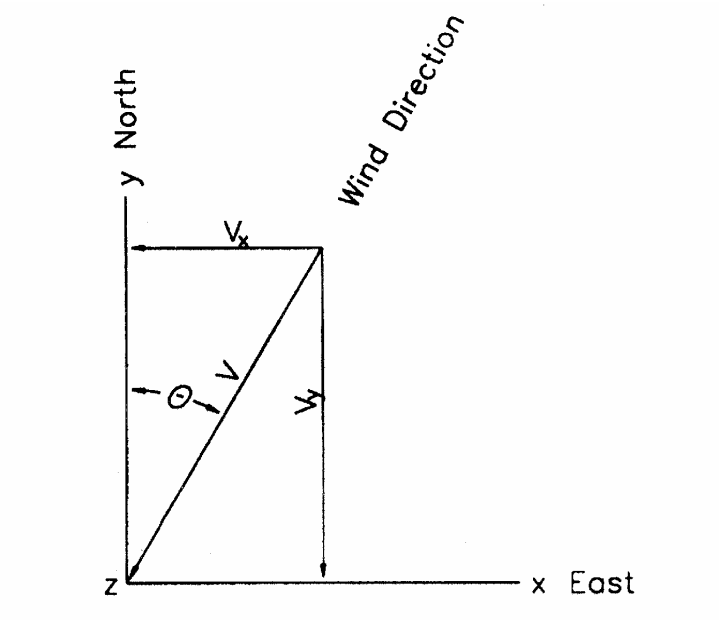

Figure 26: Cartesian coordinate system

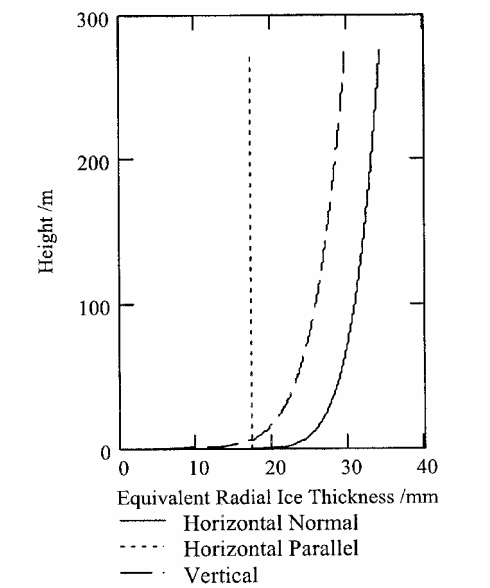

Figure 27: Ice thickness versus height

Figure 28 looks at the variation in accretion when the cylinder is parallel to the wind and then rotated along its long axis till it faces in the exact opposite direction. With the same data as before, there is zero accretion at 43° when the cylinder is parallel to the raindrop direction and at a maximum at 133° when it is normal to this. Examples are also given for flat plates.

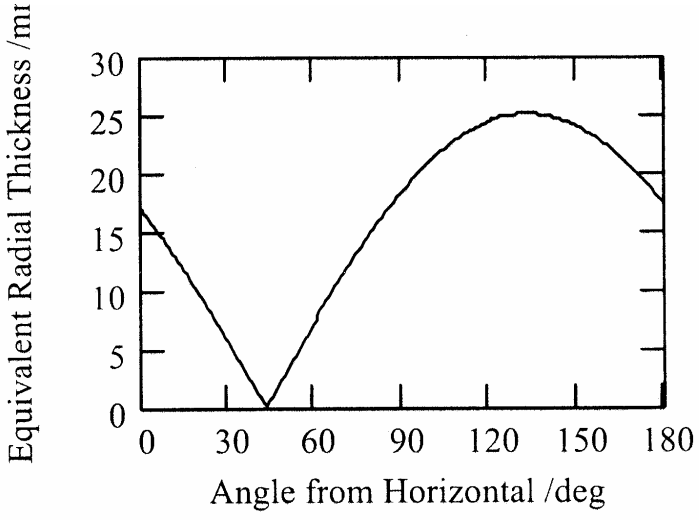

Figure 28: Cylinder parallel to wind

3.3.6 Accretion on Complex Shapes

Jones and Peabody [24] have applied standard icing conditions to determine the relative thickness of ice on structural sections. This can apply to towers, guy wires and conductors. Expressions are given for the mass per unit length on a non-round cross-section (Fig. 29) with perimeter p_o, and precipitation rate P_r:

$$(d + 2x)\cdot P_r \cdot \mathrm{d}T = \rho \cdot p(x) \cdot \mathrm{d}x \tag{52}$$

where ρ is the ice density and $p(x)$ the accretion envelope perimeter. This expression can be integrated over time to give:

$$\int_0^{\tau} \frac{P_r}{\rho} \cdot d\tau = \int_0^{t} \frac{p(x)}{d + 2\cdot x} \cdot dx \tag{53}$$

where t is the final uniform ice thickness at time τ. Similarly, the ice perimeter of an angle section of negligible material thickness (Fig. 30) made up of s outside and q inside 90° corners is given by:

$$p(x) = n\cdot L - 2\cdot q\cdot x + \frac{s}{2}\cdot \pi \cdot x \tag{54}$$

where L is the angle side length and n is number of sides of length L.

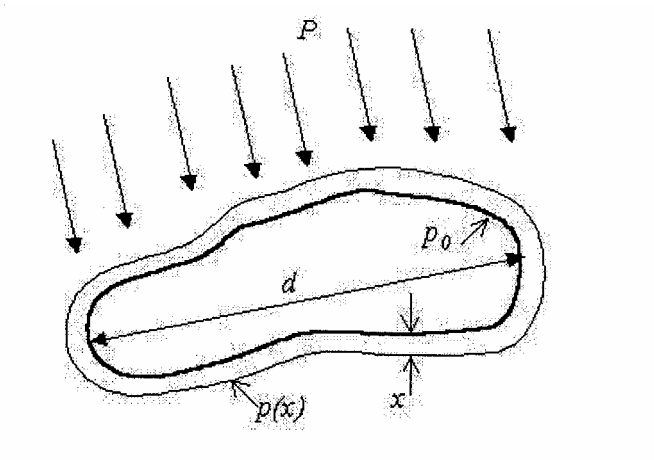

Figure 29: Freezing rain falling on a non-round cross-section with ice thickness *x*

If t_c is the uniform radial ice thickness on a cylinder from the total precipitation amount in Eq. (53), we may calculate the ice thickness that accretes on other cross sectional shapes in the same icing conditions. In particular, for an angle section, we find:

$$\pi \cdot t_c = \frac{t}{2}\left(\frac{s}{2}\cdot\pi - 2\cdot q\right) + \frac{L}{2}\left[n - \frac{1}{\sqrt{2}}\left(\frac{s}{2}\cdot\pi - 2\cdot q\right)\right]\ell n\left(\frac{\sqrt{2}\cdot t + L}{L}\right) \tag{55}$$

This transcendental equation cannot be solved analytically, but for a specified length *L* and shape given by *n*, *s* and *q*, Eq. (55) can be solved iteratively to determine the thickness *t* of the uniform layer of ice on this shape that is consistent with the uniform radial ice thickness t_c. Note that this ice thickness depends on *L*, although the uniform radial thickness does not. This happens because the shape of these objects changes as ice accretes, while a round cross section remains round.

The paper also considers squares, channel and I-beams.

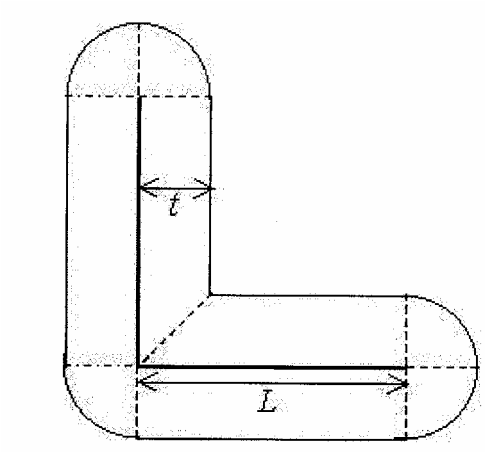

Figure 30: Ice thickness *t* on an angle section with legs of length *L*. There are four sides, five 90° outside corners, and one 90° inside corner.

3.3.7 Single and Bundled Conductors

Ice accretion loads on overhead earth wires and single and bundled phase conductors are of interest to transmission line engineers. McComber *et al.* [25] have measured ratios of ice accretion on these types of conductor. Although this paper is of field data, it can enable a transfer function for modelling single conductor loads to bundled conductors. At the Mt Valin test site the overhead earth (or ground) wire was 12.5 mm diameter steel (7.5 N/m), the single phase 35.1 mm diameter ACSR (21.4 N/m) and the bundle was a quad of the 35.1 mm ACSR spaced 406 mm apart. Other sites were also used (at Mt Bélair and Lake Lavoie) but only the Mt Valin test data is presented here. An analysis of 327 in-cloud and precipitation icing was done. The data varied widely (Fig. 31) for in-cloud rime icing but was more consistent (Fig. 32) for glaze icing. The average ground/single ratio was 1.27 and bundle/single ratio 0.83 (per conductor of the bundle) for in-cloud icing and 1.01 and 0.86 for glaze icing.

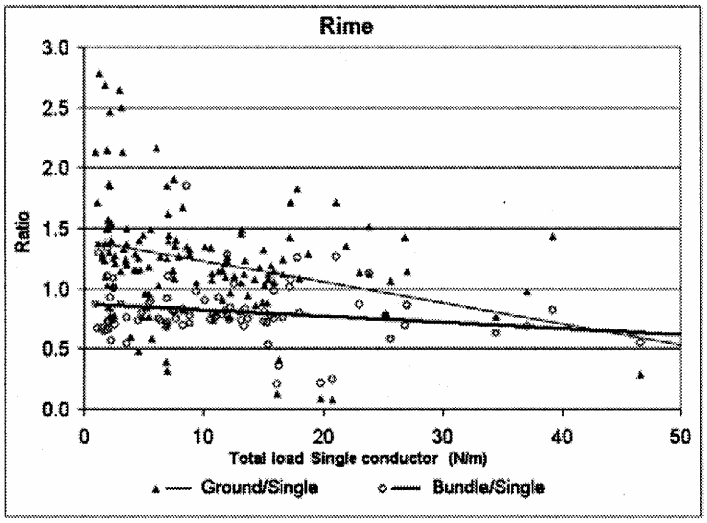

Figure 31: Ice load ratios for in-cloud icing events (231)

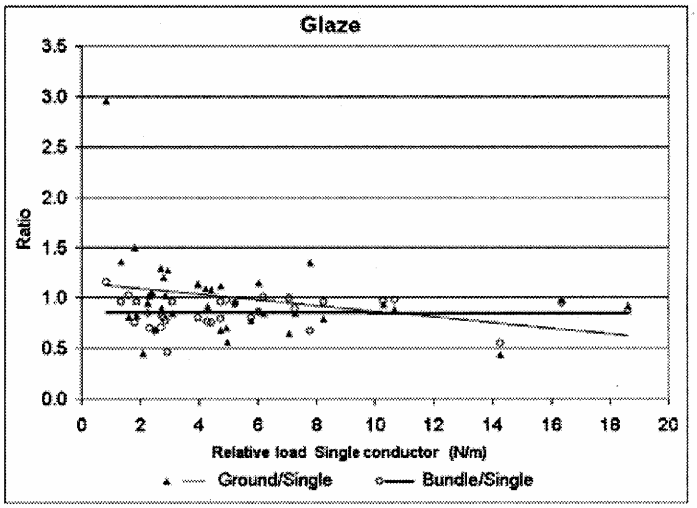

Figure 32: Ice load ratios for freezing rain events (71)

Higher ratios were obtained for small loads in both cases – although more markedly for the in-cloud icing. The full results from Mt Valin are given in Table 9.

Table 9: Average and standard deviation (SD) for ice load ratios – Results from Mt Valin

	In-Cloud Rime		Glaze	
	Average	**SD**	**Average**	**SD**
Ground/Single	1.27	0.43	1.01	0.42
Bundle/Single	0.83	0.29	0.86	0.14
Ground/Bundle	1.51	0.51	1.24	0.5

3.3.8 Data Needed for Ice Load Assessment

The basic meteorological data required to model an icing process depends on the accretion type and includes:

a) Wind speed
b) Wind direction (relative to structure)
c) Air temperature
d) Precipitation rate
e) LWC
f) Droplet size
g) Relative humidity
h) Air pressure
i) Visibility

An example was given in Section 3.2.1.3 for 3 icing models. Droplet size is difficult to measure and may have to be neglected. Visibility is useful for in-cloud icing.

3.4 Icing Climatology

3.4.1 General

Atmospheric icing occurs basically in all parts of the world where temperatures near freezing appear together with precipitation or low clouds (fog). It is outside the scope of this report to describe in details where the different icing types (in-cloud, wet or dry snow and freezing rain) can take place, and at which frequencies and intensities they may occur. It is however important to be aware of the risks for icing whenever new overhead lines, wind turbines, skilifts or other structures are planned in higher or more exposed areas than where earlier infrastructure components have been in operation for many years with no experience of icing related damage.

Traditionally, atmospheric icing has been taken as a phenomenon belonging to the northernmost regions of the Earth, such as Canada, Japan, Russia, the Nordic countries and central Europe. However, there are many reports of icing in southern France, Spain, Algeria, South Africa and Latin America as well. For most of these countries wet snow and rime icing are the most common icing types.

The frequencies and intensities of such icing depend strongly on the geographical location, with respect to direction and distance to the oceans, as well as on the local topography. Each country or region is recommended to evaluate their own risks depending on these factors. One good example from Japan is given in section 3.4.2 below. Other countries, especially Russia and many European countries have similar descriptions, see for instance [3], [28], [38], [42], [43] [46], and [50].

Within the current COST collaboration in Europe, the Action 727 "Measuring and Forecasting Atmospheric Icing on Structures" started in 2004 to investigate icing models, measuring technologies and data availability for icing in Europe, see http://www.ufa.cas.cz/cost727/index.html. The objective for the current 11 participating countries is to establish models for forecasting of icing and also establish relevant icing maps for Europe.

3.4.2 Icing Conditions in Japan

The Japanese archipelago is situated from 24 degrees N latitude to 46 degrees N latitude, running from north to south. On the north and south sides of the archipelago the ocean spreads out and the huge Asian Continent is on the north side. There are various precipitation types and diverse ice accretion phenomena in winter in Japan, because the archipelago is strongly influenced by these factors.

Glaze from freezing rain can be mainly observed in two phenomena: One phenomenon is generated in the comparatively stabilized state of the atmosphere in a ravine and a basin area between mountains. The rain comes down over the air cooled by the low temperature in the mountains, flows down to a low-lying area to form a cold basin, becomes supercooled and freeze into glaze.

When an extratropical cyclone produced by the meandering cold air in the Arctic Circle during winter to early spring passes Japan, warm air rises up over the cold air in the front of the warm front accompanying the cyclone, a temperature inversion layer is formed where snowflakes falling from the upper clouds melt and are supercooled when they pass through a layer with a temperature of 0°C or less near the surface of the earth, and the second phenomenon occurs. However, since the duration is generally short, the ice accretion load produced is comparatively small and smaller than that resulting from snow accretion mentioned later. Therefore, excepting the small amount of glaze resulting in galloping, no severe influence on a power line is experienced.

Depending on the latitude, in-cloud icing typically appears only at places that are directly exposed to clouds formed by wet air from the ocean that goes up along a mountain slope at an altitude of more than 700-800 m. Especially, warm currents flow from the sea in northern Japan, and moisture is supplied to monsoons blowing toward the Pacific Ocean in winter from the Asian Continent. Since the humid air is forced to rise along a mountain slope, supercooled clouds are produced and in-cloud icing occurs. In the central part of the Japanese archipelago, the mountain range where the altitude is comparatively high is located like a backbone, and there are flatlands along both sea sides. Since power lines that connect the flatlands go through the mountains, in-cloud icing can be frequently experienced. In addition, some of the power lines have had in-cloud icing on the southeast slope from the southeast wind produced by the low pressure which passes the northern ocean side. In Japan, although mainly soft rime ice accretion is seen, hard rime and glaze ice accretion can also be observed. The power lines in the areas with ice accretion are specifically designed by the load defined according to the method of IEC 61774 (1977) [2] based on short-term (more than about 5 years) observations.

Snow accretion occurs all over Japan excluding the islands in the south. The characteristics of snow accretion change over a large range with the weather conditions when it forms. Both density and adherence are low in snow accretion (dry) that takes place at lower than 0°C with a weak wind. Especially, snow accretion may greatly develop over a long time in a heavy snowfall area with low height above ground on the north side of the mountains and protected from wind. The snow accretion drops out all at once. Then, a conductor may jump and short-circuit of lines occurs.

Snow accretion generated at 0°C or higher is generically named wet snow accretion, and the characteristics change over a large range depending on temperature and wind velocity (or moisture content of snowflakes and snow accretion). Generally, if the wind velocity is high, density and adherence become high.

Winter weather in Japan varies remarkably between south and north of the mountains that form the backbone of the archipelago. On the north side, a lot of snow falls in winter from monsoons that blow across the sea where the warm current flows from the Asian Continent as mentioned above, and dry snow accretion occurs with a comparatively weak wind. On the contrary, on the Pacific Ocean side area, there are many fine days in winter because the monsoon is interrupted by the mountain range, and there is little precipitation.

However, harsh snow accretion loads on power lines have primarily been experienced on the Pacific Ocean side. This is because, accumulated precipitation is high but precipitation intensity is low in winter on the Continent side, while the precipitation intensity from the above-mentioned extratropical cyclone is high on the Pacific Ocean side. Commonly, the progress speed of this extratropical cyclone is comparatively fast, the duration of precipitation is short and the snow accretion load is not very large. However, when an extratropical cyclone is blocked by a high pressure in the North Pacific, this high precipitation intensity continues for a long time, and ends with harsh results. Since these phenomena quite rarely bring very high loads which do not conform to a normal extreme-value distribution (Gumbel distribution), the problem is left to measure them. Moreover, in particular, unequal loads caused by galloping from snow accretion at a wind velocity of 10 m/s, and considerable snow accretion sporadically falling on the span or phase, result in accidents.

3.4.3 Variability in Climate

As it is a current general scientific consensus that the global climate has changed more rapidly over the last 20-50 years than previously seen from historical records, and that global climate studies indicate a continued and enhanced development in similar directions, many countries and utilities question the consequences for atmospheric icing on their infrastructures in the future. Such considerations are partly included in the studies of the international project “Arctic Climate Impact Assessment” (ACIA) (www.acia.uaf.edu). A summary report of the first part was published in 2004 [100]. ACIA has not yet concluded on infrastructure, but the considerations below seem to be relevant.

A global temperature increase will be higher in northern areas (roughly north of 60°N) than nearer the equator. A higher temperature of the atmosphere will necessarily lead to higher water vapour content of the lower atmosphere. This means that there is a risk for both higher precipitation rates and liquid water contents in clouds. Combined with near freezing temperatures this may lead to more frequent and more intense icing in some areas. The general pattern is however complicated :

- In coastal areas which generally have winter temperatures a few degrees above freezing, wet snow may occur more seldom in the future. An exception may be high coastal mountains where near freezing temperatures still may occur frequently.
- In inland areas where winter temperatures are generally well below freezing, the risk of wet snow may increase, both with respect to frequency and intensity, at all elevations.
- In mountain areas the freezing level will be at higher elevations and the risk of in-cloud icing will consequently decrease in parts of mountains below this level. Above the freezing level rime icing may occur more often and with higher intensities. Wet snow may be more frequent and intense in all levels from near the freezing level.
- Freezing rain is more complex to evaluate. This is probably depending mostly of the supply of cold air for the formation of sub-freezing inversion layers. It should be noted however, that although there has been a general warming of the circumpolar air over the last 50 years, it has been a cooling of roughly 1°C during winter months over southwest Greenland, Labrador and

Newfoundland (December – February, 1954 – 2003) [100]. This *may* increase the risk for freezing rain in these areas.

The risk of wet snow accretion may be identified following a criteria based on standard meteorological parameters: minimum daily temperature between –4°C and +0.5°C, maximum daily temperature between –0.5°C and +5°C and daily precipitation level bigger than 10 mm. This criteria has been used in a study of the impact of climate evolution on accretion risks in France with two atmospheric simulation codes : Arpege-Climat (Meteo-France) and LMDZ (Centre National pour la Recherche Scientifique – Institut Pierre Simon Laplace). This study is a part of a larger French project (IMFREX) aimed at assessing the evolution of risks of extreme winds, temperatures and precipitation in France, storms in Atlantic Europe, cyclones in North Atlantic.

Concerning the wet snow accretion risk, the previous meteorological criteria has been applied to the simulation of actual climate with Arpege-Climat (40 years simulation) and LMDZ (30 years simulation) to compare the simulated risks to the observations. The behaviour of both models in the identification of the risk zones is realistic, particularly for Arpege-Climat whose resolution on France (50 km) is more precise than LMDZ (150 km in these simulations). Arpege-Climat slightly overestimates the frequencies of wet snow events, but the simulation of high daily mean precipitation levels on Eastern Pyrenees follows the observations (this particularity was at the origin of major damages on transmission lines in this area). As the resolution of LMDZ is less precise, the description of Mountain areas is less convenient.

In a simulated climate for the end of the 21st century (evolution of greenhouse gas following the “high emission” scenario A2 of IPCC), Arpege-Climat shows a restriction of the wet snow risk zones, as well as a lower frequency of meteorological conditions favourable to wet snow. The same result is also obtained with LMDZ, on the only zone in which the resolution is correct enough for a realistic description. The results obtained on the daily mean precipitation levels are not convergent, so that is difficult to assess the evolution of the intensity of events.

Finally there is a discussion on changes in wind climate. This is not as clear as for temperature. If the frequency and magnitude of wind storms will increase (in northern latitudes), then the probability of high combinations of wind and ice may increase in areas where icing frequencies increase.

4. STATISTICAL METHODS

4.1 Extreme Distributions of Icing Events

Atmospheric icing will have a great variability when measured at one location. Figure 33 shows annual maxima (and running 5-year mean values) from the longest homogeneous time series of ice measurements in the world, on the top of Studnice Mountain (800 m above sea level) in Czech Republic [33]. This test site represents nearly 60 years of continuous measurements and is fortunately still in operation.

This figure clearly shows that the design ice loads based on data from the 1950 - 60's would be quite different from those selected from the 70's and 80's. Furthermore, it is interesting to notice the development through the last decade of the 20th century. It is relevant to ask whether this dramatic increase of ice accretion is related to the parallel increase of atmospheric temperature in the same decade. This underlines the importance of careful awareness regarding ice accretions in the future, especially in the light of possible global warming which will lead to higher atmospheric humidity.

The most important conclusion from this figure is that it is more important than ever to monitor ice accretions and ice loads for power utilities in all countries where damage cost due to ice loads is high. Such time series of observations may be long, costly and difficult to obtain but are of great value for obtaining statistically reliable distributions of ice loads.

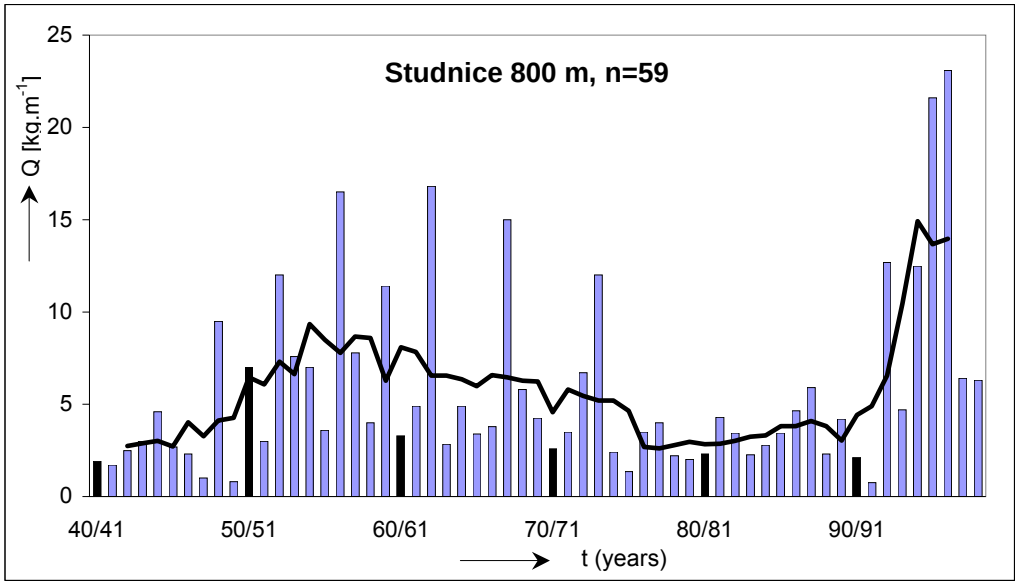

Figure 33: Ice load measurements from Studnice 1940 – 1999

4.1.1 Extreme Value Analysis of Data for Ice Loads

4.1.1.1 Background

Statistical analysis of icing data is important in all stages of overhead power network planning, design, construction and operation. The need of a large amount of available, reliable, and pertinent data containing historical information for icing events is increasing continuously, after probabilistic methods have been almost universally adopted in transmission line design. Extreme value analysis and its

application in engineering was introduced mainly by Gumbel [29], and since, many important advances in theory development have been published. These theories, used as statistical tools for design purposes, are now largely spread between designers of transmission lines. Nevertheless, for estimating meteorological design loads, long time series of observations should be analyzed for obtaining statistically reliable distributions for extreme value analysis. While such data bases for wind are relatively readily available, collecting data for icing is a costly and time consuming process.

Section 4.1.1 provides an overview of the methods for collecting icing field data, and the practice of the extreme value analysis.

4.1.1.2 Collecting Field Ice Data

There exist different means to obtain field information for icing events. These means differ mainly by the sources of information, the methods of observation and measuring, the type, contain, and length of time series in the database.

Sources of Information:

a) National weather services – data from operation of standard meteorological stations

b) Electrical facilities:
   - Previous operational experience from overhead line networks in icing exposed areas. This is perhaps the most important source of pertinent icing information for planning future lines or upgrading old ones in the concerned area.
   - Direct measurements on samples fallen on the ground or accessible non-energized line conductors or ground wires.
   - Field observations of the effect of icing on vegetation or on the neighboring distribution or telecommunication lines.
   - From especially designed measuring devices such as the Passive Ice Meter (Fig. 35, [27]) used in Quebec for freezing rain measurements, or tubular steel-rod racks as those used in Norway (Figs. 36a and 36b, [26, 28, 35]) or in the Czech Republic [33].
   - Using test spans or permanently instrumented test sections of line spans out of service.
   - Indirect icing measurements on permanently instrumented transmission lines in service.

An example of a registration of icing events on overhead power lines is the “IceDat” database [46]. The database contains information from more than 20 years continuous systematic acquisition of field icing data in Iceland, in addition to random reports of icing events dating back to 1930. The database contains more than 3000 reports grouped in more than 500 icing episodes (see Fig. 34).

4.1.1.2.1 Passive Ice Meter

The Passive Ice Meter (PIM), sketched on Fig. 35, is a simple, robust and useful instrument, designed mainly for measuring precipitation icing accumulation. Usually, it is placed 1.2 m above ground, and its metallic receiving cylinders are oriented N – S and E – W.

A network of more than 170 PIMs has been established throughout Quebec since 1974 within a grid dimension of about 50 km. A detailed description of the PIM performance and technical characteristics, as well as usefulness of the recorded data for extreme value analysis and transmission line design, may be found in [32]. In CIGELE, statistical data from the PIM network was used for establishing the averaged distributions of (i) Annual Number of Icing Event Recurrence, (ii) Icing Event Residency Period, and (iii) Annual Duration of Icing Events. These distributions are important for determining statistics based return periods for the wind speed associated with icing events in combined wind and ice load calculations.

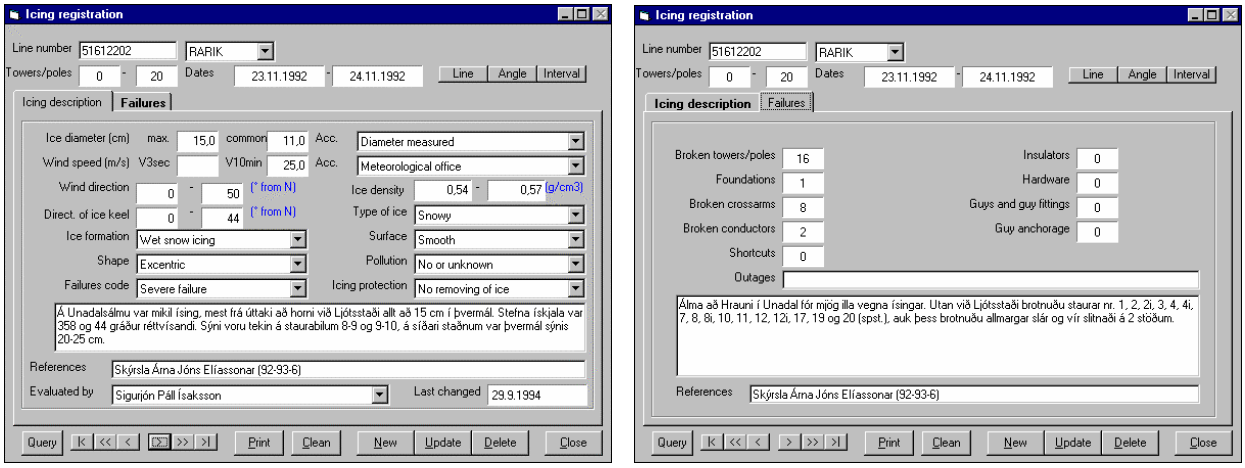

a) **b)**

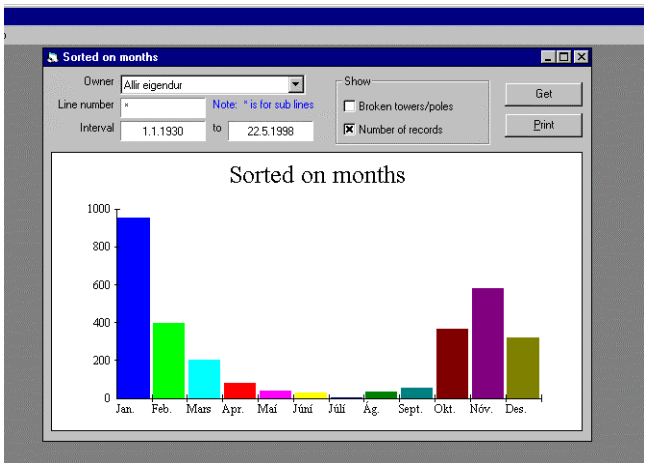

c)

Figure 34: Description windows of the "IceDat" database for **a)** icing events, **b)** failures and **c)** the distribution of icing records within the year

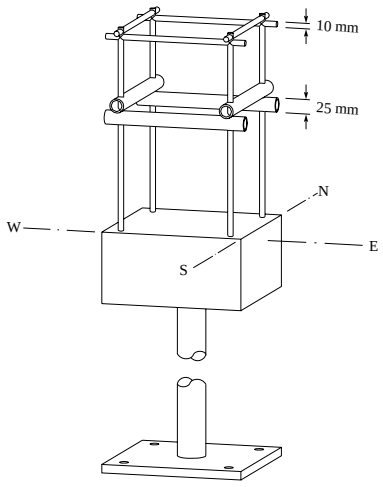

Figure 35: Passive Ice Meter

4.1.1.2.2 Icing Test Tubular Rod Racks

The icing test racks used in Norway are outlined in Figs. 36a and 36b. A 10.5-m long horizontal rod, 55 mm in diameter, is suspended 5 m above ground on a dynamometer, recording mechanically the maximum load since previous resetting. A set of dampers is installed for absorbing vibrations due to wind. Some of the racks are in addition equipped with electronic load cells that record the loads every 3 hours on a local logger. A more detailed description of these facilities, their instrumentation and maintenance may be found in [26] and [28]. Some of the test stations contain two or three racks in a group installed either at 90° to study the effect of local wind directions, or at another position to study small-scale topographical effects. Most stations were erected during the period 1978-1995 and are situated in the vicinity of existing or to-be-built high voltage line routes.

The remote locations and extreme exposures of these stations make it difficult to access them and monitor their behavior. Most of them can only be reached by helicopter, hence they have been inspected in general only every summer although mid-winter dynamometer readings have been accomplished in most years on the most important stations. However, it is obviously only occasionally that the racks can be observed with significant ice amounts. In particular, during extreme events there were no possibilities to check the measured loads (see Fig. 36b).

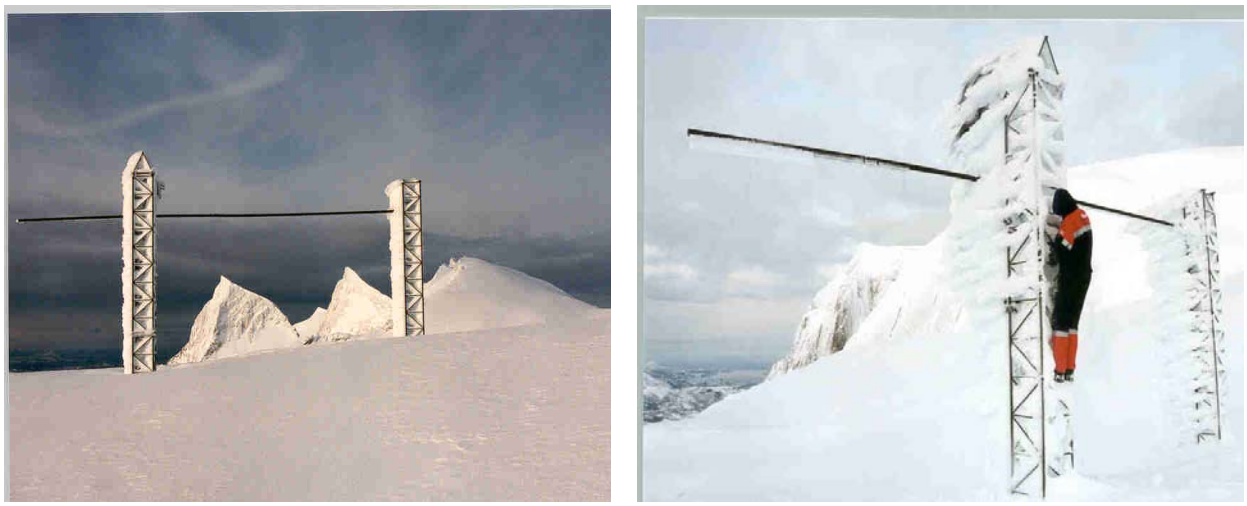

a) **b)**

Figure 36: Tubular rod rack test station in Norway

4.1.1.2.3 Indirect Icing Measurements on Permanently Instrumented Transmission Lines in Service

In Québec, a program for studying atmospheric icing and its impact on the power networks has been in progress since 1994. A warning and monitoring system, SYGIVRE, installed by Hydro-Québec, numbers now more than 30 icing measurement stations throughout the province. Most of these stations are instrumented with a modern measurement equipment furnishing real-time meteorological information available to users via satellite (Figs. 37a and 37b [36]) which consists of the following:

- an improved, recent-variant, Ice Rate Meter;
- load cell;
- electrically-heated anemometers;
- hygroscopic/ambient temperature probe;
- electrically-heated precipitation gauge.

4.1.1.2.4 Ice Rate Meter (IRM)

An IRM, developed for rime detection and accretion rate measurement, consists of a vertical, 25.4 mm long cylindrical probe, situated at the top of the instrument (Fig. 37b). When ice accretes to the probe, the frequency of 40 kHz, at which the probe is excited to vibrate, decreases at rate of about 2 Hz for each mg accreted mass. After an accretion of 60-65 mg, an electronic controller heats and deices the probe, and thus completes a cycle recorded by a cumulative counter. The hourly number of cycles, or IRM signals, can be used as a warning alarm, but also as an indirect measure of icing rate in the surrounding atmosphere. However, using the IRM for the purpose of collecting statistical data for extreme value analysis or design necessitates establishing a correlation between the hourly number of IRM signals and the actual icing accumulation rate on neighboring transmission line components – conductors, insulators, or structures. For this purpose, the measurement of the actual icing accumulation is given by load cells. More details on this may be found in [37].

4.1.1.2.5 Load Cell

Load cells are incorporated into the attachment point of a suspension insulator string [85, 86, 87] supporting one of the conductors of the instrumented line (Fig. 37a). Its readings (in volts) are proportional to the axial insulator force, and can be used for assessing the ice mass or hourly icing rate per unit length of conductor.

In Iceland, a system of nearly 40 measuring sites are operated [47]. Each site has one, two or three test spans, in a straight line, at right angles or in a triangle (see Fig. 39). The spans are standardised, being 80 m long and strung on poles 10 m high. In most cases the type of conductor in use is AAAC 28,1 mm. The spans are instrumented with data loggers for load cells and air temperature recorders (see Fig. 38). In some instances more weather parameters are measured. The first test span was built in 1972, and more than half of the sites have been in operation for more than 20 years.

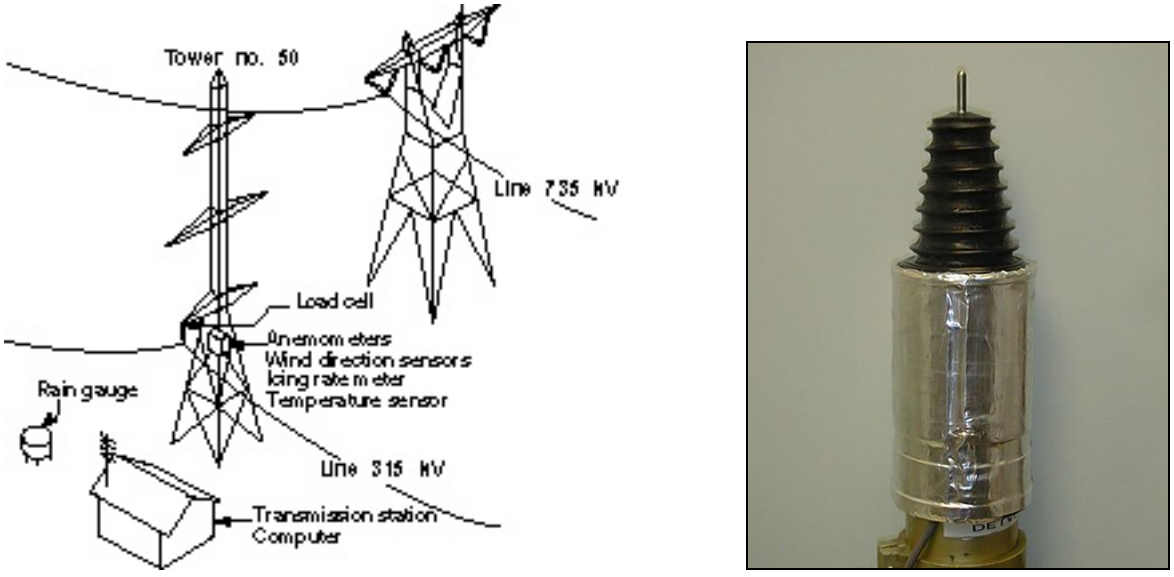

a) **b)**

Figure 37: **a)** Sketch of the Mont Bélair icing test site and measuring equipment; **b)** Ice Rate Meter

Figure 38: Top of an instumented pole in a test span

Figure 39: Iced test span in Iceland

4.1.1.3 Extreme Value Analysis

4.1.1.3.1 Distributions of Largest Extremes

Distributions of largest extremes depend on the behavior of the initial distribution at large values of the variable. The statistical theory of extremes shows that there exist three different asymptotic distributions for largest extremes [29].

The first asymptotic distribution of type I, Gumbel distribution, holds for largest extremes coming from a large class of initial distributions of exponential type – exponential, largest extremes of type I, normal,

lognormal, Weibull, gamma, etc. For the random variable ice radial thickness on transmission line conductors, *t*, this asymptotic distribution is given by the following relationship:

$$\Phi(t) = exp\left\{ - exp\left[- \frac{c_1}{\sigma_t} \cdot \left(t - \bar{t} + \frac{c_2}{c_1} \cdot \sigma_t \right) \right] \right\} \tag{56}$$

where $\bar{t}$ and σ_t are the mean and standard deviation of the annual maxima, respectively; c_1 and c_2 are constants depending on the number of years of observation *N*. For $N \cong \infty$, $c_1 \approx 1.28255$ and $c_2 \approx 0.5772$.

In general, σ_t has the same value as, or near, the standard deviation of the initial distribution, and $\bar{t}$ increases as the logarithm of the size *n* of the annual samples; The same distribution may be used for the ice mass per unit length of conductor, *m*, if this variable is chosen as representative parameter for icing amount.

Design values for *t*, with respect to the prescribed return period *T*, can be calculated by inversing (56):

$$t(T) = \bar{t} - \frac{c_2}{c_1} \cdot \sigma_t + \frac{\sigma_t}{c_1} \left\{ - \mathrm{Ln} \left[- \mathrm{Ln} \left(1 - \frac{1}{T} \right) \right] \right\} \tag{57}$$

For instance, extreme value analysis for a 20-year series of annual maxima of ice thickness of exponential type is shown in a Gumbel probability chart (Fig. 40). There are also shown the 68% and 95% confidence limits for estimating the ice thickness with a given return period [1, 29, 35].

The second asymptotic distribution or, of type II, holds for Cauchy or Pareto type – long-tailed and unlimited to the right – initial distributions.

The third asymptotic distribution or, of type III, holds for initial distributions which are bounded toward the largest values. Both type II and type III asymptotic distributions are rarely used for extreme value analysis of icing, wind or combined loads on overhead transmission lines [1, 35].

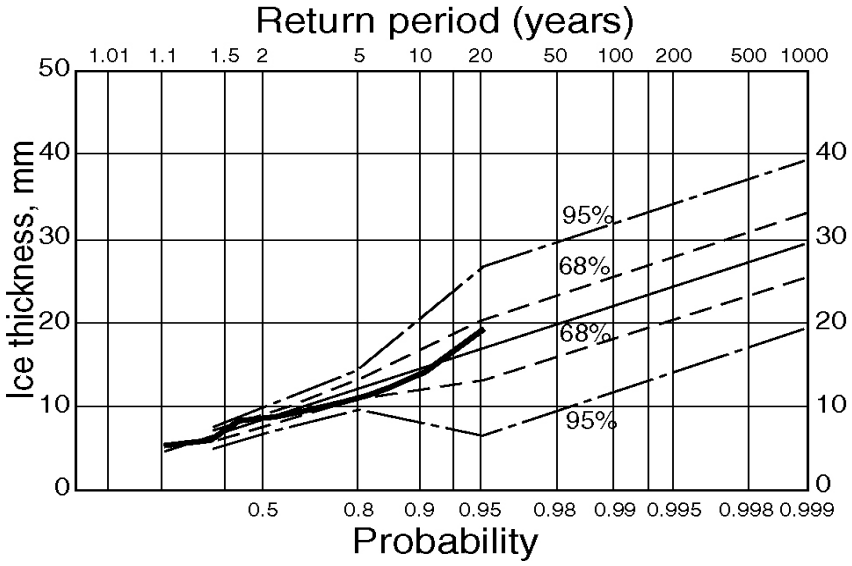

Figure 40: Gumbel probability chart for estimating ice thickness with a given return period

4.1.1.3.2 Initial (Parent) Distribution

The majority of initial distributions of icing amount – radial thickness or unit mass, are of the exponential type. In general, they may be best described by the Weibull two-parametric law, or by the Exponential or Gamma distributions which, besides, are identical to the Weibull distribution for a coefficient of variation (COV) equal to 1. The Gumbel and the Normal distributions are not always adequate for describing initial icing distributions because they are unbounded toward the left tail, i.e. toward negative values. The Weibull distribution is given by the following formula:

$$F_i(t) = 1 - exp\left[-\left(\frac{t}{c} \right)^k \right] \tag{58}$$

where c and k are the scale and shape parameters, respectively.

Various probability density functions of the Weibull distribution with mean $\bar{t}$ = 3 mm and coefficient of variation (COV) from 0.8 to 1.7, are shown in Fig. 41.

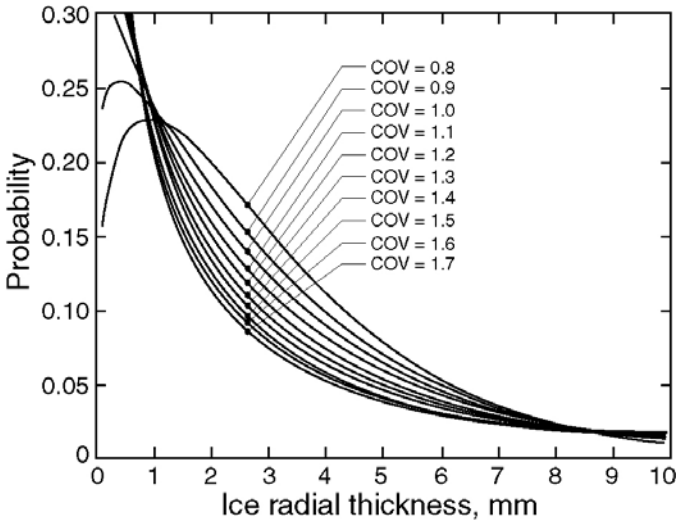

Figure 41: Weibull probability density functions for ice thickness $\bar{t}$ = 3 mm, and various COV

4.1.1.3.3 Convergence of Icing Annual Maxima of Exponential Type Toward the Gumbel Asymptotic Distribution of Type I

As mentioned above, collecting icing data is difficult, costly and time consuming process. There are rarely available time series of icing data longer than 10-20 years. For instance, the data base from the Norwegian rack network contains time series of 4 to 21 years [35]. The average number of years of observation, for the Hydro-Québec Passive Ice Meter Network, is 16 years [27], and much shorter for the recent system SYGIVRE. As a world longest continuous time series, for annual maxima of ice thickness, can be indicated that in Studnice, Czech Republic, where icing measurements on tubular rod rack have been performed since 1941 [33] (see Fig. 33). Such long-time series of icing observations are of great scientific and practical interest. They allow for a better understanding the variations of the climate during the last decades.

The convergence toward the Gumbel distribution of icing annual maxima coming from initial distributions of exponential type was studied in [34] using computer-performed numerical simulations. The minimal number of years of observation N_c, for which the variations of the extrapolated 500-year ice thickness, $t(500)$, are stabilized into the 68% confidence band limits was used as an estimate of the rapidity of convergence toward the asymptotic Gumbel distribution (Fig. 42, [34]). The width of the 68% confidence band, which is almost independent from the number of years of observation N [29], was evaluated for convenience for N = 200 years. The results from these simulations are shown in Fig. 38, for Weibull initial distributions with various COV, and in Table 10, for four different initial distributions of exponential type.

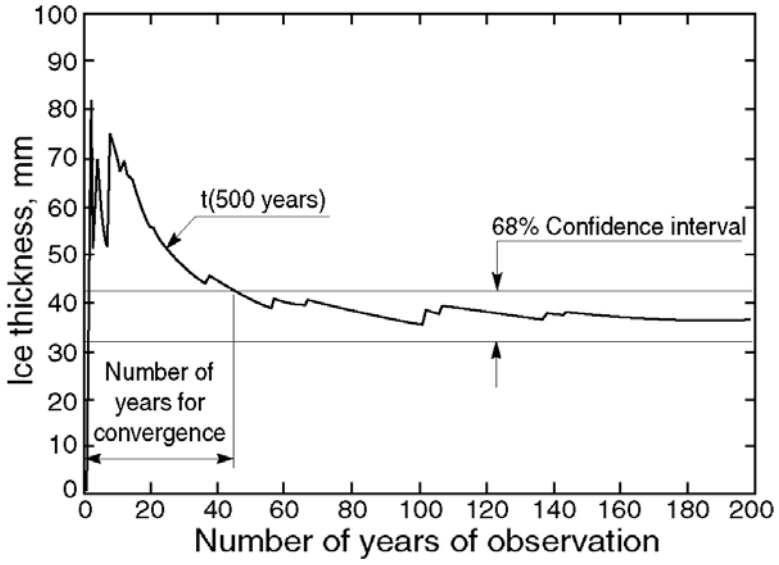

Figure 42: Typical convergence of 500-year return period ice thickness, $t(500)$, toward the asymptotic Gumbel distribution

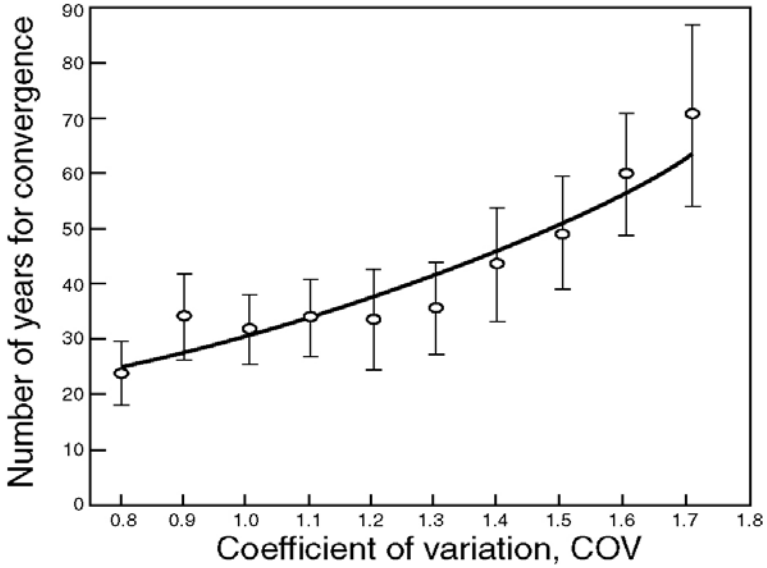

Figure 43: Convergence of annual maxima of ice thickness from Weibull initial distributions with different COV toward the asymptotic Gumbel distribution

Table 10: Averaged number of years for convergence, N_c

COV	Initial (parent) distribution of ice thickness			
	Gumbel	Gamma	Weibull	Lognormal
0.8	24	27	25	44
0.9	25	28	28	48
1.0	26	29	31	52
1.1	28	31	34	56
1.2	29	32	38	61
1.3	30	33	42	66
1.4	31	35	46	71
1.5	32	37	52	77
1.6	34	40	57	84
1.7	35	43	64	91
Mean:	30 ± 3	32 ± 4	42 ± 10	65 ± 12

4.1.1.3.4 Tests for Acceptance or Rejection of Aberrant Members of the Time Series

Given the limited possibility of visual or video inspection of most of the stations because of their distant location, high altitude or very severe climatic conditions during winter season (Fig. 36b), some suspiciously or aberrantly large annual maxima not consistent with the remaining data should be tested for acceptance or rejection from the studied time series. These tests should begin with the screening of data and the exclusion of outliers for various reasons: recording mistakes, inadequate measurements, interpretation difficulties, etc.

The fitting of the empirical data for annual maxima of icing with the Gumbel distribution is not always satisfactory enough. The great variability of the empirical measurement data, the relatively small number of years of observation available [35], and the presence of an aberrantly large measurement, non-coherent with the other members of the time series, have the following consequences: (i) the observation data plotted on Gumbel probability paper do not approach a straight line; and (ii) the 95%, and even the 68% confidence intervals become uselessly wide. Current, but non-correct practice in this case is to seek for another distribution fitting better the empirical data. It should be clear that, for a time series with a small number of years of observation, what is currently the case for icing data, the classical χ^2 or Kolmogorov's test for goodness of fit are not applicable. The goodness of fit may be estimated only visually on probability paper. For these reasons, the following recommendations can be done for a statistically correct solution:

1. Using the theoretically justified Gumbel asymptotical distribution of type I. The use of the asymptotical largest value distribution of type II is justified only if it is established that the initial icing amount distribution is of Cauchy's or Pareto's types.
2. Using tests for acceptance or rejection of aberrant data for annual maxima. Two very simple tests, giving almost similar results, may be recommended.
   - The first consists of checking if the plotting position of a suspiciously aberrant annual maximum lies out of the 95% confidence interval constructed for the truncated series after eliminating the suspected maximum.
   - In the second method, the observed return period $T_o = n$ of the largest value, G_n, in a sample of n observations, is compared with the theoretical return period T_t of the same annual maximum, but determined by the theoretical straight line [27, 29]. If the theoretical return period $T_t > 2 \cdot T_o$, the largest maximum is rejected; if not, accepted.

These tests were successfully used for analysing the data from the Norwegian rack network [35]. The results, for the evaluated 100-year unit ice mass in kg/m, showed a very good agreement with estimations from measurements made on actual neighbouring line routes in the same area.

3. Increasing the length of the time series used in the analysis by continuous increasing the number of years of observation in the subsequent winter seasons. This is the best, but the most difficult and costly way for improving the extreme value analysis. It may have two different consequences: (i) To justify the previous rejection of aberrant annual maxima, and thus to justify keeping the same or near extreme value distribution obtained from the truncated series. (ii) To confirm the trend of increased slope for the distribution of annual maxima in the last few observed years. In this case, it is rather more appropriate, for fitting procedures and estimating parameters, to use only the data from the right tail of the empirical distribution.

Because the calendar year ends in the middle of the freezing rain storm season, one could argue that it makes more sense to choose maximum ice thickness for the season rather than for the calendar year. In one study [81], the parameters of the extreme value distribution based on whether the calendar or seasonal year were used.

4.1.1.3.5 Discussions

Extreme value analysis, prognosis of icing and combined wind and ice loads for design purposes should be done only on the basis of statistical analysis of reliable data from sufficiently long time series (number of years of observation).

It is greatly recommendable, in accordance with the prescriptions of the IEC, the implementation of an ice observation program for collecting field data in each country concerned by the impact of atmospheric icing on the overhead power transmission network.

The largest values of type I distribution, (Gumbel), is often used as asymptotic distribution of annual maxima of icing – ice radial thickness or unit ice mass, for transmission line reliability and design calculations.

There are theoretical and practical reasons against the use of the asymptotic distributions of largest extremes of type II, holding for Pareto type initial distributions, and of type III, for bounded toward the right initial distributions.

A great majority of initial distributions of ice radial thickness (or ice unit mass) are of the exponential type – Weibull, exponential, gamma, lognormal, and more rarely Gumbel and normal. The distribution of annual maxima taken from all these distributions converges more or less rapidly toward the asymptotic distribution of type I (Gumbel). The minimal number of years of observation, to ensure that the extrapolated value of icing amount to be within 68% confidence limits, is evaluated to be between 24 and 35 years for the Gumbel initial distribution, 27 – 43 years for gamma, 25 – 64 years for Weibull, and 44 – 91 years for lognormal, as a function of the COV in the range of 0.8 – 1.7.

The estimated by extrapolation 500-year return period icing amount is smallest for the Gumbel initial distribution, followed by Weibull, lognormal, and gamma. The estimated 68% confidence interval is narrowest for the Gumbel initial distribution, followed by Weibull, lognormal and gamma.

4.1.2 Extreme Value Analysis of Wet Snow Accretion

4.1.2.1 Inadequacy of Gumbel Distributions for Irregular Events

Generally, type I extreme value distribution (Gumbel distribution) is adopted for wet snow accretion loads. Pézard [80] pointed out that in some areas where there is almost no snow accretion in a normal year, large snow accretion could be seen in very rare cases, and suggested that the Poisson type distribution would be better than the Gumbel distribution. In fact, for some areas in Japan, it has been found that, when estimating snow load based on meteorological records, data samples may indicate larger values of sample standard deviations than the mean values and this throws doubt on the application of the type-I distribution. Occurrence of heavy wet snow load is a phenomenon which happens only when several conditions are satisfied, such as a high intensity of precipitation, an air temperature suitable for accretion, suitable wind speed and direction, together with sufficient time for accretion. Note that such conditions do not promote the shedding of snow from wire.

To highlight these irregular conditions, Fig. 44 illustrates a time series plot of wet snow loads in the meteorological station “Le Tech” in south of France (altitude 548 m) from 1960 to 2002. These loads were not measured but estimated from meteorological basic parameters (air temperature, precipitation, wind, relative humidity) through cylindrical sleeve accretion model of Admirat (see Section 3.2.3.3).

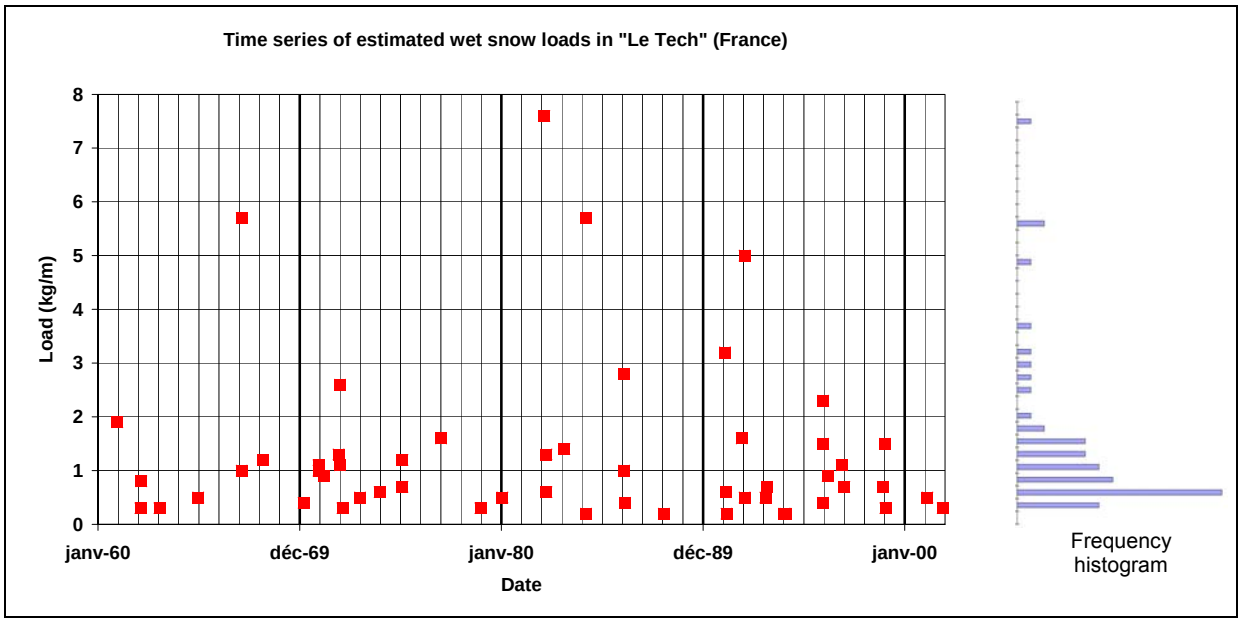

Figure 44: Example of time series plot for wet snow loads

During the 43 years period, 56 accretion situations were detected. Although this station is among the most exposed of the region, no load occurred for 13 years within the period. Finally, the distribution of annual maxima of icing may show an irregular pattern: many years without any icing event and a few years with severe overloads. A physical explanation of this special pattern could lie in the threshold effect of temperature on these icing events. For instance, in regions with relatively mild climate, all the conditions for icing might be easily obtained but one: temperature. For in-cloud icing, it is necessary that the temperature be below 0°C and this may explain the rarity of events. For wet snow, there are 2 temperature thresholds, usually around -1 to +2°C, which make the phenomenon even more rare than in-cloud icing, in accordance with the observations. Nevertheless, these events are severe enough when they occur so they could not be neglected.
As a result, the use of Gumbel laws (or more generally Generalized Extreme Value (GEV) distributions) is not satisfactory, either for theoretical and practical reasons. The theoretical reason is that Extreme Value Analysis requires the selection of identically distributed extremes, i.e. extreme data issued from the same parent law. In the case of irregular accretion events, yearly extremes might be very big values

or very low values, sometimes null depending on the year. Obviously, yearly extremes are not issued from identical distributions. This is revealed by practical difficulties, illustrated on the Gumbel plot in Fig. 45.

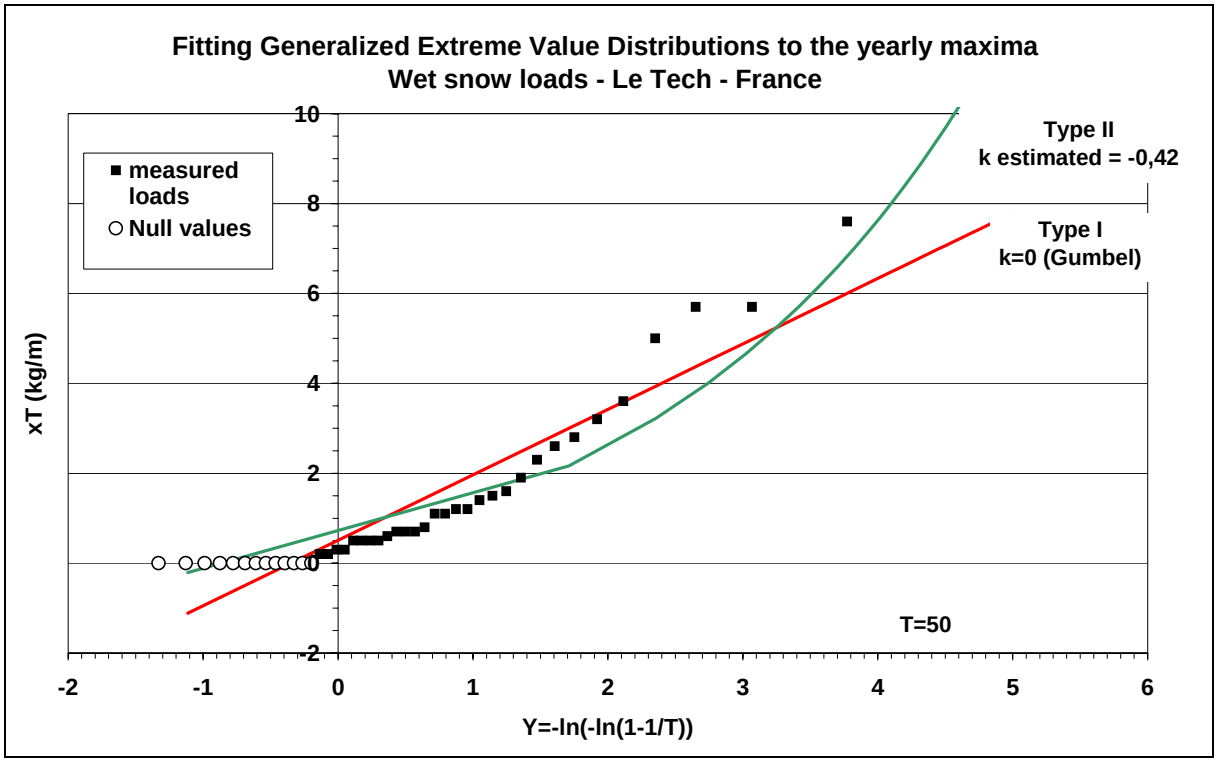

Figure 45: Inadequacy of GEV(Gumbel) distributions to fit the yearly maxima

Due to the method itself, we must select 13 null values (white dots in Fig. 45) and 30 estimated loads. With such data, fitting a straight line (assuming a Gumbel law) is obviously inadequate. The shape of the plot could lead to the false impression that the data is distributed versus a type II extreme distribution: the estimated shape parameter of the GEV distribution is negative (k=-0,42). However, the fitting is here again obviously inadequate.

To cope with these difficulties, Pézard [80] tried to find other probability distribution functions that would better fit this data, and showed that the gamma distribution may be well-suited to represent such a phenomenon. To ease the curve fitting, he determined that the parameter p1 of the gamma distribution be taken slightly lower than 0 in order to get a finite value for the density function f(0), for instance $p1 \cong -0.03$. Although this method gives practical results, it is however not supported by any Extreme Value Theory. Further research on this field eventually lead to the choice of Peak Over Threshold (POT) methods, described hereafter.

Conversely, in regions with rougher climate, some in-cloud icing patterns may come closer to a Gumbel distribution. In this case, it is supposed that the temperature conditions have been more often met, the increasing effect of altitude may also play an important role, as discussed in Chapter 5.

4.1.2.2 Peak Over Threshold (POT) methods

In the Peak Over Threshold (POT) methods, the selected extremes are not the yearly maxima (as for Gumbel), but the values exceeding a threshold, on which a Generalized Pareto Distribution is fitted. The Generalized Pareto Distribution (GPD) is a generalization of the Pareto Distribution. The GPD was introduced by Pickands in 1975 [88] to model excesses over a threshold. Since then, it has been applied to model extreme events in many different fields: insurance, finance, hydrology [89], winds [90].

As for any Extreme Value Analysis, POT methods rely on the condition that the selected extremes are independent and identically distributed, i.e. issued from the same parent law [91]. Then, if the threshold S is selected "high enough", the excesses are distributed following a Generalized Pareto Distribution given by:

$$P(x) = 1 - \left[1 - \frac{k}{\alpha}\cdot(x - S)\right]^{1/k} \qquad k\neq 0 \qquad (59a)$$

$$P(x) = 1 - exp\left[-\frac{(x - S)}{\alpha}\right] \qquad k=0 \qquad (59b)$$

α is the scale parameter; S is the threshold analogous to a position parameter; k is the shape parameter depending on the type of extreme distribution: k=0 for type I, k<0 for type II and k>0 for type III, as for GEV distributions. When k=0 (type I), the GPD reduces to a simple exponential distribution.

The global procedure is the following:

1. collect the data for M years
2. select a threshold S "high enough"
3. order the N excesses $\{x_1 \leq \ldots \leq x_N\}$ over this threshold
4. position the N points of coordinates $(P^*(x_i)\ ;\ x_i)$, $P^*(x_i)$ being the "plotting position" usually estimated by (i-0.35)/N or i/(N+1).
5. fit the GPD on these points and estimate the parameters k and α.

The T-return period value is then given by:

$$X_T = S + \frac{\alpha}{k}\left[1 - \left(\frac{N}{M}\cdot T\right)^{-k}\right] \qquad k\neq 0 \qquad (60a)$$

$$X_T = S + \alpha\, ln\left(\frac{N}{M}\cdot T\right) \qquad k=0 \qquad (60b)$$

The main difficulty with POT methods is the choice of the threshold S [92]: "*the threshold be set high enough so that only true peaks* […] *are selected. The threshold must be set low enough to ensure that enough data are selected for satisfactory determination of the distribution parameters*". One method consists of plotting the mean of the excesses (x_i-S) as a function of the threshold S ("mean residual life plot" [93]). For a GPD, this graph should be a straight line with slope $-k/(1+k)$ and intercept $\alpha/(1+k)$. An appropriate threshold can be chosen by selecting the lowest value above which the graph is a straight line. Although it is theoretically possible to determine the values of k and α from this line, interpretation difficulties may occur depending on the number of points available. Figure 46 gives such a graph applied to the previous data of wet snow loads in France.

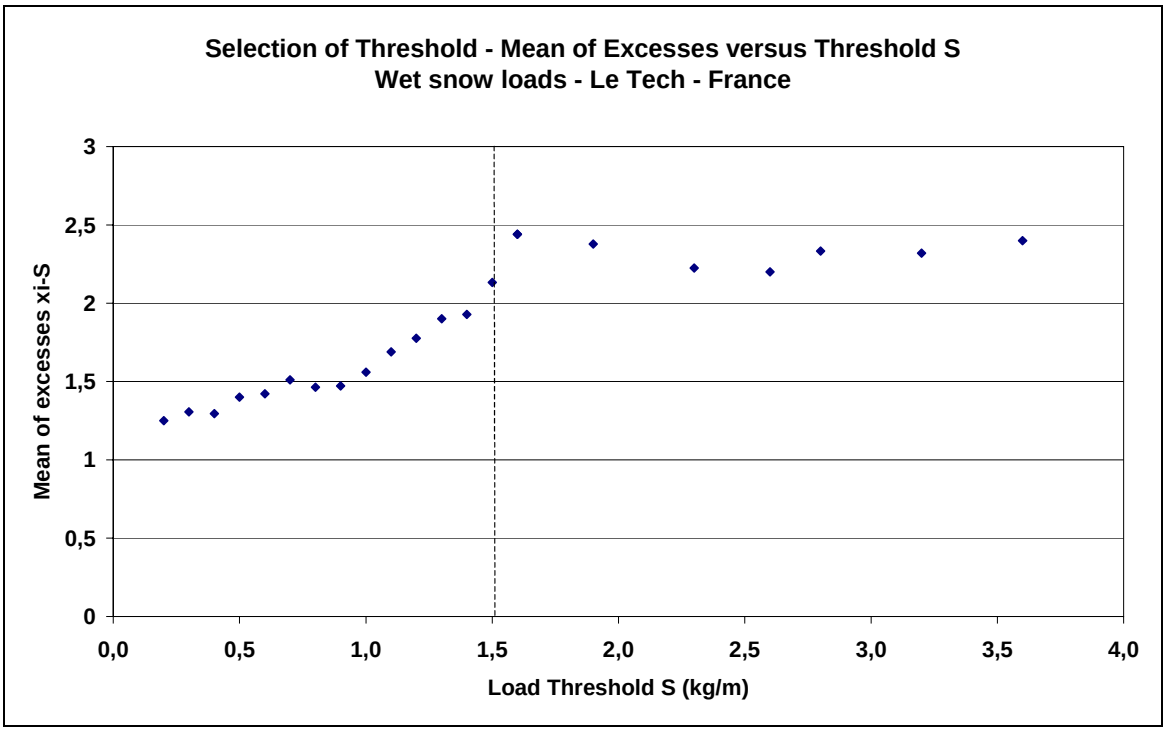

Figure 46: A method for selecting the threshold

In this example, the selected threshold *S* is 1.5 kg/m, which lead to the selection of only 12 values. More straightforward methods consist in choosing a threshold corresponding to a high percentile of the data (the *x*% biggest) or for a given value of excess rate *N*/*M* [84]. The horizontality of the line above threshold indicates the value of *k* is close to 0, suggesting a type I distribution. The intercept gives a value of α close to 2.

The most common and more precise method used for estimating the parameters *k* and α is the Probability Weighted Moments method. The parameters α and *k* can be deduced from the two first statistical moments b_0 and b_1 of the extreme value *X*. Unbiased estimates of these moments for a set of *N* ordered values $\{x_1 \leq x_2 \leq \ldots \leq x_N\}$ are given by [94]:

$$b_0 = \frac{1}{N}\sum_{i=1}^{N} x_i \ , \ b_1 = \frac{1}{N}\sum_{i=1}^{N} x_i \times P^*(x_i) \qquad (61a, b)$$

Estimates of parameters *k* and α are given by [84]:

$$k = (4 \cdot b_1 - 3 \cdot b_0 + S) / (b_0 - 2 \cdot b_1) \qquad (62a)$$

$$\alpha = (b_0 - S)(1 + k) \qquad (62b)$$

In the example above, the estimated value of the shape parameter k is almost null (k = -0.03), confirming the data above threshold is distributed following a type I form. The estimated α is 1.98, close to the previous approximate value given by the mean of excesses line. The final extreme value distribution is a simple exponential form fitted on the 12 values above the threshold *S*, as illustrated in Fig. 47.

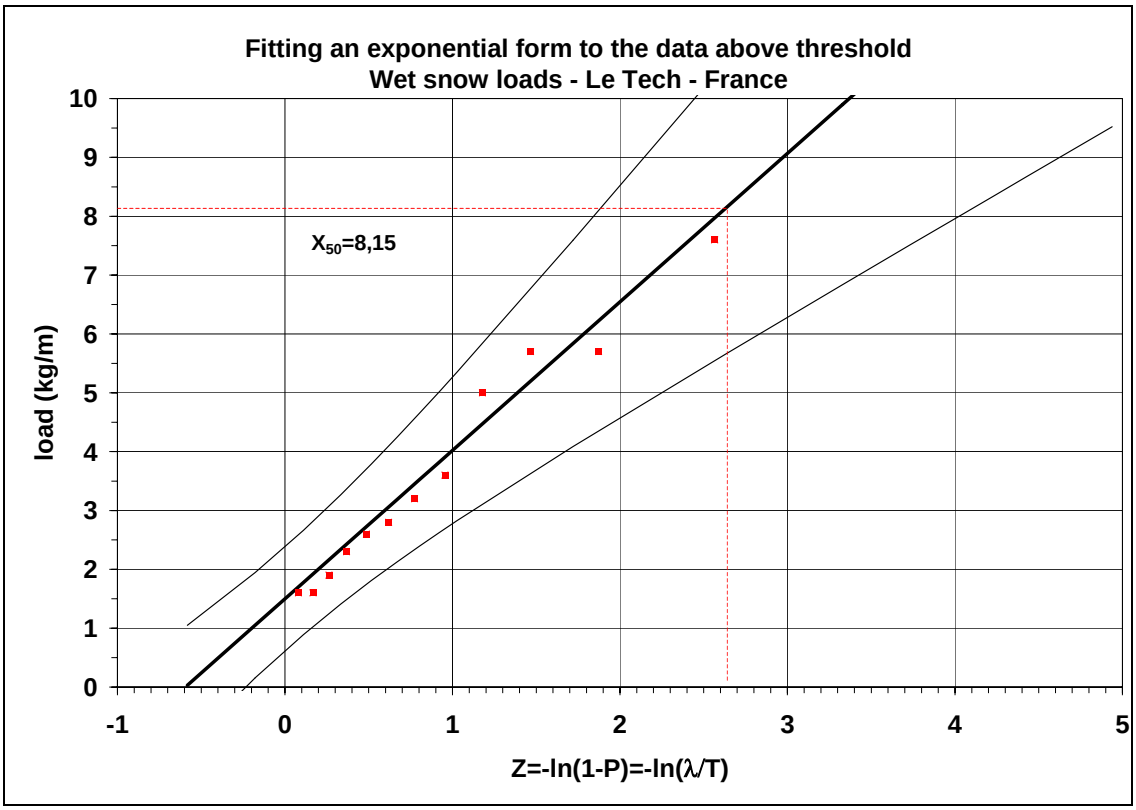

Figure 47: Fitting an exponential form to the data above the threshold

Modelling wet snow load with exponential forms fitted to data above thresholds has been generalized in France [95]. The dashed lines give the 90% confidence interval, the standard deviation of the sampling error being given by (for k=0) [92]:

$$\sigma_{GPD}[X_T] = \left[\frac{\alpha^2}{N} \left\{ 1 + \left[ln\left(\frac{N}{M} \cdot T \right) \right]^2 \right\} \right]^{\frac{1}{2}} \qquad (63)$$

As the number N of selected extremes is low (N=12) the confidence interval is large. This reflects the uncertainty linked to irregular and relatively rare event. As for any statistical method, a large number of data, meaning a large observation period leads to a better precision. One can also see that the uncertainty grows with the slope α, meaning a larger variation in the selected extremes.

4.1.2.3 Discussion

POT methods are more recent and computationally more demanding than methods based on yearly largest extremes modelled by GEV distributions. In particular, the choice of the threshold must be made with care, and one must also pay attention to select only independent values. This method is however suitable for irregular events like wet snow accretion in mild climate areas, for which GEV distributions are inadequate.

These methods are now spreading even for more regular phenomena. They were applied recently to model extreme ice thickness on overhead line cables in Canada and USA [84]. To quote this reference, in some years "*there is more than one severe ice storm, each of which may cause larger ice loads than*

the most severe storms in milder years. The epochal methods do not include these large, but not worst-of-the-year, ice thickness in the estimation of the parameter of the extreme value distribution". Applied to regular phenomena, POT methods often allows to select more data than the number of years (*N*>*M*), leading to minimize the uncertainty on the estimates of T-return period values.

One could also add that the use of a threshold for the selection of the extreme values prevents from selecting data issued from too different parent laws, any Extreme Value Analysis method requiring identically distributed samples. The difficulty arising when trying to fit Gumbel laws to wet snow data in mild climate probably comes from the fact that different origin phenomena are responsible for very big and low wet snow loads, leading to mixed distributions, thus different extreme distributions.

4.2 Transfer Function Modelling

Before construction of a transmission line, an analysis is undertaken to establish whether a particular line route is suitable. One aspect of this analysis involves usually the prediction of the long-term maximum ice load along the proposed line route. Typically, ice loads are measured by a number of punctual measurement stations and the maximum ice load along this line route can be estimated from past experience and available climatological data from the stations. Guidelines to achieve such a transfer function modeling are provided in the following sections.

4.2.1 Transfer Function Modelling of Glaze Icing

4.2.1.1 Introduction

The analysis of very large ice database is always difficult because of the geographical repartition of measurement sites and the temporal behaviour of icing events. However, it becomes important to analyse the past icing events and, if possible, their progression from one location to another in order to better design overhead lines. Houde *et al.* [78] proposed a method to characterize spatial patterns for the distribution of icing events in different regions of the province of Québec. Measurement stations are considered as a fixed mesh in space and an icing event is defined in time and space as the group of stations affected by the same meteorological phenomenon. This precise definition of the notion of event helps to estimate the probability that an icing event is progressing from one station to another, and also to determine progression pattern in space. For this purpose, the available meteorological data are divided into two sets. The first one covers period of observation up to 20 years at 180 stations deployed throughout the province of Québec and is based on ice measurements obtained through PIM (Fig. 35). The second set covers periods of observation up to 8 years at 23 stations and is based on an improved IRM (Fig. 37b).

4.2.1.2 Houde *et al.* Model [78]

The two databases are built around the notion of icing events defined as the period between the first beginning of a freezing rain and the time where no more ice is still on the instrument. This means that the accumulation and the persistence are considered as two states of the same event. Sometimes, an event can have more then one accumulation period and last for days and even for weeks. This is a natural definition when investigating the total load on the structure at any given time but not relevant when studying precipitations and relations between stations on this basis. In order to analyse the meteorological events, only the accumulation period is considered so an event in the database is split into smaller events defined as a period of accumulation. This allows the analysis of stations in term of sharing the same meteorological event.

Geographical distance between stations cannot reflect the spatial association because there are many factors limiting the area affected by an icing event such as rivers, lakes, mountains, plains, etc. Houde *et al.* [78] proposed to define spatial correlation based on the probability that two stations share the same accumulation event. Let π_{ij} the probability that the station *j* is affected by an event when there is an icing

event at station *i*. The natural estimator of this probability is $p_{ij} = n_{ij} / n_i$, where n_i is the number of events at station *i* and n_{ij} is the number of events shared by stations *i* and *j*. The result is a matrix of probability that is transformed into a distance matrix ***D*** between stations with the relation:

$$d_{ij} = 1 \frac{n_i \cdot p_{ij} + n_j \cdot p_{ji}}{n_i + n_j} \tag{64}$$

The distance is 0 if stations *i* and *j* always share the same events and 1 if the stations never share any common event. To interpret the distance matrix and identify spatial patterns, Houde *et al.* perform hierarchical clustering with association by single linkage. This allows them to define a classification tree for the PIM and IRM dataset respectively. Different spatial patterns come out the hierarchical clustering. For instance, a first spatial pattern is defined around the Montreal region associated to a group of stations affected by the St-Lawrence River and the plain around it.

The matrix Π reflects the fact that two stations *i* and *j* are likely to share a particular icing event. For a spatial pattern, some parameters such as temperature, accumulation, etc. influence these probabilities. In order to explain the spatial propagation of icing events in a given pattern, the relation between stations *i* and *j* and the observed variables, temperature, accumulation, duration and accumulation rate are analysed. For instance, the most important variables to explain the correlation of the events for the group of stations in the Montreal region are the accumulation rate and duration of the event.

4.2.1.3 Laflamme Model [32]

Laflamme [79] has demonstrated that it is possible to obtain acceptable extreme distributions from 20 years of freezing rain data. He pooled extreme values from three stations at a time and obtained regional instead of punctual extreme values. These stations actually formed triangles with 50 km sides, and covered sufficient area to catch large icing values of small icing storms. He then fitted an extreme value distribution to the triangles of maximum icing thicknesses with an estimated error of the order of 10%.

Laflamme [32] proposed to use the network of PIM to produce maps of freezing rain season in the province of Québec. For instance, from the maps of the earliest and latest dates of freezing rain, he showed that, in the Northern part of Québec, the freezing rain season starts as early as September 15, while in the Southern part, it starts around October 20.

He also demonstrated the usefulness of the recorded data for extreme value analysis and transmission line design. With a fine grid network, it is possible to detect any anomaly in the data and to make the proper correction when necessary. Even though the sampling rate is slow (twice a day), the data are very consistent because the ice deposits stay long enough on the PIM, generally more than 12 hours. A few icing episodes might have been missed in the middle of the day, but this fact cannot affect the analysis of major ice storms.

A contour map of ice thickness is prepared by first plotting the values for the appropriate return period at the observing location. Contours at appropriate intervals are drawn based on the analyst's judgment and knowledge of the climatology of freezing precipitation. Maximum ice thicknesses for a 100-year return period have been plotted on the St-Lawrence valley map [32] as shown in Fig. 48. Another type of map is illustrated in Fig. 49 where contour curves of return periods of 15-mm ice thickness are plotted. Laflamme [32] also produced maps of the frequency of freezing rain events and persistence of ice deposit from the PIM database.

Freezing rain maps are very useful to define ice load zones for determining limit strength of structures. The PIM database can also be used to produce risk analyses of other problems related to overhead conductors such as flashovers of iced insulators and conductor galloping.

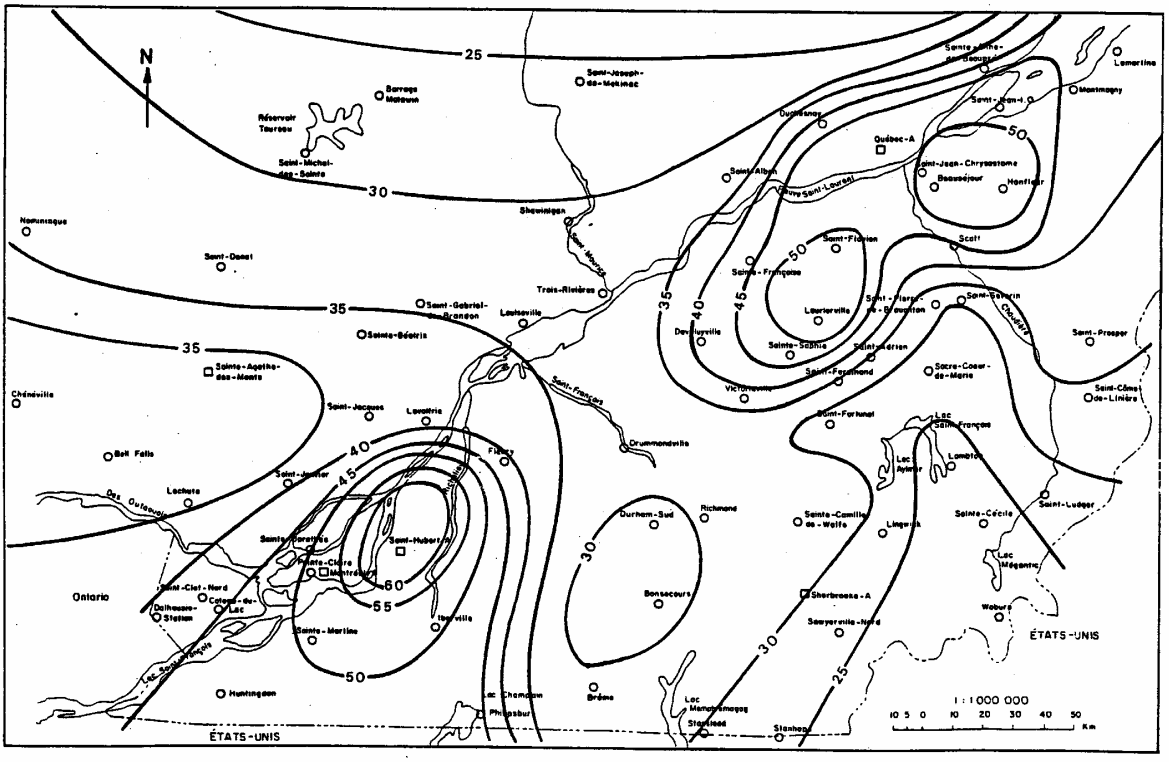

Figure 48: Maximum ice thickness (mm) for a 100-year return period – Reference [32]

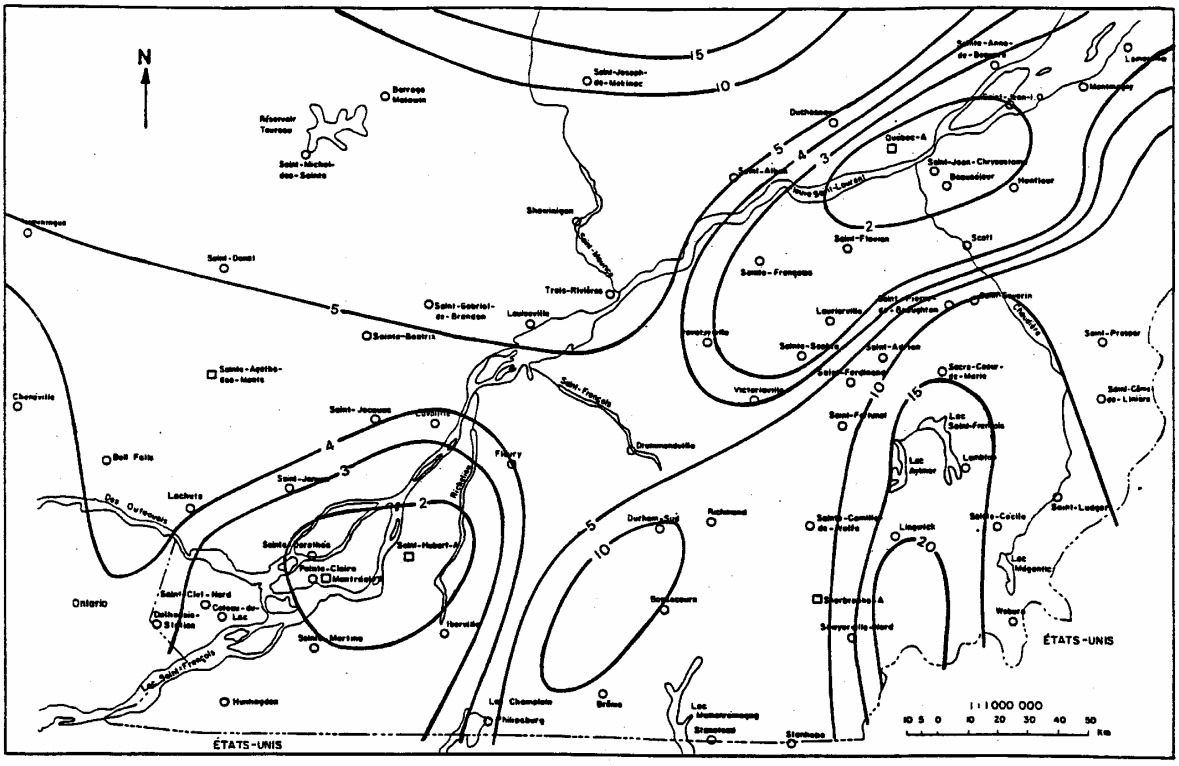

Figure 49: Return period (years) of a 15-mm ice thickness – Reference [32]

Generally, only locations having long periods of record (greater than 15 years) are used in the contour analysis since the statistical sampling error decreases with increasing length of record.

4.2.2 Transfer Function Modelling of Rime Icing

4.2.2.1 Introduction

Applying models for rime ice accretion requires reasonable estimates of non-measured parameters like cloud droplet size distributions and liquid water content. In his paper, Harstveit [45] demonstrates a method to use regular meteorological observations in order to obtain a classification of icing severity for in-cloud icing according to a recent ISO standard [3].

The method is based on simultaneous observations of:

- cloud base on lowland stations,
- observations of visibility on (nearby) elevated stations and
- some optical visual range measurements.

The ISO classification for in-cloud icing (see Section 3.3.1.4) is a sort of logarithmic classification from R1 to R10 representing a mass of ice from 0,5 kg/m for R1 to 50 kg/m for R9, on a 30 mm diameter cylinder (return period = 50 years). R10 is used for extreme locations where adequate meteorological evaluations should be made. The ISO standard then provides calculation rules for any type of structure other than overhead power line conductors.

4.2.2.2 Harstveit Model

The general rate of icing is given by Eq. (11). Expressing this formula in specific terms, the mass per unit length, m, becomes:

$$\frac{dm}{dt} = \alpha_1 \cdot \alpha_2 \cdot \alpha_3 \cdot w \cdot v \cdot D \tag{65}$$

where D is the diameter of the object.

α_1, α_2 and α_3 are factors representing processes that may reduce the icing rate and are called *collision efficiency*, *sticking efficiency* and *accretion efficiency*, respectively (see Section 3.2.2.3.1). For rime icing only α_1 and α_3 need to be accounted for. Harstveit [45] then shows that these quantities are dynamic, especially with respect to the growing ice accretion and to some extent interdependent. This can roughly be expressed as:

$$\alpha_1 = f_1(v, D, d) \tag{66}$$

and

$$\alpha_3 = f_2(v, w, D, T_a, \alpha_1) \tag{67}$$

where d is the median volume droplet diameter (MVD) and T_a the ambient air temperature. These functions are further developed in [45].

From hourly observations (METAR) of cloud cover (0 to 9) and cloud base (intervals 100 feet) he found good relations to fog frequencies of neighbouring hills both in the Oslo area and in Northern Norway.

Following Mie's theory for scattering of light in fog, the liquid water content and MVD may be found from measurements of "meteorological optical range", MOR, assuming an adiabatic lapse rate of liquid water above the cloud base.

Then the vertical temperature and wind speed profiles may be found from radiosonde measurements from certain locations in the country.

Based on the above information, icing events and accreted ice mass can be estimated for selected heights in representative areas around the METAR stations.

When the thermodynamics for ice melting is included, it is also possible to identify ice-shedding episodes and hence to start with realistic initial values by the next icing event.

Figures 50 and 51 show the results for the two seasons 1997/98 and 1998/99, respectively, for 6 height levels from 600 m asl to 1 200 m asl.

Other studies (not published) show reasonable correlations with Statnett's network of ice measuring racks [35].

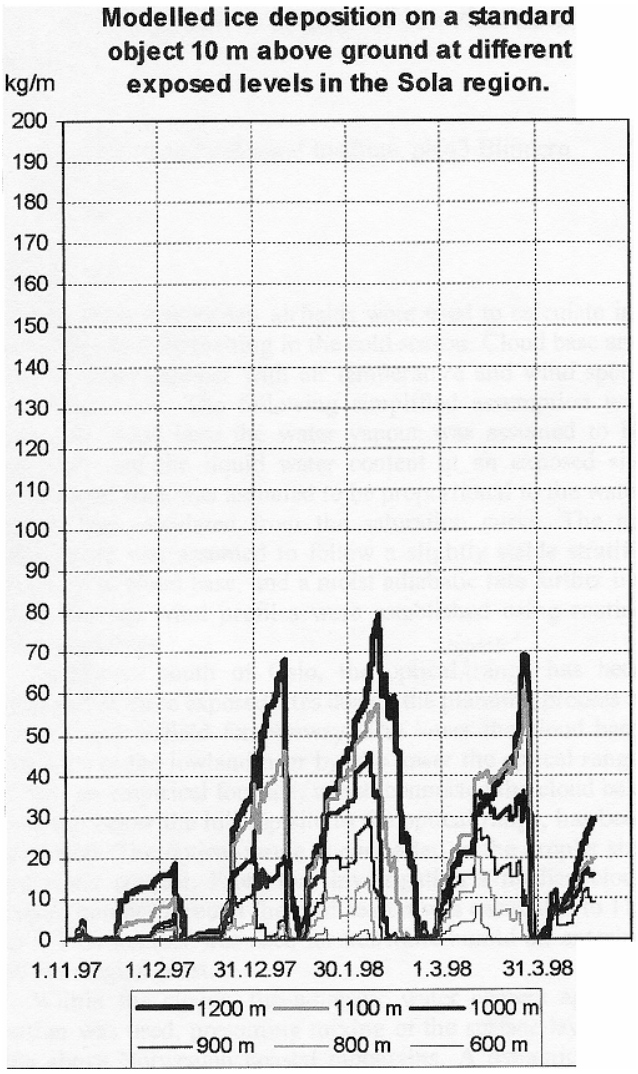

Figure 50: Calculated ice loads for different heights in the Sola area 1997/98

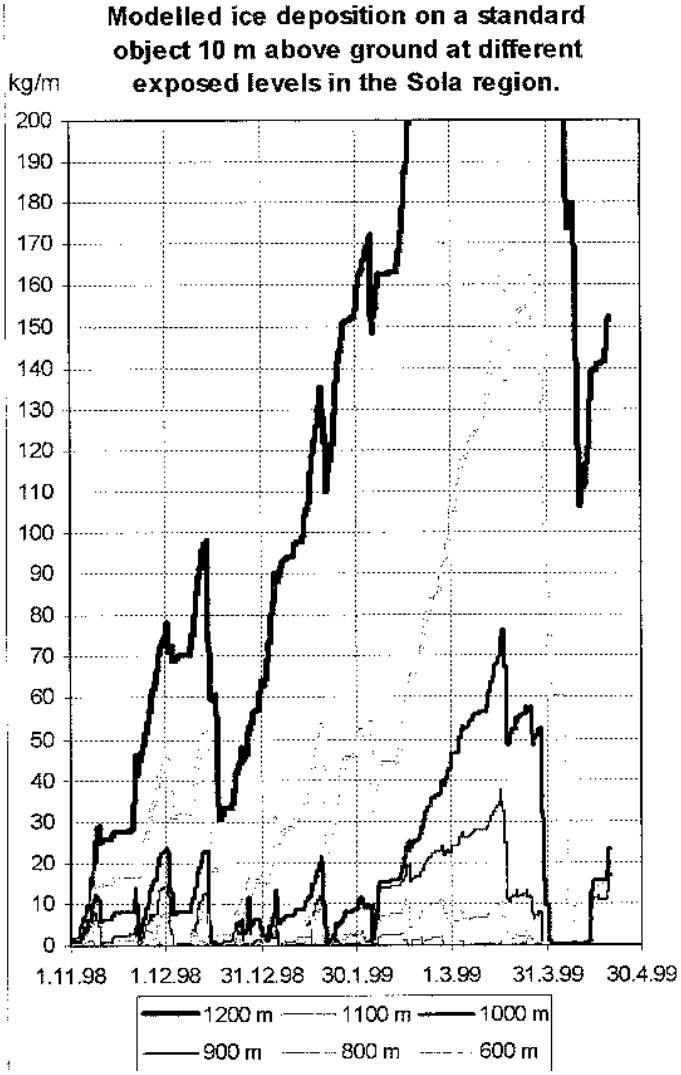

Figure 51: Calculated ice loads for different heights in the Sola area 1998/99

4.2.3 Transfer Function Modelling of Wet Snow Accretion

4.2.3.1 Introduction

Krishnasamy and Fikke [50] reported a procedure to estimate wet-snow loads along transmission line route in Norway. This procedure utilizes historical values of precipitation at stations in the general vicinity of the line route. The procedure takes into consideration the effects of height above sea level, terrain and historical experience in predicting the loads. In general, the proposed procedure reasonably predicts ice/wet snow loads along the line route. The usefulness and the accuracy of the method are described hereafter by applying it to a proposed transmission line in Southern Norway.

4.2.3.2 Procedure For Predicting Ice/Wet-Snow Loads At Weather Stations [50]

Three procedures are described to predict ice/wet snow loads at weather stations. Each procedure varies in the manner the "reference precipitation" value is chosen for the weather stations. A "reference precipitation" is a value that realistically represents the precipitation for a station. The steps in choosing the representative precipitation values for each procedure are described below in a flowchart (Fig. 52) and applied to a proposed corridor for a new 420 kV line in Southern Norway. The Norwegian Meteorological Institute (MI) has precipitation data for a number of locations from 1895 and to the present. A significant part of these data are quality controlled on a 24-hour basis. A lot of the remaining data are however controlled on a monthly basis to ensure that monthly totals are homogeneous and reliable for climatic assessments. Based on these two types of data, two procedures were applied for ice load assessments: procedure #1 is based on the actual extreme values on record of 24 hour totals (without statistical extreme value calculations), and procedure #2 is based on extreme value analyses of time series of monthly precipitation data.

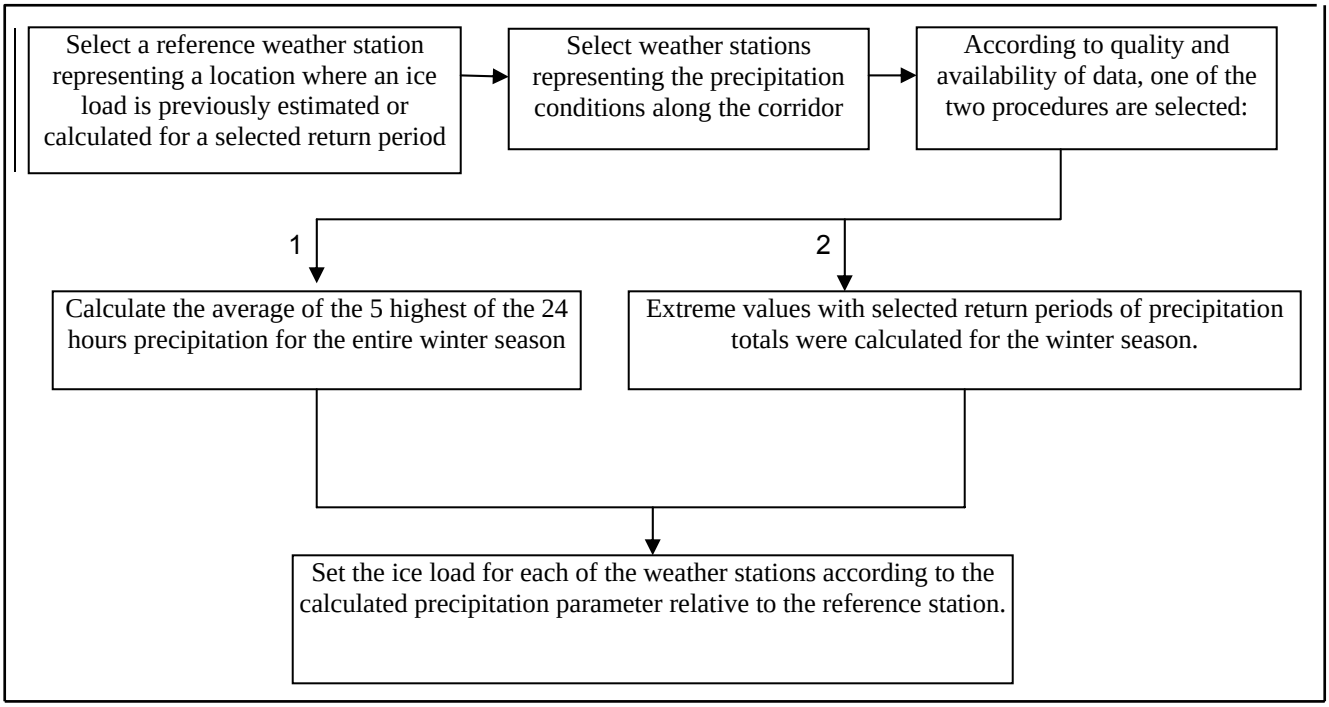

Figure 52: Flowchart of the steps in choosing the representative precipitation values for each procedure

In addition to the ice loads generated from the procedures described in Fig. 52, a local exposure factor (LEF) was established to account for the local exposure of the line compared the nearest weather station.

The precipitation data, including local variations in precipitation above sea level, were generated by the MI [51]. The transmission line corridor was divided in 88 sections where the LEF was estimated according to topographical characteristics and the local ice loads was calculated for each section. Figure 53 shows the calculated loads according to this method together with the loads that were given for the line according to traditional subjective evaluations.

The resulting loads for this line are shown in Fig. 53 together with the loads that were estimated on a subjective basis from experience with ice load assessments in Norway.

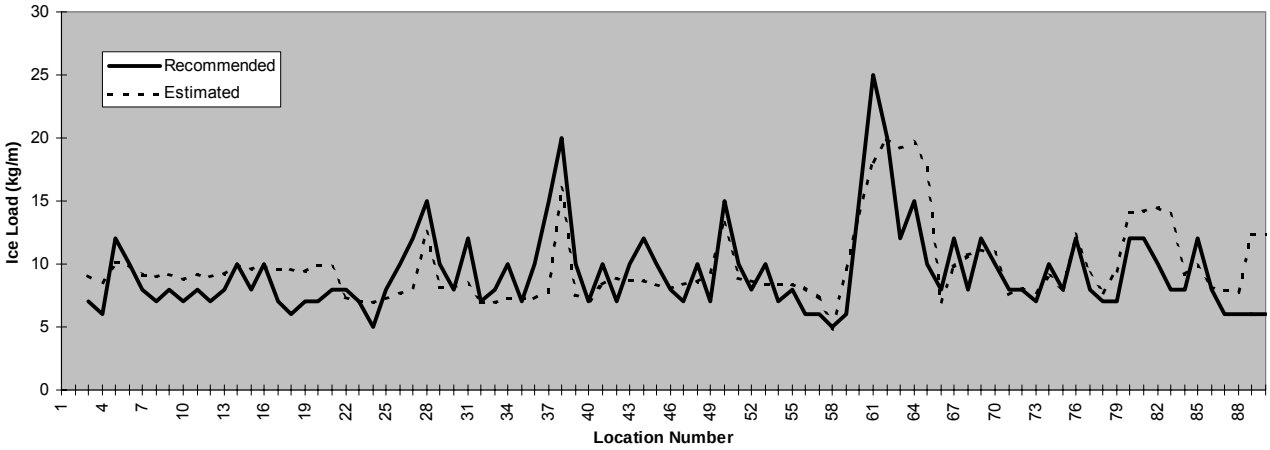

Figure 53: Calculated ("recommended") ice loads along the line route shown together with ice loads estimated according to design experience

5. TOPOGRAPHICAL EFFECTS

5.1 Background

Topography [3] modifies the vertical motions of the air masses, which, in turn, modify the cloud structure, precipitation intensity and, by these, the icing conditions. The influence of terrain is generally different for in-cloud icing and for precipitation icing. In general, topography is the basis for defining icing zones. For instance, a typical topographical description might include the distance from the coast, elevation above sea level, presence of plains and valleys, high mountains situated on high level areas, etc.

Standards of Russian Federation (RF) decided to establish regional icing maps taking into account topography. For this purpose “oroclimatic” (from “orography” (or “topogragphy”) and “climate”) terrain standardization is used. In Section 5.2.1, it is considered that radial thickness of the ice load is converted to a relative density of 0.9 and to the 10 mm diameter conductor placed at 10 m height [38].

A considerable amount of work has also been carried out by EA Technology at their various field sites. This is summarized in the IWAIS 2000 paper by Wareing and Chetwood [19] and presented in Section 5.2.2.

Several studies have been carried out in Iceland with regard to topographical influence on wet snow accretion as presented in Section 5.2.3.

5.2 Variations of Ice Thickness With Topography

5.2.1 Russian Icing Maps

An ice load having a given return period and calculated from the observations data from one meteorological station is valid only for the terrain with surface characteristics identical to those at the site of the meteorological station. In order to extend the observation data from individual meteorological stations to the whole territory, it is necessary to find the laws of their space-time distribution, and the relation between loads and the physical and geographical conditions: the type of terrain, the presence of large water reservoirs and forests.

The type of terrain (topography) greatly affects ice loads, which creates many "spots" and "specks" on the icing map. Dividing a territory into the icing regions is only possible on the basis of the terrain standardization. This standardization is oroclimatic, i.e. it considers from one side a climatic factor – prevailing wind direction, and from the other –surface (orographic) characteristics of the terrain.

In practice two major oroclimatic types are applied for dividing the RF territory into the icing regions: undulating terrain (plains and hills) and mountainous terrain. For the undulating terrain two types of macro-topography are marked out: plain and heights, which differ by the value of relative elevation (Table 11). The terrain type "heights" is divided into six subtypes, defined by the degree of exposure to the ice-carrying flow (windward and leeward slope, a valley exposed to or screened from the ice-carrying flow, etc.).

The next step of standardization is to define the meso-scale topography, or simplified “meso-topography”. “Meso-scale” is usually in the order of 10 – 1000 km. Larger scale characteristics can be called “macro-scale” and smaller scale characteristics “local-scale”. On the heights the watersheds are marked out as a type of meso-topography, which in its turn is divided into 6 subtypes similar to the subtypes of macro-topography [39].

The mountainous terrain is divided into two types of macro-topography, according to the characteristics of the main chains: outlying exposed regions, and inside, mainly screened regions. Each of the two types of macro-topography is divided into several meso-terrain types, corresponding to the shapes of mountainous surface with linear dimensions from several tens to several hundreds of kilometers (foothill

plains, intermountain valleys, outside range slopes, closed valleys and hollows). The types of meso-terrain, in their turn, are subdivided into a number of oroclimatic subtypes - local sites with specific conditions of a certain micro-terrain (bottoms of valleys and hollows, exposed slope sites, etc.) [40].

Based on the above standardization, a map of the terrain types is drawn for a given region. Terrain standardization allows ascertaining the quantitative relation between the ice load and the height of the site for orographycally similar territories.

The main morphometric characteristics needed to allocate macro- meso- and micro-terrain are described in Table 12 [44], where:

a) H – true altitude above the sea level, m;
b) ΔH – relative altitude – exceeding of the highest terrain element above the medium level of the nearest plain surface, m. These terrain elements must have the same spatial scale;
c) ℓ – shortest distance from the highest terrain element to the nearest plain surface, kilometers;
d) β - steepness of the slopes defined from:

$$\sin \beta = \frac{\Delta H}{\ell} \tag{68}$$

Table 12: Main morphometric characteristics of the macro- meso- and micro-terrain (excepting mountains)

Terrain	H (m)	ΔH (m)	ℓ (km)	β (degree)
macro-	0 - 750	0 - 750	more than 50	less than 1
meso-	0 - 750	0 - 750	3 – 50	1 – 3
micro-	0 - 750	less than 80	less than 3	more than 3

For an undulating terrain the relation between equivalent ice thickness and the height above the sea level is determined for each type and each subtype of macro- and meso-terrain. When the number of meteorological stations is not enough to determine this relation for each type (or subtype) of macro- and meso-terrain, it is possible to combine several types of terrain basing on the exposure to the prevailing wind direction during icing. For example, the following types of macro-terrain: peaks of heights, windward slopes, and exposed valleys – can be combined into one macro-terrain type: exposed shapes.

In the absence of meteorological station data for the elevated sites of the territory, the abovementioned relations are drawn using the values of equivalent ice thickness, obtained analytically from the observation data of the meteorological stations, situated on the plain from the side of windward slope. For these data the coefficient K_p is introduced:

$$K_p = e^{(\lambda - r)\cdot\varphi\cdot\Delta H} \tag{69}$$

where λ and φ are coefficients depending on the geographical situation and slope direction to the ice-carrying flow; r is a factor of ice-forming atmospheric phenomena, depending on synoptic conditions in a given region; ΔH is relative elevation of the site above the plain from a windward slope side [41].

Table 11: Types of macro- and meso-topographies for undulating terrain.

Macro-topography	Subtypes of macro-topography	Exposure to the ice-carrying flow	Types of meso-topography	Subtypes of meso-topography	Exposure to the ice-carrying flow
Plain (H = 0 – 750 meters above sea level, ΔH *less* than 100 meters)	-	Exposed	-	-	-
Heights (H = 0 – 750 meters[1], ΔH *more* than 100 meters)	I. Peak	Exposed	Watersheds (H = 0 – 750 meters, ΔH *more* than 100 meters)	a. Peak	Exposed
	II. Windward slope	Exposed		b. Windward slope	Exposed
	III. Parallel to the wind slope	Exposed		c. Parallel to the wind slope	Exposed
	IV. Leeward slope	Screened		d. Leeward slope	Screened
	V. Exposed valley	Exposed	-	e. Exposed valley	Exposed
	VI. Screened valley	Screened	-	f. Screened valley	Screened

[1]Terrains with heights more than 750 meters are considered as mountains and have to be studied with special methods.

When determining the relation between equivalent ice thickness and the site height it is advisable to consider an influence of micro-terrain on the ice load. For this purpose the observation data of meteorological stations, situated in various micro-terrain conditions, are referred to an open plain, using the coefficients K_{mr}, obtained from the long-term measurements in the field [42]. For example, for the type of micro-terrain "windward hill slope" this coefficient K_{mr} = 1.1 - 1.4 in the range of relative elevations of the hill points above the plain from 20 to 80 meters.

Determining the relation of ice load to height for the mountainous regions is much more difficult. The main difficulty consists of the fact, that there are not enough meteorological station observations, except for narrow slope valleys, for the slopes and crests. Experimental ice measurements in such poorly examined mountainous areas allow drawing icing maps with sufficient approximation [40].

If the period of such experimental measurements reaches 1 to 3-5 years, probability estimation of ice load is made by means of approximation of the empirical distributions. With the shorter duration of the measurements the obtained data are referred to the observation data of a meteorological station using approximate statistical methods.

In mountainous regions the relation between the ice load and the height is determined for the oroclimatic types of terrain, thus taking into account macro-, meso- and micro-topography.

Mathematical methods of constructing the above relationships are different for undulating terrain and mountainous terrain.

For undulating terrain and for individual sites in mountainous terrain the ice load to height relationships are drawn using simple graphical methods and analytical regression calculation (Fig. 54).

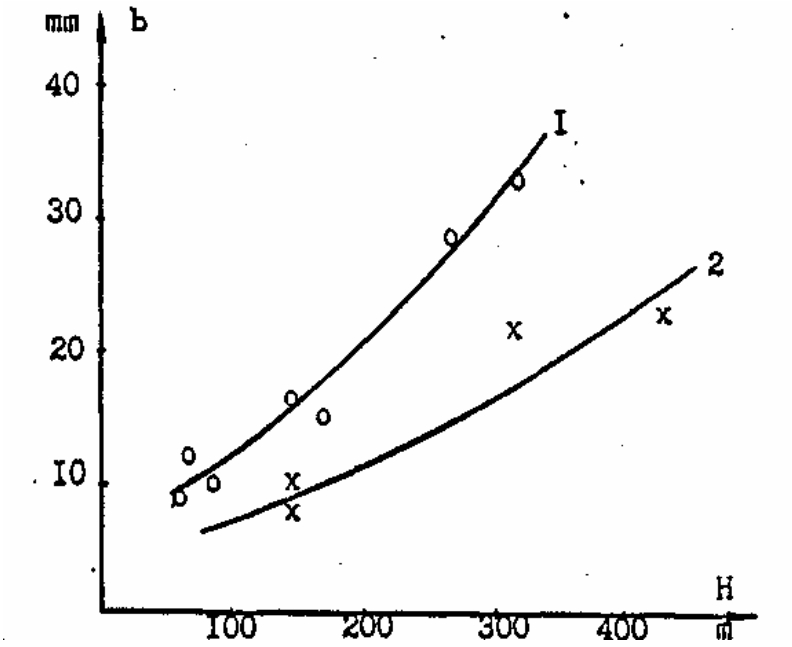

Figure 54: Relationship between ice thickness *t* and the height above the sea level *H* for exposed (1) and screened (2) types of macro- and meso-topography for undulating terrain

For mountainous terrain it is more advisable to draw the upper envelopes of maximum parameter values

at a given value of an argument (Fig. 55).

When drawing a regional icing map, one should also consider an influence of other geographical factors: the presence of near-by large water pools, forests, etc. The relation between ice thickness and the height of the site is determined taking into account the said factors.

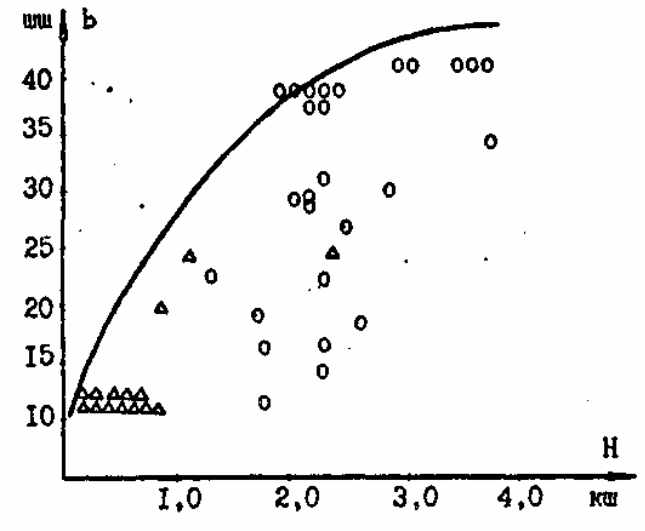

Figure 55: Relationship between ice thickness *t* and height above the sea level *H* for the slopes of outside mountain chains, based on the data of meteorological stations (∆) and experimental measurements at expedition points (o)

The borders of icing regions are drawn along the contour curves (curves of equal height). These curves are defined for each region and each type of the terrain from the relations between ice loads and height with the gradation 5 mm.

The regional icing maps are drawn on a hypsometric scheme on a 1:500000 scale. In mountainous regions besides the borders along the contour curves, natural orographic borders are considered, too.

Additional data ascertaining ice load values in the regions with few meteorological stations are obtained from the experience of OHL operation. The main requirement to such data is availability of reasonably valid measurements of deposit mass or its dimensions, and precise definition of a deposit type or its density. Of great importance is the reference of these measurements to a certain geographical point. To use these data probability estimation is needed, which is possible from the analysis of OHL operational experience for a number of years.

5.2.2 UK Wind and Icing Maps

In the UK, wind/icing maps exist for overhead lines which split the country up into specific areas according to their wind and snow/ice susceptibilities. This Section summarized the result of work in 1988 to determine a wind and ice load map of the UK that demonstrated the difference in load with geographical position and land height above mean sea level. This was incorporated into a Technical note, EAT 111, and a new standard ENATS 43-40. These included snow/ice maps in 100 m increments from sea level to 500 m in height.

5.2.2.1 Standard ENATS 43-40

ENATS 43-40 [82] uses combined wind/ice parameters based on mean hourly wind speeds and radial ice thickness at a density of 914 kg/m^3. The wind loads were classified in six ranges (1-6) and the ice loads in five ranges (A-E). Figure 56 shows a UK wind/ice map for 0 to 100 m above sea-level. There is a map for each land height from 0 m up to 500 m in 100 m increments. This enables line design and components to be specified and used according to the environment. The complete set of wind/ice maps are given in Appendix I. Other examples of icing maps are given in Appendix II. Typically, a line would be constructed based on a wind/ice combination as described in Tables 13 and 14.

Table 13: Wind Ordinate in ENATS 43-40 – Reference [82]

Wind Ordinate	Wind Pressure (N/m^2)
1	190
2	380
3	570
4	760
5	950

Table 14: Radial Ice Ordinates in ENATS 43-40 – Reference [82]

Ice Ordinate	Radial Thickness (mm)
A	5
B	10
C	15
D	20
E	25

So a “2B” wind/icing zone would be an area which could expect a wind load of 380 N/m^2 and a radial ice thickness of 10 mm.

This work was an alternative to adopting the UK wind/ice codes as expressed in BS 8100 [62].

5.2.2.2 BS 8100

The application of BS 8100 [62] methodology considers Wind only, Wind and Ice and Ice only conditions. The maps presented here are from BS 8100 Part 1, 1996.

It should be noted that with the publication of BSEN 50341 “Overhead Electrical Lines Exceeding 45kV AC”, the industry has recognized that wood pole overhead lines at 66 and 132kV will be affected. More recently, the requirements of BSEN 50423 addresses overhead lines below 45kV also.

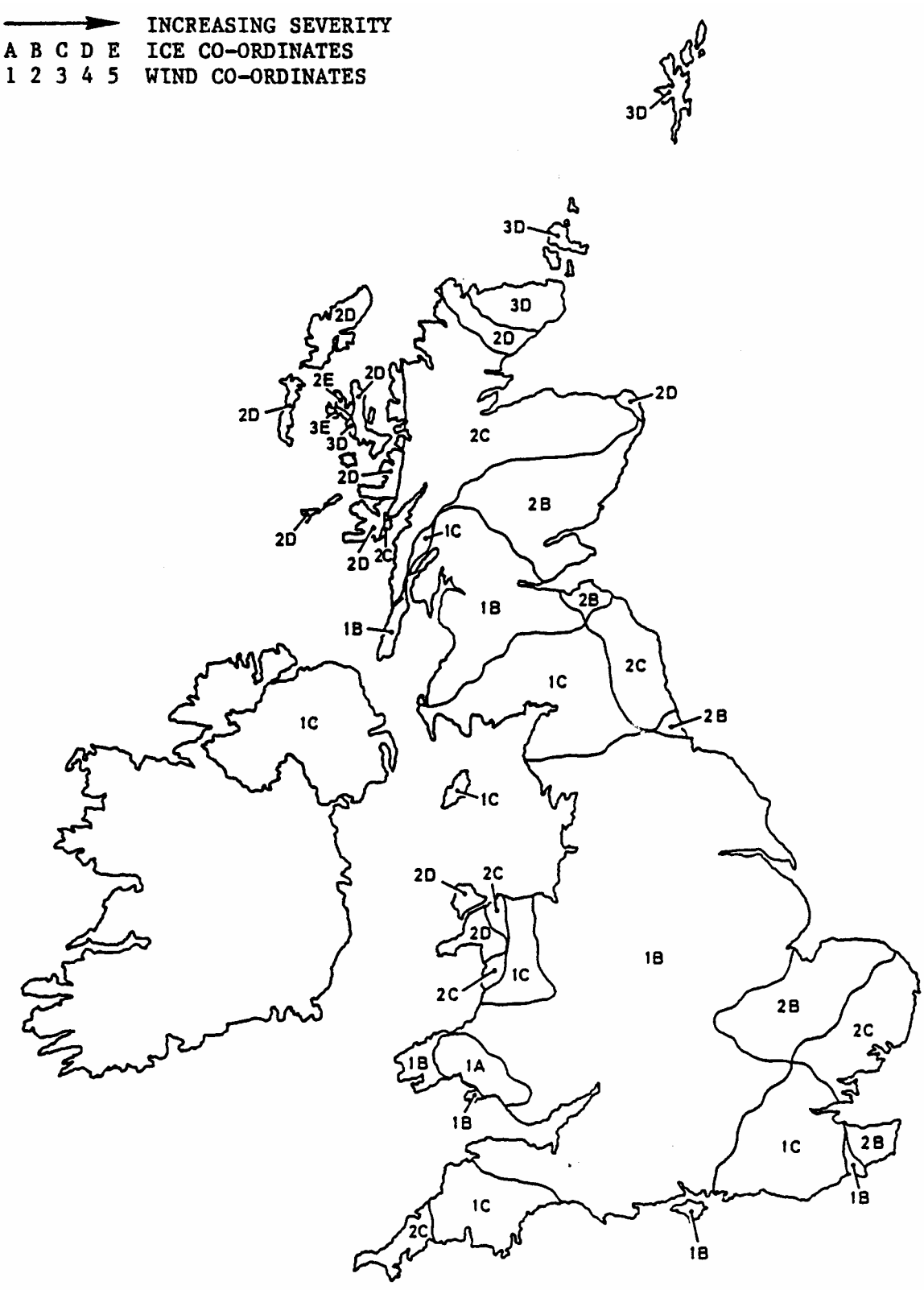

Figure 56: Sea level ENATS 43-40 wind/ice map

The UK National Normative Aspect (NNA) of BSEN 50341 (BSEN 50341-3-9) has been drafted around the use of BS 8100 Part 1 using probabilistic methods (deemed 'General Approach') and also around the use of ENATS 43-40 maps using deterministic methods (deemed 'Empirical Approach'). The BSEN 50341 includes the two UK wind/icing maps mentioned. From the two maps, users are able, with the aid of associated software, to assess line performance against user-defined line and site parameters.

5.2.2.2.1 Treatment of Accretion Rate with Height

General Approach

The basic wind speed, $\overline{V_B}$, is obtained from the wind maps in BS 8100 Part 1 which are based on the GB Meteorological Office data. The data is presented as the maximum mean hourly wind speed independent of direction, at a height 10m above level ground in basic open terrain category III (see Table 15), at the site of the structure. The data has an annual probability of occurrence of 0.02 (i.e. a return period of 50 years). The appropriate map for the GB is shown in Fig. 57 adjusted for sea level. For each 100m above mean sea level (AMSL), the map value is increased by 10% to obtain $\overline{V_B}$ at 10m above the general ground level.

Variation of Wind Speed with Height

Sites in Level Terrain

For all sites in level terrain, the mean wind speed, $\overline{V_z}$, at a height *z* metres above the site ground level shall be taken as:

$$\overline{V_z} = \overline{V_B}\left(\frac{z - h_e}{10}\right)^{\alpha} \quad for\ z \geq 10 + h_e \tag{70}$$

$$\overline{V_z} = \frac{\overline{V_B}}{2}\left(1 + \frac{z}{10 + H_e}\right) \quad for\ z < 10 + H_e \tag{71}$$

where α is the power law index of variation of speed with height to be obtained from Table 15 appropriate to the site terrain and H_e is the effective height of surface obstructions to be obtained from Table 15, appropriate to the site terrain.

Dynamic Pressure

The dynamic pressure, q_z at height *z* shall be taken as:

$$q_z = \left(\frac{\rho_a}{2}\right)\overline{V_z}^2 \tag{72}$$

where ρ_a is the density of air, which may be taken as 1,22 kg/m^3 for Great Britain.

Note: *z* shall be taken as the mean height of the conductors under swung condition when calculating conductor loadings or the mean height of the tower panel being considered when calculating tower wind loadings.

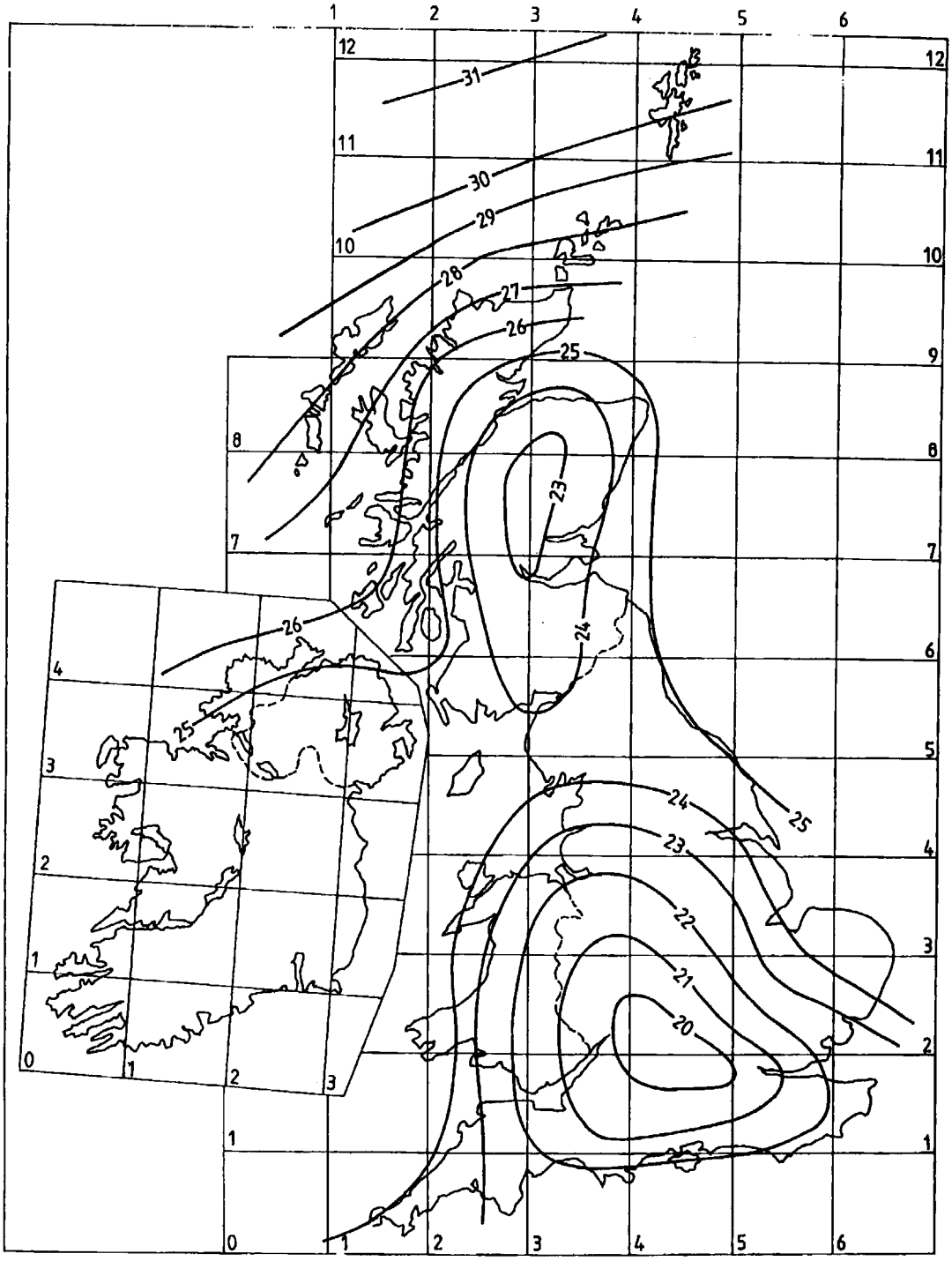

NOTE 1. Values are at sea level in basic open terrain, category III

NOTE 2. Values are in metres per second.

Map 1. **Basic mean hourly wind speeds for UK, V_b (metres per second)**

Figure 57: Wind loads under BS 8100 – Reference [62]
Table 15: Terrain Characteristics – Reference [62]

Category	Terrain description	Terrain roughness factor K_R	Power law index of variation of wind speed with height α	Effective height H_e (m)
I (z_o = 0,003 m)	Snow covered flat or rolling ground without obstructions; large flat areas of tarmac; flat coastal areas with off-sea wind	1,20	0,125	0
II (z_o = 0,01 m)	Flat grassland, parkland or bare soil, without hedges and with very few isolated obstructions	1,10	0,14	0
III (z_o = 0,03 m)	Basic open terrain, typical GB farmland, nearly flat or gently undulating countryside, fields with crops, fences or low hedges, or isolated trees	1,00	0,165	0
IV (z_o = 0,10 m)	Farmland with frequent high hedges, occasional small farm structures, houses or trees	0,86	0,190	2
V (z_o = 0,30 m)	Dense woodland, domestic housing typically covering 10% to 20% of the plan area	0,72	0,230	10

NOTE 1 z_o is the terrain aerodynamic roughness parameter
NOTE 2 The lower (smoother) of any two possible categories should be adopted where the environs of the site are difficult to define or may change
NOTE 3 The terrain description should apply to environs extending several kilometres upwind from the site
NOTE 4 Higher (rougher) categories that occur within only a few kilometres upwind from the site, may not be sufficiently extensive to develop an equilibrium wind profile and should not generally be used for determining the terrain category
NOTE 5 In urban areas (z_o = 0,8m) where towers rise above the general level of the surrounding buildings, category V should be adopted. Specialist advice should be sought where considerations of local accelerations from adjacent high buildings could affect the tower design.

Combined Wind and Ice Load

Ice Thickness in Conjunction With Wind

The basic ice thickness in conjunction with wind, on conductors for the UK, shall be taken as:

$$r_B = k_I \left[r_w + \left(\frac{H - 200}{25} \right) \right] \qquad (73)$$

But not less than $k_I \cdot r_w$, where:

k_I and *a* are as defined in ice only case;
r_B is the ice thickness when wind is not considered, i.e. ice load only.
H is the height of the conductor above sea level.
r_w is the radial ice thickness in mm in conjunction with wind, to be obtained from Fig. 58, appropriate to the position of the site. Alternatively, r_w may be derived from records, having an annual probability of occurrence of 0,5.

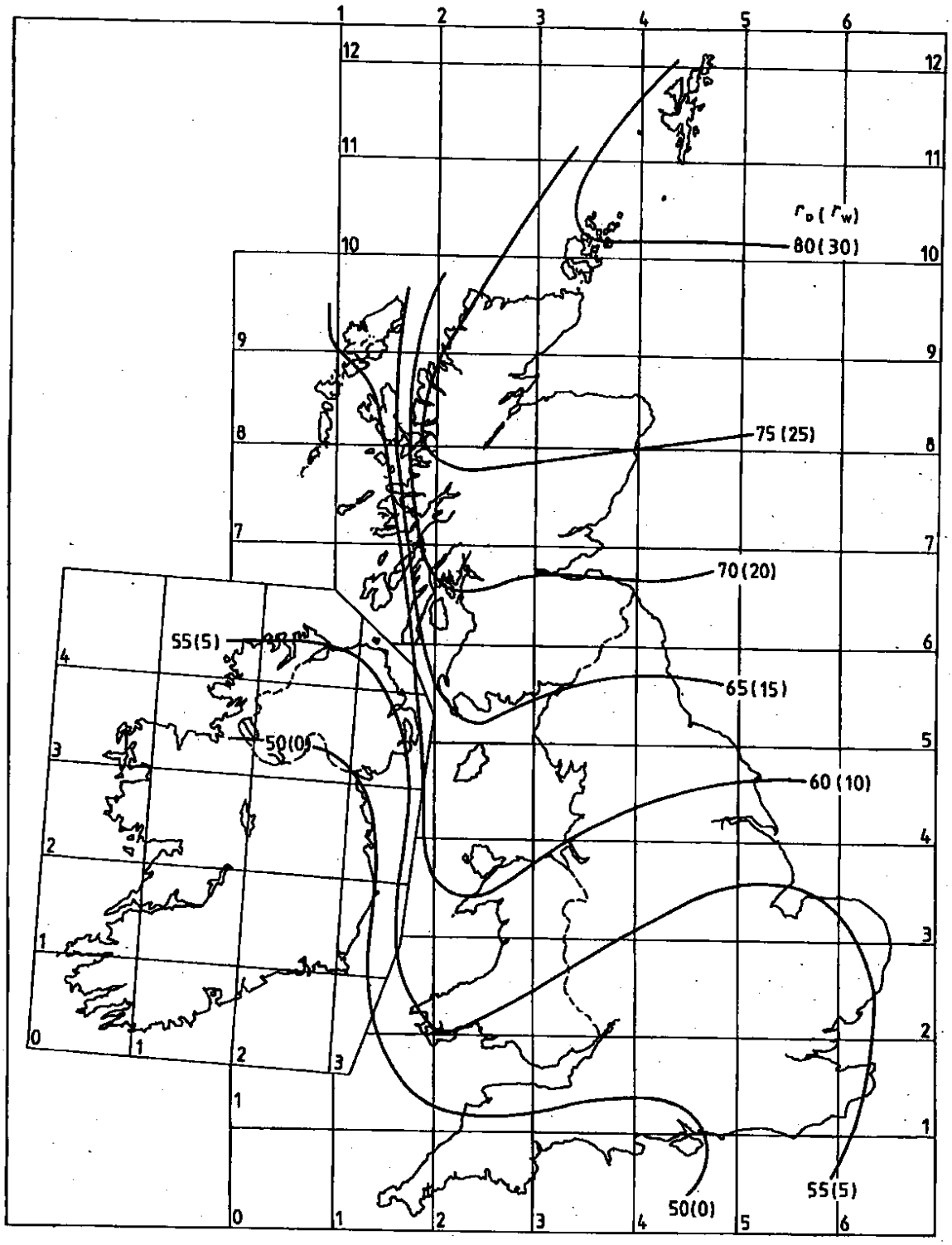

All thicknesses are in millimetres.

Map 2. Ice thickness for UK, r_o and r_w (in millimetres)

Figure 58: Ice loads under BS 8100 – Reference [62]

5.2.3 Topographical Influence on Wet Snow Accretion

In complex terrain, there may be large spatial variability in wet snow accretion. Studies have shown [48, 49] that mountains may favor wet snow icing upstream by increasing precipitation, creating a low level inversion and a barrier wind (see Fig. 59). Wet snow icing may also be favored locally immediately downstream of mountains, by increased precipitation (spill-over), or by strong local winds, such as gap winds in mountain passes or atmospheric gravity waves over the lee slopes (see Fig. 60).

In the “IceDat” database [46], the most serious damages of the Icelandic overhead distribution lines occur where lines run perpendicular to a dominating strong local wind. The lines at most risk run typically across valleys or fjords, downstream of a mountain pass or downstream of mountain slopes that favor gravity waves in the wind.

Probably the best attempts toward wet snow modeling based on dynamic weather models are described in [48,49]. This model includes realistic description of mountains and is probably the first direct approach to connect wet snow modeling with regular weather forecasting models (Figs. 61 and 62).

Mountains may favour wet snow icing upstream by:

- **Increasing precipitation (up to several 100 of %)**

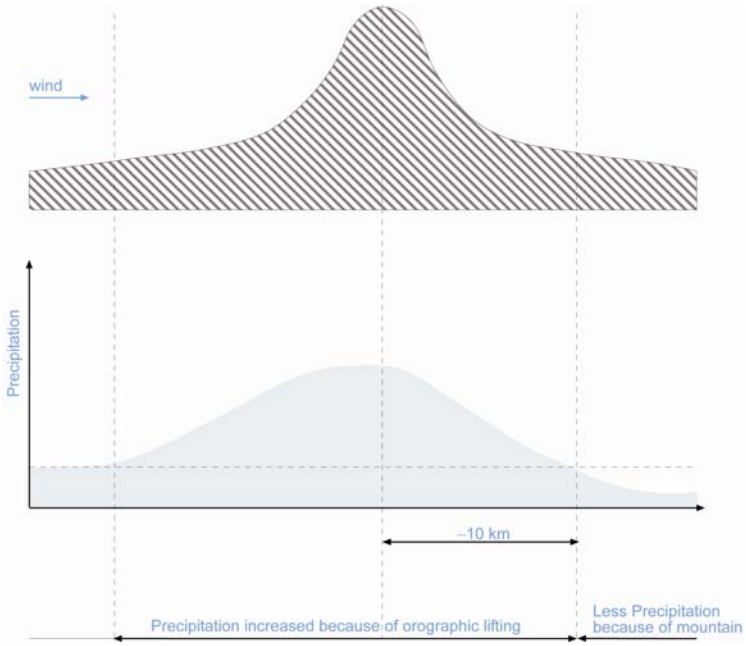

- **Creating a low level inversion**

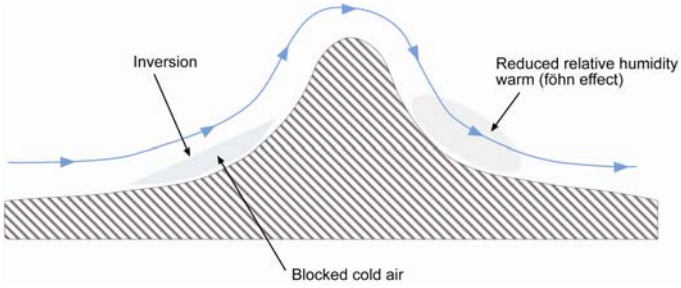

- **Creating a barrier/corner wind**

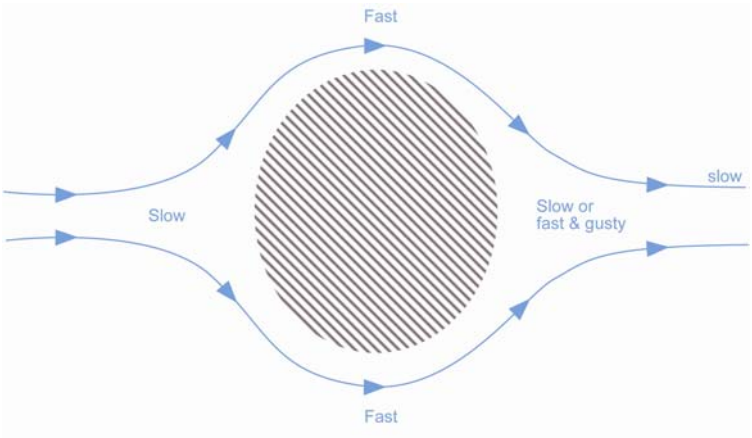

Figure 59: Schematic picture of the mountain influence on wet snow icing: upstream

Mountains may favour wet snow icing downstream by:

- **Increasing precipitation (up to several 100 of %)**

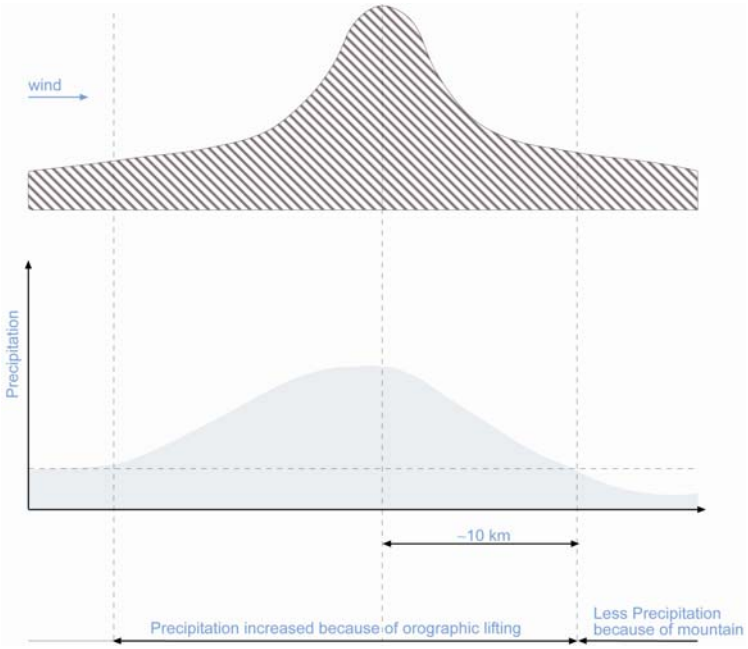

- **Increasing wind speed, e.g. through gravity waves**

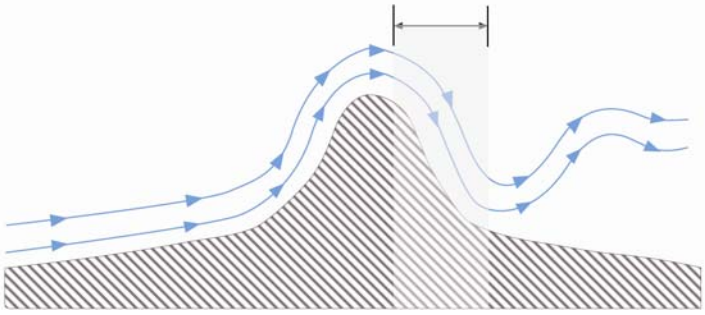

- **Reducing relative humidity while snowflakes may still be wet and sticky**

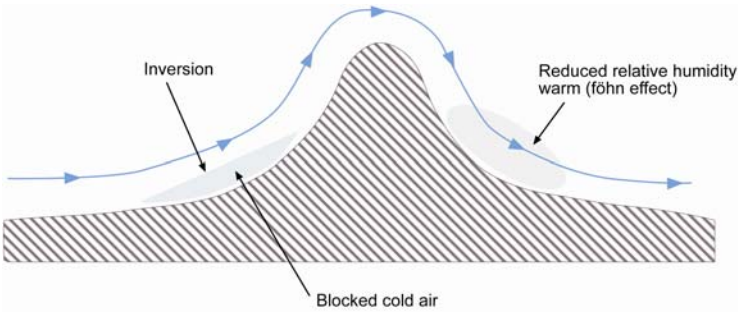

Figure 60: Schematic picture of the mountain influence on wet snow icing: downstream

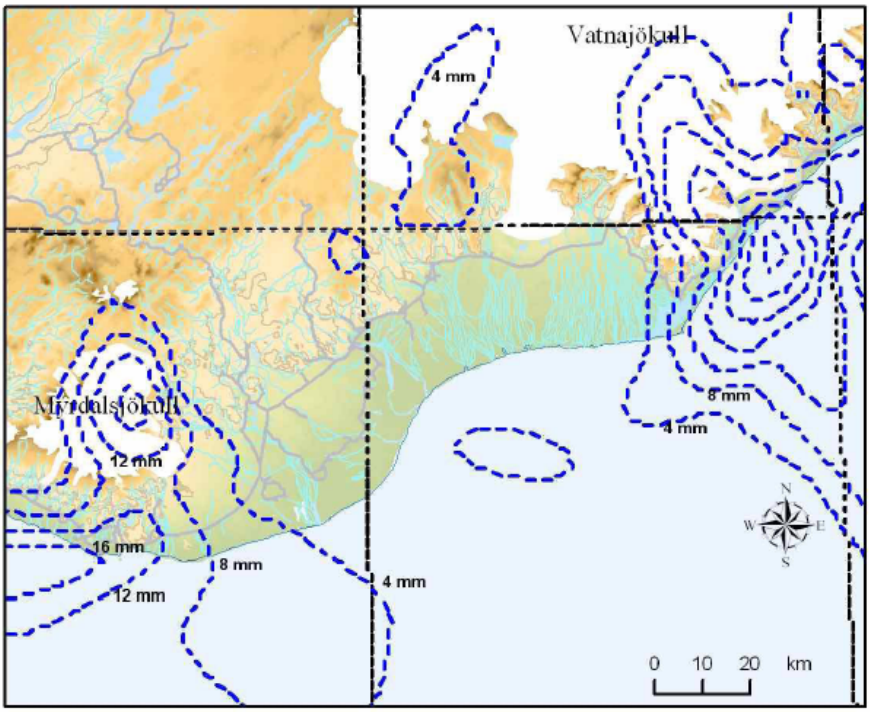

Figure 61: Precipitation (mm) as simulated by a dynamic weather model during a wet snow event upstream of mountains [48, 49]

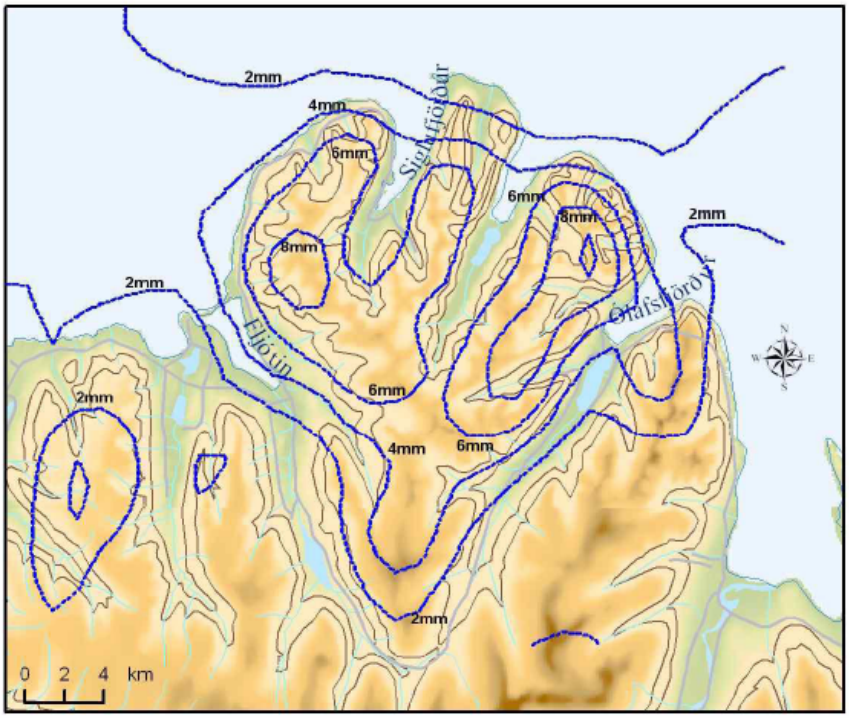

Figure 62: Precipitation (mm) as simulated by a dynamic weather model during a wet snow event downstream of mountains [48, 49]

6. APPLICATION OF ATMOSPHERIC BOUNDARY LAYER MODELS

6.1 Principles of a Weather Forecasting System

Modern meteorology and weather forecasts are based on mathematical models that describe the dynamical and physical processes in the atmosphere. However, before the models can run they need a detailed description of the state of the atmosphere at the starting point for the model. For this purpose observations are made at fixed hours worldwide of air temperature, air pressure, wind, humidity, clouds, precipitation, etc., both on the ground by manned or automatic weather stations, and vertically by radiosondes fixed to balloons that may reach throughout 80 – 90 % of the atmosphere. Satellites provide now important supplementary information, especially over areas where there is little conventional information (oceans, polar regions, etc.).

This chapter is mainly based on [96].

More important for icing is of course the water (vapour) cycle in the lower atmosphere near the earth's surface. This is still the most difficult part, but since it is so important for cloud formation, initiation of precipitation, precipitation intensity, etc., this weather element is object for wide global studies. One of the most studies of this kind is the "Global Energy and Water Cycle Experiment" (GEWEX) and its sub-project "Global Water Vapor Project" (GVaP). GEWEX is headed by the World Meteorological Organization (WMO) in collaboration with the UNESCO World Climate Research Programme. It has been going on for many years and the results are constantly being implemented in dynamic and physical models for the atmosphere, both for climatic studies and indeed also for forecasting purposes.
More information on this can be found in www.gewex.org.

A weather forecasting system consists then accordingly of two main parts, a data assimilation system and a forecasting model. The purpose of the data assimilation is to combine observations and forecasts in an optimal way in order to produce initial values for the unknown parameters in the 3D computer model of the atmosphere.

The forecasting model itself is a system of time-dependent partial differential equations, and if solved in a limited domain needs both initial and boundary conditions. The system of partial differential equations is discretized in space, and integrated forward by a time stepping scheme.

A meteorological model is, in principle, a mathematical description of the atmosphere based on the following physical laws:

1. Newton's second law of mechanics (the sum of forces on an air "parcel" equals the mass times acceleration of the parcel)
2. Equation of state (thermodynamic)
3. Conservation of mass

The output of a weather forecasting model consists both of variables in the equations, for example winds, vertical velocities, temperature, pressure and humidity, as well as output from parameterization of other variables, for example surface fluxes of heat and momentum and components of radiation.

6.2 Nesting of Models

Nesting in this context means that we are using a model with relatively coarse resolution on a large domain (macro- and meso-scale) to provide initial and boundary conditions for a model with a relatively fine resolution on a smaller domain. The boundary conditions are time-dependent and are made continuous in time by interpolation. For stability reasons the "jumps" in resolution form one model to another cannot be too big. Therefore it is necessary to combine models of several levels of resolution, one included into the other, to obtain good and realistic results for weather phenomena near the ground. See illustration in Fig. 63.

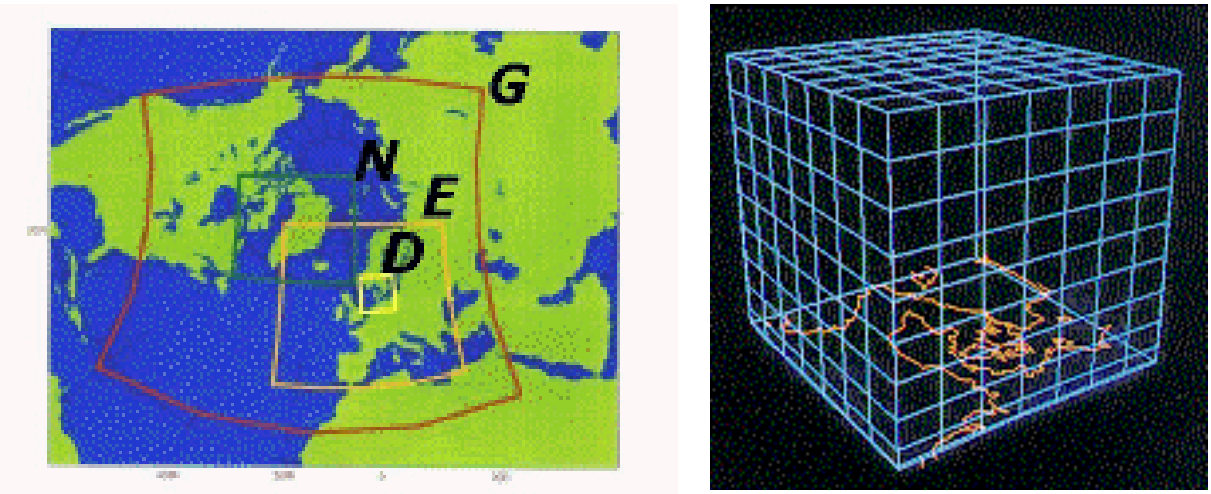

Figure 63: Illustration of model nesting. A semi-global model "G" gives boundary conditions to regional and local models stepwise as shown in left figure. The local model "D" (right figure) has its boundary forced by the outer model on 5 sides and by the earth characteristics in the bottom plane. (From dmi.dk)

What can we achieve by nesting? Some important features are:

- Use of more accurate topography and surface fields.
- Fields with more accurate spatial variation, for example in the case of wind in mountainous terrain.
- Prediction of turbulence.
- More efficient use of computer resources, running with fine resolution on a large domain is very costly.
- Better spatial variations of parameterised fields, for example cloud cover and precipitation.
- Possibilities for local data assimilation.
- Better predictability for local short-range forecasts.

Model nesting have been used for a number of years and the experience with the performance of fine scale models, say in the 0,1 - 1 km range, is continuously improving. Especially this is important for stable air conditions that prevail under freezing rain (and in some cases also wet snow). Air pressure, temperature, wind direction, wind speed and turbulence parameters can be very well modelled in modern computers also in detail for very complex terrain.

Icing models depend on many other types of data that may not be directly available in the resolution we want. In particular, the water cycle in the atmosphere has to be improved in order to be sufficient for describing all types of icing phenomena. However, there are great ongoing international efforts to improve the descriptions of processes involving water and therefore it is important to check current status whenever meteorological models shall be used for icing purposes.

6.3 Examples of Application

As mentioned in 6.1, the water, in its various forms, is not yet sufficiently described in meteorological models to make them fully applicable for calculations of atmospheric icing. However, a complete icing model also includes parameters for air temperature, wind speed, wind direction and often turbulence.

The latter parameters can be much better described in space by 3D atmospheric models, compared with interpolations from regular measurement networks, especially in more complex terrain.

Since complete icing studies are still to be done, three examples of application of such models on wind conditions in mountainous terrains are showed in the following. It should be noted that such model outputs could be used together with measurements of precipitation rates or cloud observations in order to improve icing assessments within the model areas. In particular such model experiments could improve combined wind and ice load estimates.

The first example is shown in Fig. 64. The wind conditions are known to be very extreme in the valley and fjord areas shown with light yellow and light green colours. Two double circuit 132 kV lines were planned to cross this area transverse to the wind, and the Norwegian wind code indicated a gust wind speed of 75 m/s at the top conductor height of 30 m. A model set-up was established as outlined in Section 6.2. The model results showed significantly lower winds, especially concerning the vertial wind profile and the design gust wind speed was reduced to 60 m/s. The model output was in this case well confirmed by measurements.

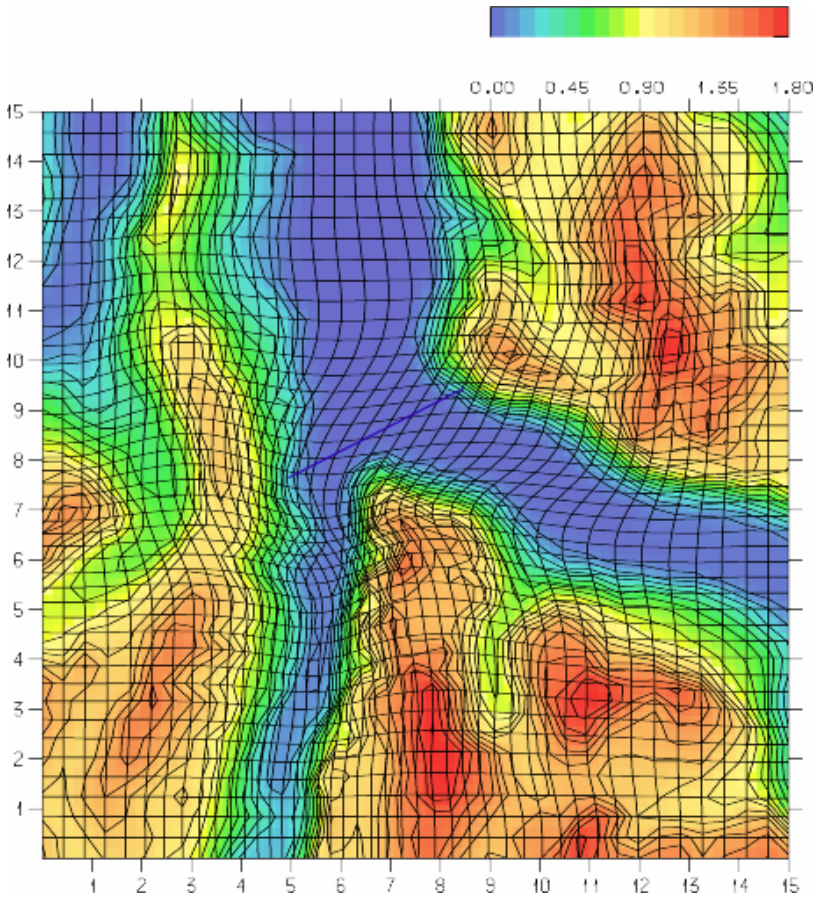

Figure 64: 15x15 km^2 model topography of Sunndalsøra area, Norway. Fjord to the north (upwards), valleys towards S (down) and SE (down right from center). Height contours every 100 m and colour scale (km) shown on the top. The mountains reach over 1500 m asl (marked with red). A new 132 kV transmission line is crossing the two valleys near the fjord bottom (solid line). From [97].

In the second example, a similar model was established to identify the turbulence characteristics along a 3 km long fjord crossing in western Norway. Figure 65 shows the wind and turbulence conditions in a vertical plane, perpendicular to the span, behind a 1400 m high mountain on the western (upwind) side.

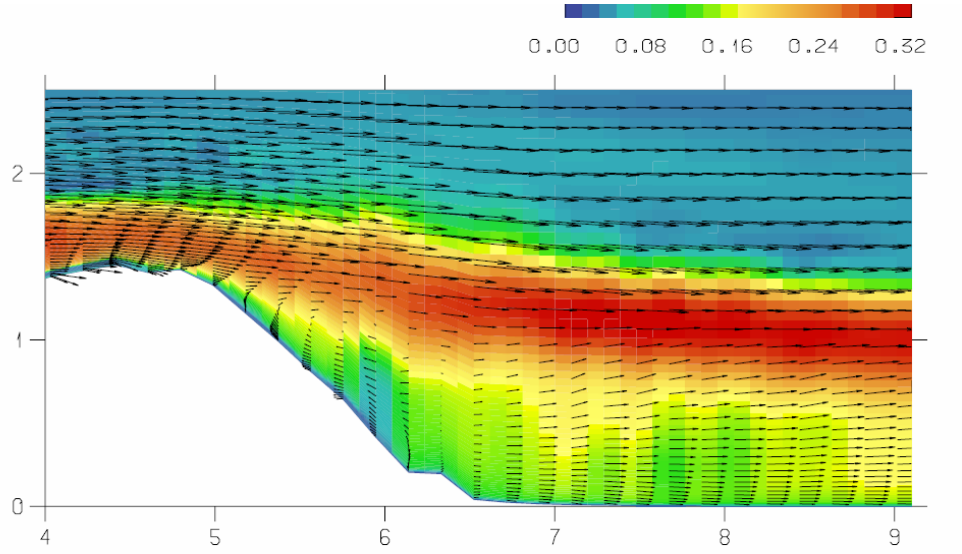

Figure 65: An example of the wind distribution in a vertical plane from south (centre bottom of Fig. 64) over Sunndalsøra towards north (right) over the fjord. Horizontal and vertical length unit: km. The turbulence intensity is shown with the colour code on top of figure (normalized values), blue: low turbulence, red: high turbulence. Note the near constant wind speed with height at the position of the line, approximately 6.8 km from the southern (left) boarder of the model. From [97].

Figure 66 shows another graphic representation of model outputs from the first example. The vertical plane can be inserted to illustrate the 3D model output. The grid distances in both examples are of the order 200 – 500 m.

Figure 67 shows an example where the topography influences the surface wind in a stable stratification of the atmospheric boundary layer. The figure shows a situation where a cold SE wind is blowing from land over the sea and is influenced by coastal islands. It is seen from the figure that local winds may be totally opposite (direction change of 180°) within a few km and in both places almost perpendicular to the main wind direction. A local vortex appears also west of the northern tip of the island. Similar wind patterns may be found in all areas where freezing rain occurs. Then there is always a temperature inversion with cold air near the ground (freezing layer) and warmer air aloft (melting layer).

Such models cannot be used directly for extreme value calculations. However, it may often be useful to compare one site with another, and hence have better foundations for assessing differences in wind, ice or combined wind and ice loadings. Also, certain case studies could be important for failure analyses for certain events in either remote areas or in areas with particular topographical characteristics.

Model studies like the ones presented above have often been produced by so-called “Computer Fluid Dynamics” (CFD) models. The innermost models used above (for instance in Fig. 67) could well be of the same kind. However, the great advantage with the nested model system described above is that it is dynamic and takes care of the actual stability of the atmosphere. Also they require much less computer resources than traditional CFD calculations.

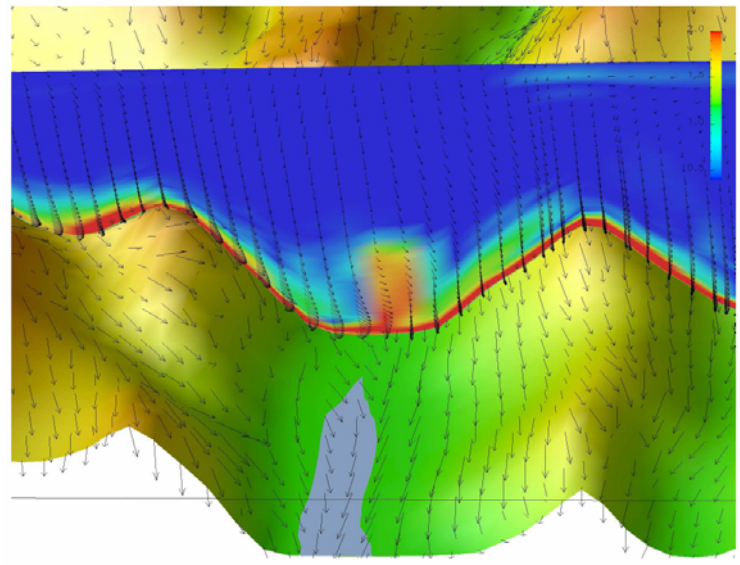

Figure 66: Same model as Fig. 64, but seen from North. (This is "upside-down" compared with Fig. 64. S: upwards, N: downwards, E: left and W: right.). Arrows show wind speed and direction over the surface (2 m height) as well as in a vertical plane, approximately where the 132 kV lines cross the valley bottom. Colours in the vertical cross section represent turbulent kinetic energy (relative scale, blue: low turbulence, red: high turbulence). From [97].

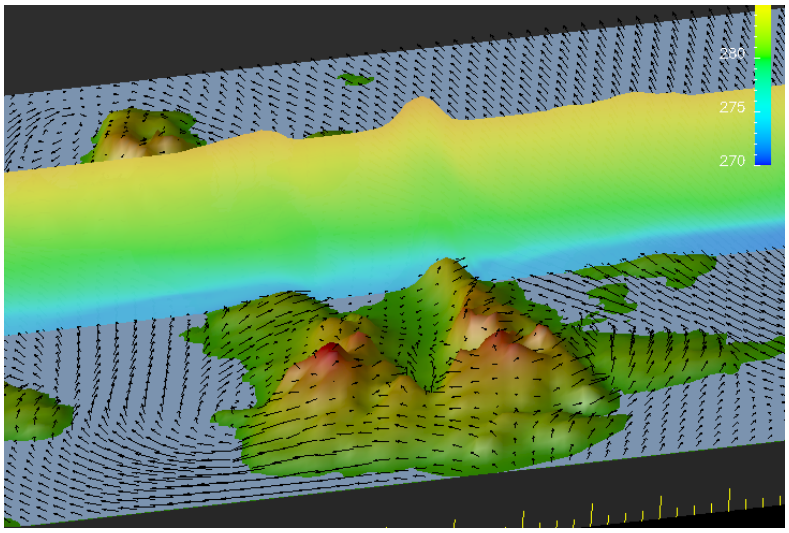

Figure 67: A model study of the wind pattern around the island Vannøya, Northern Norway, in a situation with strong SE winds and a strong temperature inversion near the surface. The grid size is 250 m (distance between arrows). The highest mountain of Vannøya is 1033 m asl (peak at lower left). The vertical cross section plane shows the vertical temperature distribution (scale in °K on top right). A well-mixed cold air layer is near the ground and a well-mixed warmer layer above. This is resulting in a wind flow around the island that is much stronger influenced by the topography than in a neutral atmosphere. See for instance the western sound (lower left part of figure) where the wind is blowing from east (almost perpendicular to the main airflow) and north of the highest peak where there is a strong wind blowing from west, and from southwest in the eastern sound.

7. CONCLUSIONS AND FUTURE WORK

Ice load modeling is still in the development stage. All icing models should have been calibrated for the specific icing types, structures, climatological conditions and topographic locations of their intended use. It is important to appreciate that the accuracy of the ice load predictions depends upon the quality of climatological data used as input into the models. The reliability of the prediction increases as the length of the climatological data records and the frequency of icing events increase.

It is important to monitor ice accretions and ice loads for power utilities in all countries where damage cost due to ice loads is high. Such time series of observations may be long, costly and difficult to obtain but are of great value for obtaining statistically reliable distributions of ice loads. Generally, the Gumbel distribution is adopted for extreme value distribution of ice loads. However, POT methods are more suitable for irregular events like wet snow accretion in mild climate areas, for which GEV distribution are inadequate. It is highly recommended to keep the initial distributions, including date and time, as a reference for future analyses in the study of loads on structures. More research is needed in this field.

However, care should be taken in correlating data from meteorological stations to the actual line route because of the influence of the topography, without applying appropriate transfer models. The estimated ice load values should be adjusted appropriately to account for height differences, unusual terrain changes and other unique features associated with the line route, such as valleys, hills, etc. In general, topography is the basis for defining ice load maps which split the country up into specific areas according to their wind and snow/ice susceptibilities.

The science of meteorology has developed significantly during the last decades. In particular, the combination (nesting) of operational forecasting models with turbulence models of smaller scales, e.g. down to 100 – 300 m grid size, has already provided results that make them interesting for overhead line applications.

Finally, it is relevant to underline the importance of careful awareness regarding ice accretions in the future, especially in the light of a varying climate. Increased temperatures of the atmosphere will consequently lead to higher atmospheric humidity. The variability and projected changes in climate may affect the icing conditions, mostly in northern latitudes. However, the pattern is relatively complex, but it may be likely that the frequency of wet snow may decrease in coastal lowlands and increase in inland (continental) areas. Rime icing may decrease in lower mountain areas and increase in higher altitudes. It is not so obvious how freezing rain may be affected. The frequencies and intensities of such icing depend strongly on the geographical location with respect to the seas as well as on the local topography. Each country or region is recommended to evaluate their own risks depending on these factors.

8. REFERENCES

[1] "Design criteria of overhead transmission lines", IEC 60826 – Ed. 3.0 (2003).

[2] "Overhead lines – Meteorological data for assessing climatic loads", IEC Technical Report 61774, First Edition, August 1997.

[3] "Atmospheric Icing of Structures", ISO 12494, First Edition, August 2001.

[4] CIGRÉ Brochure 109 "Improved design criteria of overhead transmission lines based on reliability concepts", 1996.

[5] CIGRÉ TB 179, "Guidelines for Field Measurement of Ice Loadings on Overhead Power Line Conductors", August 2000.

[6] Farzaneh M., "Ice Accretion on High-Voltage Conductors and Insulators and Related Phenomena", Philosophical Transactions of the Royal Society, Vol. 358, No. 1776, November 2000, pp. 2971–3005.

[7] Schaub, W.R., "Methods to Estimate Ice Accumulations on Surface Structures", 7th IWAIS, University of Chicoutimi, Canada, June 1996.

[8] Chaîné, P.H. and Skeates, P., "Ice Accretion Handbook (Freezing and Precipitation)", *Industrial Meteorology – Study VI*, Environment Canada, Toronto, Canada, 1974.

[9] McComber, P. and Govani, J.W., *Proc. 42nd Annual Eastern Snow Conference*, Montreal, Canada, 1983.

[10] Schaub, W.R., *2nd Conference on Mountainous Meteorology*, America Meteorological Society, Rostes, MA 1981, pp. 41-45.

[11] Thom, H.C.S., *Proc. Chicago Design Symposium*, North Western University, Evanstan, 1L, 1970, pp. 17-34.

[12] Makkonen, L., "Modelling of Ice Accretion on Wires", *J. Climate and Applied Meteorology* 23, 1984, pp. 929-39.

[13] Makkonen, L., CRREL Monograph 84-2, CRREL, Hanover, NH 1984.

[14] Chaîné, P.M. and Castonguay. A., "New Approach to Radial Ice Thickness Concept Applied to Bundle-Like Conductors", *Industrial Meteorology – Study IV*, Environment Canada, Toronto, Canada, 1974.

[15] McComber, P., "A non-circular accretion shape freezing rain model for transmission line icing", 9th IWAIS, EA Technology, Chester, UK, June 2000.

[16] Poots, G., "Ice and Snow Accretion on Structures", Research Studies Press Ltd, Somerset, UK, 1996.

[17] Chen, Y., Farzaneh, M., Lozowski, E.P., Szilder, K., *9th IWAIS*, EA Technology, Chester, UK, June 2000.

[18] Mason, B.J. (1971) "Physics of Clouds", Clarenden Press, Oxford 2nd Edition p610.

[19] Wareing, J.B., Chetwood, P., "Ice load data from Deadwater Fell", *IWAIS 2000*, Chester, UK, June 2000.

[20] Admirat, P. and Sakamoto, Y., "Wet snow on overhead lines: State of the Art", *Proc. 4th IWAIS*, Paris, France, 1988.

[21] Savadjiev, K. and Farzaneh, M., "Modelling wind and ice loads on overhead power line conductors", IWAIS 2002, Brno, Czech Republic, 17-20 June, 2002.

[22] Peabody, A. and Jones, K.F., "Effect of wind on variation of ice thickness", IWAIS 2002, Brno, Czech Republic, June 17-20, 2002.

[23] Best, A.C., "The Size Distribution of Raindrops", Quarterly J. of Royal Met. Soc., Vol. 76, pp. 418-428, 1950.

[24] Jones, K.F. and Peabody, A., "The Application of a Uniform Radial Ice Thickness to Structural Sections", IWAIS 2002, Brno, Czech Republic, 17-20 June, 2002.

[25] McComber, P., Druez, J., Sabourin, G., "Comparison of ice loads on ground wires, single and bundled conductors", *IWAIS 2002*, Brno, Czech Republic, 17-20 June, 2002.

[26] Ervik, M and Fikke, S (1982a). "Development of a mathematical model to estimate ice loading on transmission lines by use of general climatological data," *IEEE Transactions On Power Apparatus & Systems*, Vol PAS-101, No 6, pp 1497-1503.

[27] Farzaneh, M. and Savadjiev, K., (2001).“Icing Events Occurrence in Quebec: Statistical Analysis of Field Data” *International Journal of Offshore and Polar Engineering*, Vol. 11, No 1, March 2001, pp. 9-15.
[28] Fikke, S, Schjetne, K and Evensen, BD (1982). “Ice Load Measurements and Design Practice,” *Proceedings of the 1st International Workshop on Atmospheric Icing of Structures*, Hanover, NH, USA, pp 277-289.
[29] Gumbel, E J, (1958). *Statistics of Extremes*, Publ by Columbia University Press.
[30] Foder, M.H. (2001), “ISO 12494 ‘Atmospheric Icing of Structures’ and How to Use It”, *Proceedings of the 11th International Offshore and Polar Engineering Conference*, Volume I, June 17-22, Stavanger, Norway, pp. 678-685.
[31] Krishnasamy, S. and Kulendran, S. (1996). “Combined Wind and Ice Loads from Historical Extreme Wind and Ice Data,” *Proceedings of the 7th International Workshop on Atmospheric Icing of Structures*, Chicoutimi, Québec, pp.119-124.
[32] Laflamme, J. and Périard, G., “The Climate of Freezing Rain Over the Province of Québec in Canada: A Preliminary Analysis,” *Proceedings of the 7th International Workshop on Atmospheric Icing of Structures,* Chicoutimi, Québec, pp. 19-24, 1996.
[33] Popolansky, F., Kruzik, J., Lehky, P., Hrabanek, J, and Lago, J. (1998). “Ice Monitoring at Stand Studnice. Tuned Vibration Control of Overhead Line Conductors”, *CIGRE Paper 22-105*, Session – 1998, Paris.
[34] Savadjiev, K. and Farzaneh, M. (2002). “Modeling Asymptotic Distributions of Extreme Icing from Various Initial Distributions,” *10th International Workshop on Atmospheric Icing of Structures*, Brno, Czech Republic, June, 2002.
[35] Savadjiev K., Farzaneh, M. and Fikke, S. (2001). “Extreme Value Analysis of Ice Accretion Data from Norwegian Measurement Rack Network”, *Proceedings of the 11th International Offshore and Polar Engineering Conference*, June 17-22, Stavanger, Norway.
[36] Savadjiev, K., Farzaneh, M., McComber, P., Druez, J. and Paradis, A., “Analysis and Interpretation of Icing Rate Meter and Load Cell Measurements on the Mt. Bélair Icing Site,” *The 9th International Offshore and Polar Engineering Conference (ISOPE 1999)*, Brest, France, 1999.
[37] Savadjiev, K. and Farzaneh, M., “Modeling of Icing and Ice Shedding on Overhead Power Lines Based on Statistical Analysis of Meteorological Data,” *Accepted for publication in IEEE – Transactions of Power Delivery* (Jan. 2004).
[38] Bourgsdorf, V.V., Nikiforov, E.P., Bassarskaya, T.A., Golikova, T.N., Lomilina, L.E. and Toporkova, G.D., “Methodology of compiling the regional ice-load maps used in design and operation of OH transmission lines“, SPO ORGRES, Moscow, 1976.
[39] Lomilina, L.E., “Methodological principles of construction of regional wind-speed maps“, Elektricheskije stanzii, No. 8, 1985.
[40] Podresov, O.A., “Maximum wind and ice loads in the mountainous regions of the USSR“, Trans. Wind and ice loads on the structures of OH lines in mountainous regions, Moscow, 1986, p.p.49-57.
[41] Bassarskaya, T.A., Golikova, T.N., Lomilina, L.E., Nikiforov, E.P. and Toporkova, G.D., “Ice and ice-wind loads on OH line conductors“, *CIGRE Symposium 22-81*, Sweden, Stockholm, 1981, 111-08.
[42] Lomilina, L.E. and Nikiforov, E.P., “Estimation of macro-terrain influence on ice loads basing on experimental data“, Synopsis of the reports of the meeting “Influence of climatic factors on OH transmission lines”, Moscow, 1983.
[43] Golikova, T.N., Toporkova, G.D. and Nikitina, L.G., “Ascertaining ice-load maps of the USSR territory“, Trans. “Improving the reliability of High voltage transmission lines”. Moscow, Energoatomizdat, 1989, p.p.107-122.
[44] Lomilina, L.E., Terrain typification for the construction of the regional wind- and ice-load maps. Moscow, Energoatomizdat, 1989, pp. 122 – 126.
[45] Harstveit, K., “Using routine meteorological data from airfields to produce a map of ice risk zones in Norway”, *Proc.10th IWAIS*, Brno, Czech Republic, June 2002.
[46] Ísaksson, S.P., Elíasson, Á.J., Thorsteins, E., “Icing Database – Acquisition and Registration of Data”, *Proc. of the 8th International Workshop on Atmospheric Icing of Structures,* Reykjavík, Iceland, 8-11 June 1998, pp 235-240.

[47] Thorsteins, E., Elíasson, Á.J., “Iceload Measurements in Test Spans in Iceland – Statistical Analysis of Data”, *Proc. of the 8th International Workshop on Atmospheric Icing of Structures*, Reykjavík, Iceland, 8-11 June 1998, pp 285-289.
[48] Ólafsson, H., Elíasson, Á.J. and Thorsteins, E., "Orographic Influence on Wet Snow Icing - Part I", *Proc. (CD-Rom) of the 10th International Workshop on Atmospheric Icing of Structures*, Brno, Czech Republic, 17–20 June, 2002.
[49] Ólafsson, H., Elíasson, Á.J. and Thorsteins, E., "Orographic Influence on Wet Snow Icing - Part II", *Proc. (CD-Rom) of the 10th International Workshop on Atmospheric Icing of Structures*, Brno, Czech Republic, 17 – 20, June, 2002.
[50] Krishnasamy, S. and Fikke, S., “An objective approach for selecting ice or wet-snow design loads on transmission lines” in G. Poots (ed.) Phil. Trans. R. Soc., vol 358 number 1776, pp 3007-3033. London, November 2000.
[51] “Ryfylke Og Setesdalen Vaerstatistikk For Kraftlinjetraseer”, Report No. 05/96 KLIMA, Prepared by Det Norske Meteorologiske Institutt, Oslo, Norway, January 1996.
[52] Anderson, R.S. and Richmond, M.C., "Ontario-Hydro Wind and Ice Loading Model", Meteorological Research Inc., California, 1977.
[53] Langmur, I. and Blodgett, K.B., "A Mathematical Investigation of Water Droplet Trajectories", Tech. Report No. 5418, U.S. Army Air Force, 1946.
[54] Canadian Electricity Association, “Beta testing of icing models“, CEA Report No ST-331-C, April 1998.
[55] Canadian Electricity Association, “Validation of accretion models for freezing application using field data“, CEA 331 T 992 (A-D), 166 p, 1998.
[56] Eliasson, A.J. and Thorsteins, E., “Data analysis of icing measurements in Iceland“, *5th IWAIS*, Budapest, Hungary, June 1993.
[57] Wareing, J.B., “Ice accretion loads on different conductors to apply to ETR 111 line design“, EATL Report 4720, January 1999.
[58] Grenier, J.C., Admirat, P. and Maccagnan, M., “Theoretical Study of Heat Balance During the Growth of Wet Snow Sleeves on Electrical Conductors”, *3rd IWAIS*, Vancouver, Canada, 1986.
[59] Wu, S. and Liu, Z., “Comprehensive Report on Problem of Ice (Snow) – Line of Power System in China“, *Proc. 5th IWAIS*, Tokyo, Japan, 1990.
[60] Jones, K.F., “A Simple Model for Freezing Rain Ice Loads”, *Proc. of the 7th International Workshop on Atmospheric Icing of Structures*, Chicoutimi, Canada, 1996, p. 412-416.
[61] Jones, K.F., “Ice Accretion in Freezing Rain”, CRREL Report 96-2, Cold Regions Research and Engineering Laboratory, Hanover, New Hampshire.
[62] British Standard Lattice Towers and Masts, Part 1, Code of Practice for Loading, BS8100, Part 1, 1996.
[63] Kuroiwa, D., “Icing and Snow Accretion on Electric Wires”, U.S. Army CRREL Report, 17-3, p. 10, 1965.
[64] Mitten, P. and Makkonen, L., “Development of an Operational Ice and Wind Load Model for Transmission Lines”, Draft Report submitted to Atmospheric Environment Services, Toronto, Ontario, Canada, 1989.
[65] Yip, T.C., “Estimating Icing Amounts Caused by Freezing Precipitation in Canada”, *Proceedings of the 6th IWAIS*, Budapest, Hungary, 20-22 September, 1993.
[66] Stallabrass, J.R. and Hearty, P.F., “The Icing of Cylinders in Conditions of Simulated Sea Spray”, Mechanical Engineering Report MD-50, NRC No. 9782 National Research Council, Ottawa, Canada, 1967.
[67] McKay, G.A. and Thompson, H.A., “Estimating the Hazard of Ice Accretion in Canada from Climatological Data”, *Journal of Applied Meteorology*, Vol. 8, No. 6, pp. 927-935, 1969.
[68] Haldar, A., Mitten, P. and Makkonen, L., “Assessment of probabilistic climatic loadings on existing 230kV steel transmission line”, *Proc. 4th IWAIS*, Paris, France, 1988.
[69] Canadian Climate Centre, “Climatological Ice Accretion Modelling”, Report No. 84-10, Atmospheric Environment Service, Downsview, Ontario, p. 195, 1984.
[70] Goodwin, E.J., Mozer, J.D., DiGioia, A.M. and Power, B.A., “Predicting Ice and Snow Loads for Transmission Line Design”, *Proc. 1st IWAIS*, L.D. Minsk (Ed.), 1-3 June, 1982, Hanover, New Hampshire, CRREL Special Report 83-17, pp. 267-273, 1983.

[71] Makkonen, L. and Fuji, Y., “The Amount of Icicles on Power Line Cables”, 5th IWAIS, 1990.
[72] MEP, “Software Implementation for Climatological Ice Accretion Modelling Project”, Report prepared for the Atmospheric Environment Service under DSS Contract No. OISE.KM147-3-1425, 1984.
[73] Finstad, K., Master’s Thesis, University of Alberta, 1988.
[74] Imai, I., “Studies on Ice Accretion”, *Research on Snow and Ice*, No. 1, pp. 35-44, 1953.
[75] Leavengood, D.C., “Meteorology, Can It Be Useful?”, Canadian Electrical Association, Paper 73-TR-221, 1973.
[76] McComber, P., “Numerical Simulation of Ice Accretion on Cables”, *Proc. 1st IWAIS*, U.S. Army CRREL Special Report 83-17, 1983.
[77] Sakamoto, Y. and Miura, A., “Comparative Study of Wet Snow Models for Estimating Snow Load on Power Lines Based on General Meteorological Parameters”, *Proceedings of the 6th IWAIS*, Budapest, Hungary, 20-22 September, 1993, pp. 133-138.
[78] Houde, L., Guesdon, C., Farzaneh, M. and Chouinard, L., “Analysis of Spatial Patterns for Icing Events in Québec”, *Proceedings of the 9th IWAIS*, Chester, United Kingdom, June 2000.
[79] Laflamme, J., “Spatial Variation of Extreme Values for Freezing Rain”, *Atmospheric Research* 36 (1995), pp. 195-206.
[80] Pézard, J., “A Method to Estimate Icing Loads on Overhead Lines”, *Atmospheric Research* 36 (1995), pp. 303-310.
[81] Laflamme, J., “Spatial Variation of Extreme Values in the Case of Freezing Rain Icing”, *Proceedings of the 6th IWAIS*, Budapest, Hungary, 20-22 September, 1993.
[82] ENATS 43-40 “High voltage single circuit overhead lines on wood poles” (1988).
[83] Admirat, P., Maccagnan, M. and De Goncourt, B., “Influence of Joule effect and of climatic conditions on liquid water content of snow on conductors”, *Proc. 4th IWAIS*, Paris, France, 1988.
[84] Jones, K.F. and Morris, R., “Investigation of the Differences in the Application of the Canadian and U.S. Methodology for Estimates of Ice Loads for a 50-yr Return Period”, Ice Storm Mitigation Interest Group, CEATI Report No. T003700-3306, June 2002.
[85] Hardy, C., Brunelle, J., Chevalier, J., Manoukian, B. & Villandré, R., "Telemonitoring of Climatic Loads on Hydro-Québec 735 kV Lines", *Proceedings of the 7th IWAIS*, Chicoutimi, 3-7 June 1996.
[86] Hardy, C., Brunelle, J., Chevalier, J., Manoukian, B. & Villandré, R., "Telemonitoring of Climatic Loads on Hydro-Québec 735 kV Lines, *J. of Atmospheric Research*, vol. 46, 1998, pp. 181-191.
[87] Hardy, C., Brunelle, J., Beauséjour, Y., Lanoie, R., Laflamme, J.N., & Bellerive, J.P., "Monitoring the Effects of Environmental Factors on Hydro-Québec's Overhead Lines", CIGRE SC22 Main Session, Paris, August 1998.
[88] Pickands, J., "Statistical Inference Using Extreme Order Statistics", The Annual of Statistics, 3, pp. 119-131, 1975.
[89] Hosking, J.R. and Wallis, J.R., “Parameter and Quantile Estimation for the Generalized Pareto Distribution”, Technometrics, 29, No 3, pp. 339-349, 1987.
[90] Walshaw, D., “Getting the most from your extreme wind data: a step by step guide”, J. res. Natl. Inst. Stand. Technol., 99, pp. 399-411, 1994.
[91] Le Du, M. and Laurent, C., “T-Return Period Values of Meteorological design Parameters”, *Proceedings of the 11th IWAIS*, Montreal, June 2005.
[92] Plautikof, J.P., Brabson, B.B., Lister, D.H. and Adcock, S.T., “A review of methods to calculate extreme wind speeds”, Meteorol. Appl. 6, pp. 119-132, 1999.
[93] Coles, S., “An introduction to statistical modelling of extreme values”, Springer Verlag, London, 2001.
[94] Hosking, J.R., Wallis, J.R. and Wood, E.F., “Estimation of the Generalized Extreme Value distribution by the method of probability weighted moments”, Technometrics, vol. 27, no. 3, pp. 251-26, 1985.
[95] Laurent, C. and Parey, S., “Tests on Adjustment Laws of Wet Snow and Rime Loads in France”, *Proceedings of the 11th IWAIS*, Montreal, June 2005.
[96] Fikke, S., “Modern Meteorology and Atmospheric Icing”, *Proceedings of the 11th IWAIS*, Montreal, June 2005.
[97] Holstad, A., Lie, I., Utnes, T. and Ødegaard, V., „ Wind conditions in Sunndalsøra: A study using fine-scale models“, The Norwegian Meteorological Institute, Research Report No. 125, Oslo, July 2001.

[98] Lie, I., “Wind conditions in Fjærlandsfjorden”, The Norwegian Meteorological Institute, Research Report No. 129, Oslo, November 2001.
[99] Gayraud, G., “Risques d’accrétion d’hydrométéores sur les conducteurs électriques aériens“, Météo-France, DP/SERV/BEC, SEBEAC00691, 3 octobre 2002.
[100] *ACIA, Impacts of a Warming Arctic: Arctic Climate Impact Assessment.* Cambridge University Press, 2004.
[101] Admirat, P., "Microphysical aspects of experiments in Japan", EDF/DER/INAG 3365, n°1, 56 p., March 1984.
[102] Admirat, P. and Dalle, B., "Les études expérimentales d'accrétion de neige collante sur les lignes aériennes", Journée d'études SEE, Gif sur Yvette, 43-49, avril 1985.
[103] Admirat, P., and Sakamoto, Y., "Quantitative results and proposed mechanisms on wet snow accretion in the Ishiuchi wind-tunnel facilities", IWAIS 1986, Vancouver, May 1986.
[104] Grenier, J.C., Admirat, P. and MacCagnan, M., "Theoretical study of the heat balance during the growth of wet snow sleeves on electrical conductors", IWAIS 1986, Vancouver, May 1986.
[105] Admirat, P., MacCagnan, M., Lapeyre, J.L., and Sakamoto, Y., "Thermodynamic simulation of the accretion of wet snow study of the heat balance during the growth of wet snow sleeves on electrical conductors". IWAIS 1988, Paris, Sept. 1988.
[106] Admirat, P. and Sakamoto, Y., "Calibration of a wet snow accumulation model on real cases in Japan and France", IWAIS 1988, Paris, Sept. 1988.
[107] Pashinsky, V.A.., *Atmospheric loads on structures*. Kiev. 1999. – 185 p. (in Ukrainian).
[108] Colbeck, S.C. and Ackley, S.F., “Mechanisms for Ice Bonding in Wet Snow Accretions on Power Lines”, *Proc. 1st IWAIS*, Hanover, New Hampshire, 1983.
[109] Hardy, C., Leblond, A. and Gagnon, D., “Theoretical Assessment of Ice Loading of Cables as a Function of their Torsional Stiffness”, Proc. 11th IWAIS, Montréal, June 12-16, 2005, pp. 303-308.

9. APPENDIX I: UK WIND/ICING MAPS

Wind/icing maps are very useful for overhead line design purpose. This appendix presents typical examples of such maps.

For instance, in the UK, wind/icing maps exist for overhead lines which split the country up into specific areas according to their wind and snow/ice susceptibilities. Figures 68 to 72 present a series of maps which cover the range of land height from 0 m up to 500 m in 100 m increments respectively, according to ENATS 43-40. The different wind/ice combinations are described in Tables 13 and 14.

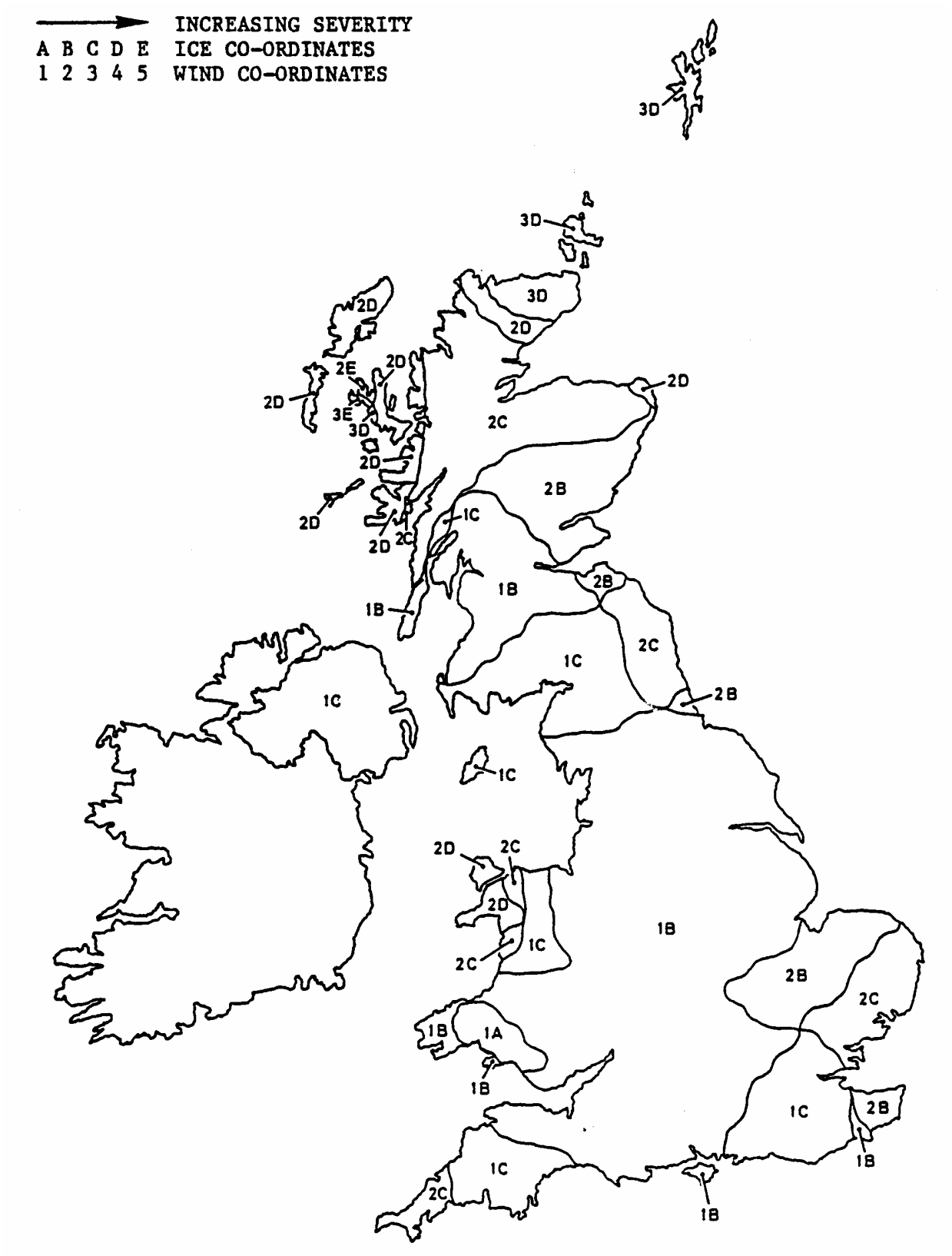

Figure 68: Wind/Icing Zones for site heights of 0 to 100 m

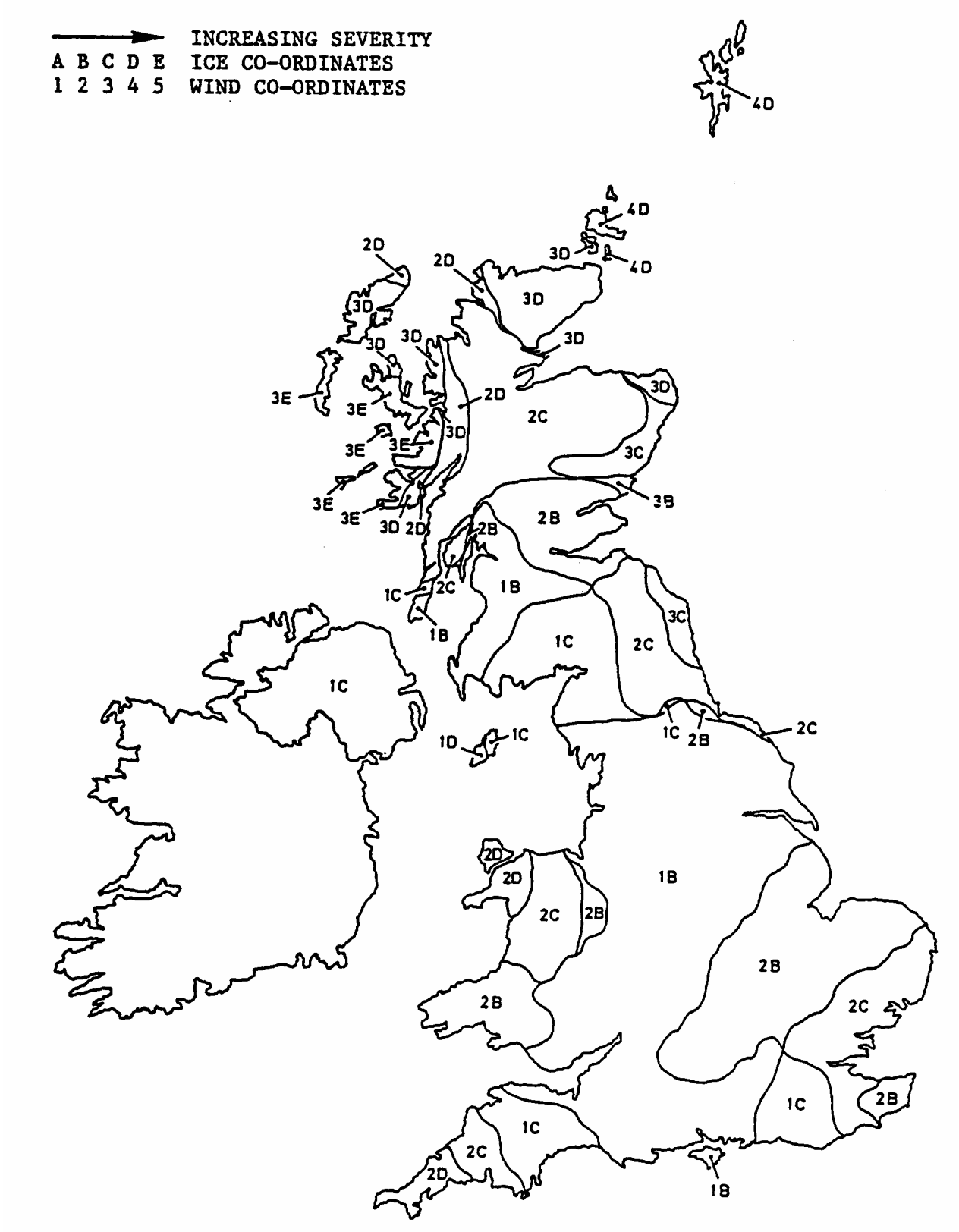

Figure 69: Wind/Icing Zones for site heights of 100 to 200 m

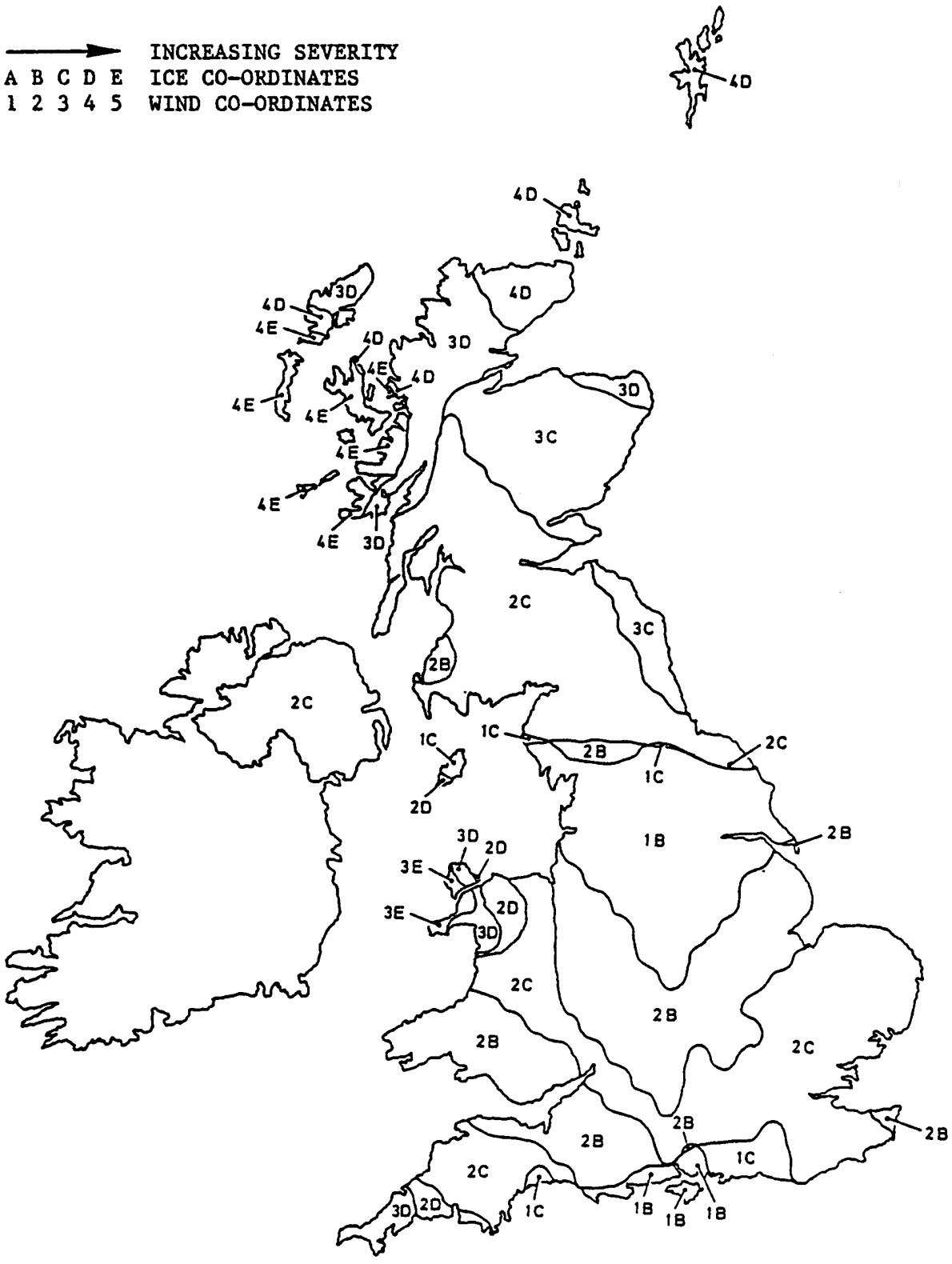

Figure 70: Wind/Icing Zones for site heights of 200 to 300 m

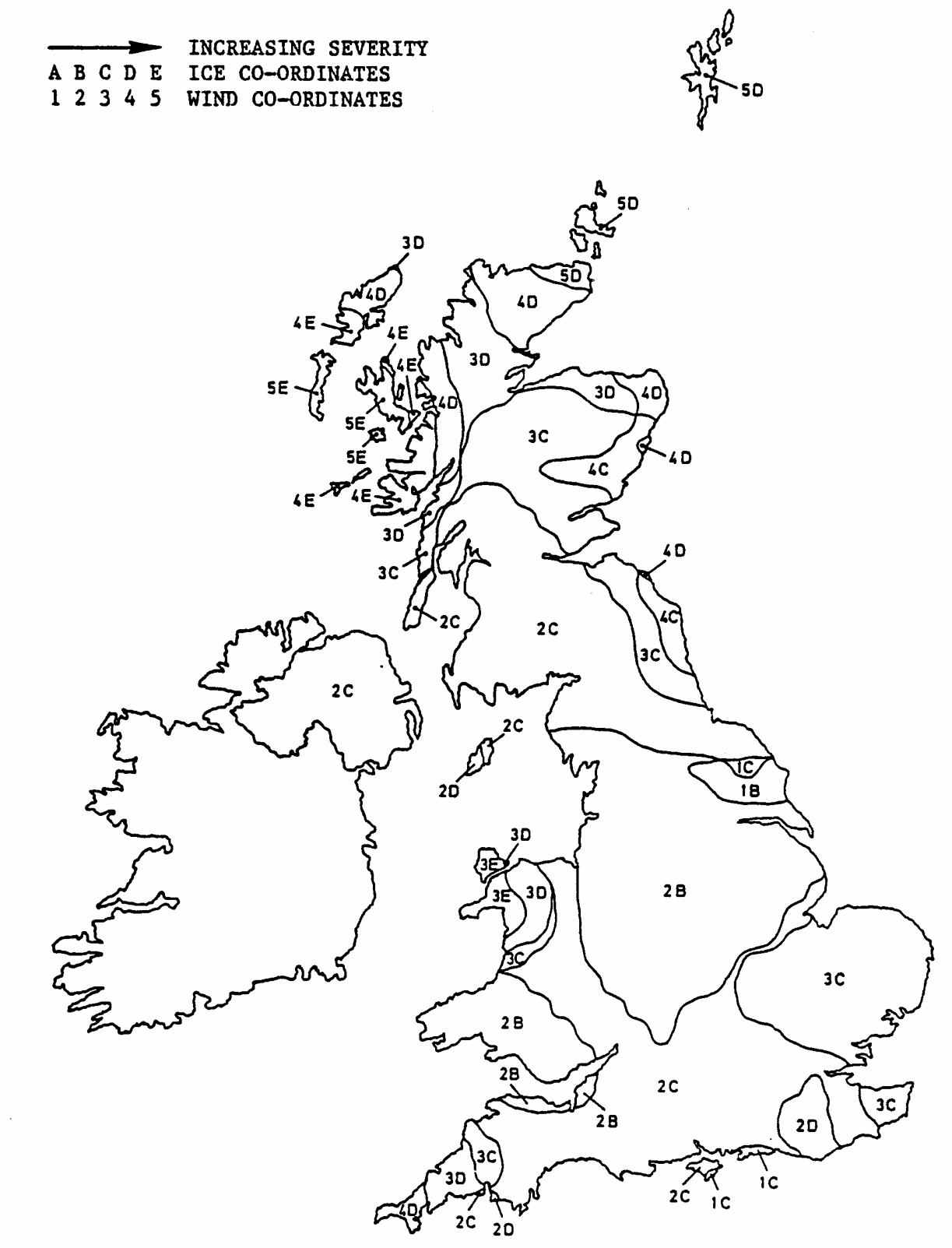

Figure 71: Wind/Icing Zones for site heights of 300 to 400 m

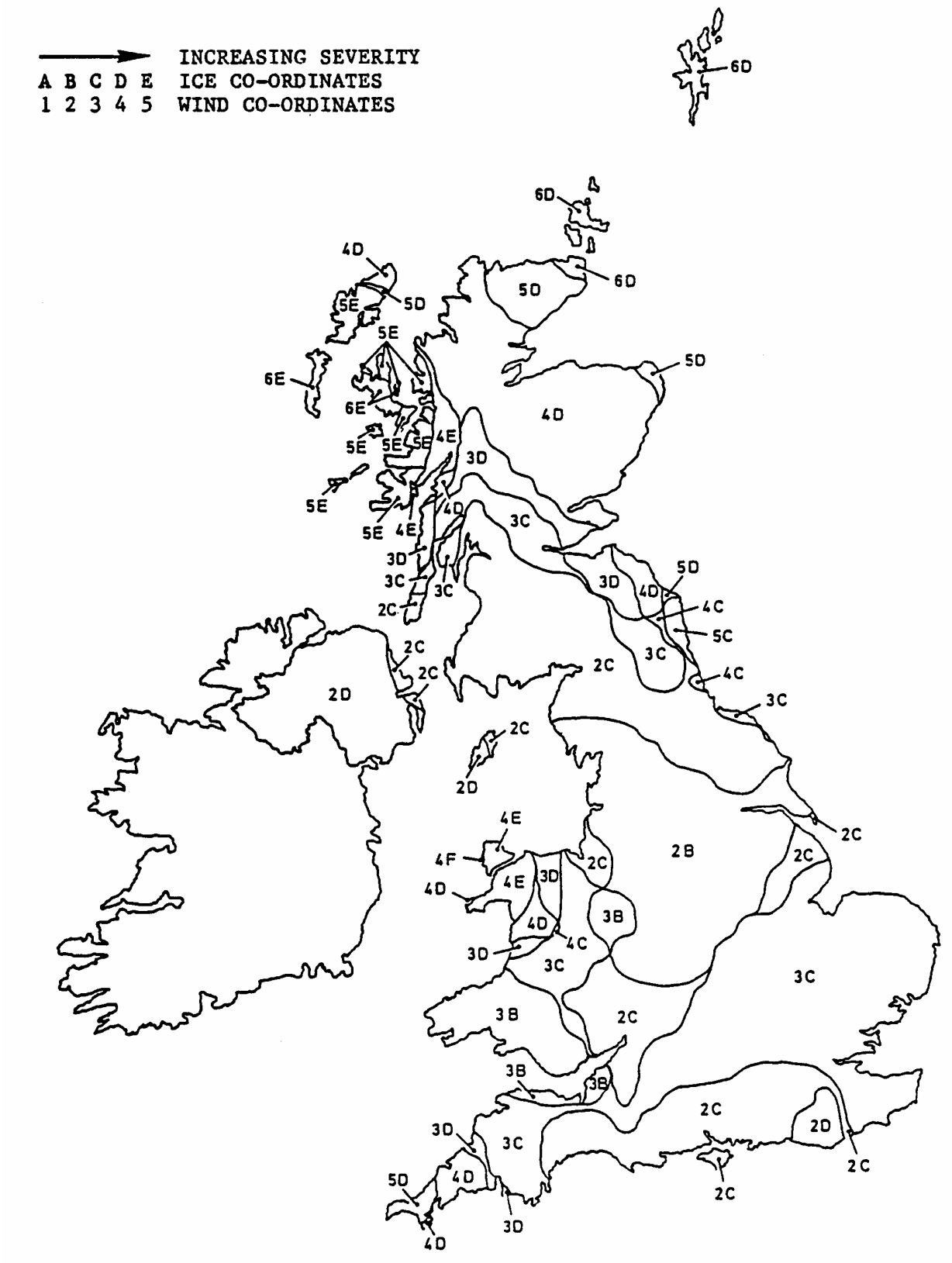

Figure 72: Wind/Icing Zones for site heights of 400 to 500 m

10. APPENDIX II: UKRAINE ICING MAPS

This appendix presents typical examples of icing maps from Ukraine.

The main problem of Ukrainian weather station data is a “human” factor – inaccuracy of measurements. In that way and by some else amplifications the data of weather stations which are situated in one region and in the same conditions may be quite different. For example for Kiev region (territory near 30 000 square kilometers) difference between ice loads are 330% (Borispol – Fastov, distance between is 82 km), 290% (Borispol – Mironovka, distance between is 77 km) and 250% (Borispol – Barishevka, distance between is 25 km). These weather stations are situated in equal conditions.

Figure 73 shows the icing map of the Kiev region.

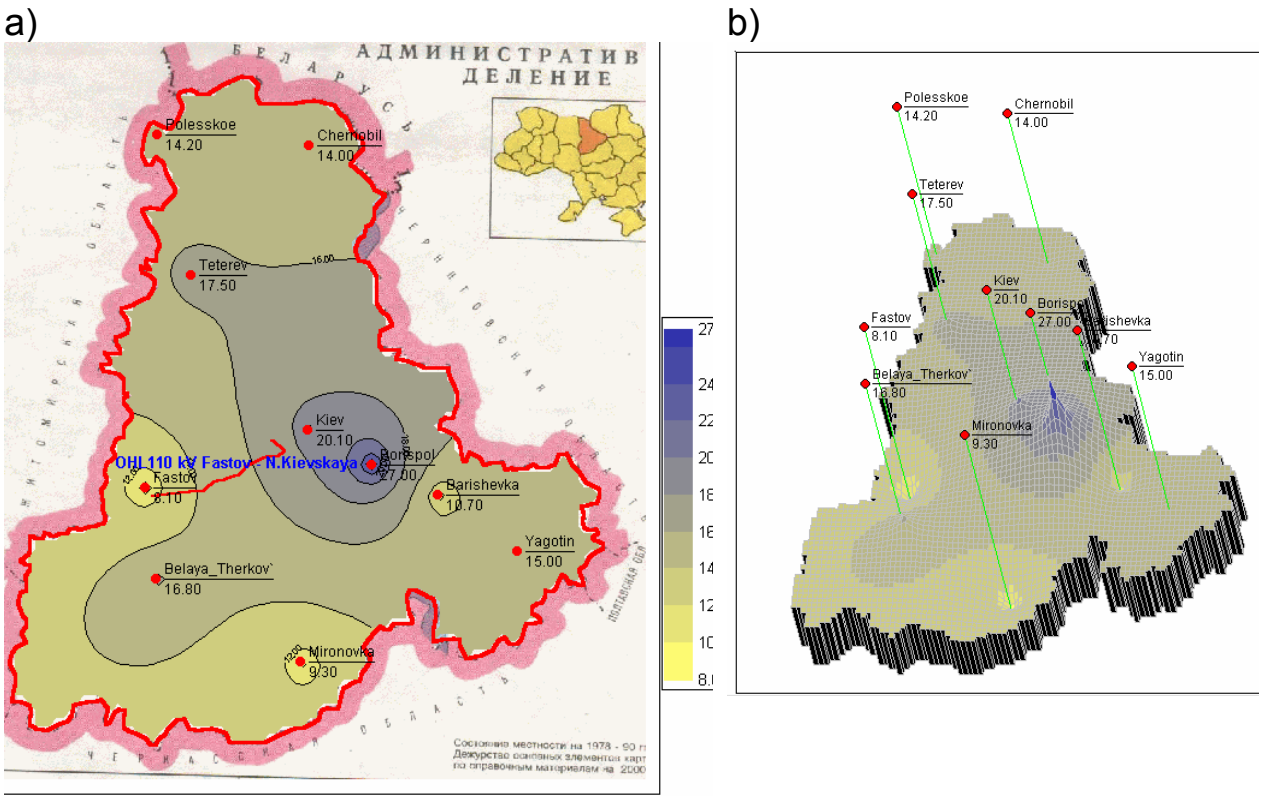

Figure 73: Map of Kiev region zoning by ice load on 1 meter conductor with 10 mm diameter, located on 10 m height above ground level, for return period 50 years, N/m
a) icing map; b) three-dimensional view

For OHTL “Fastov – Novokievskaya” 110 kW (red line on Fig. 73a) with length 57 km the difference of icing load on line route is 150 % (see Fig. 74).

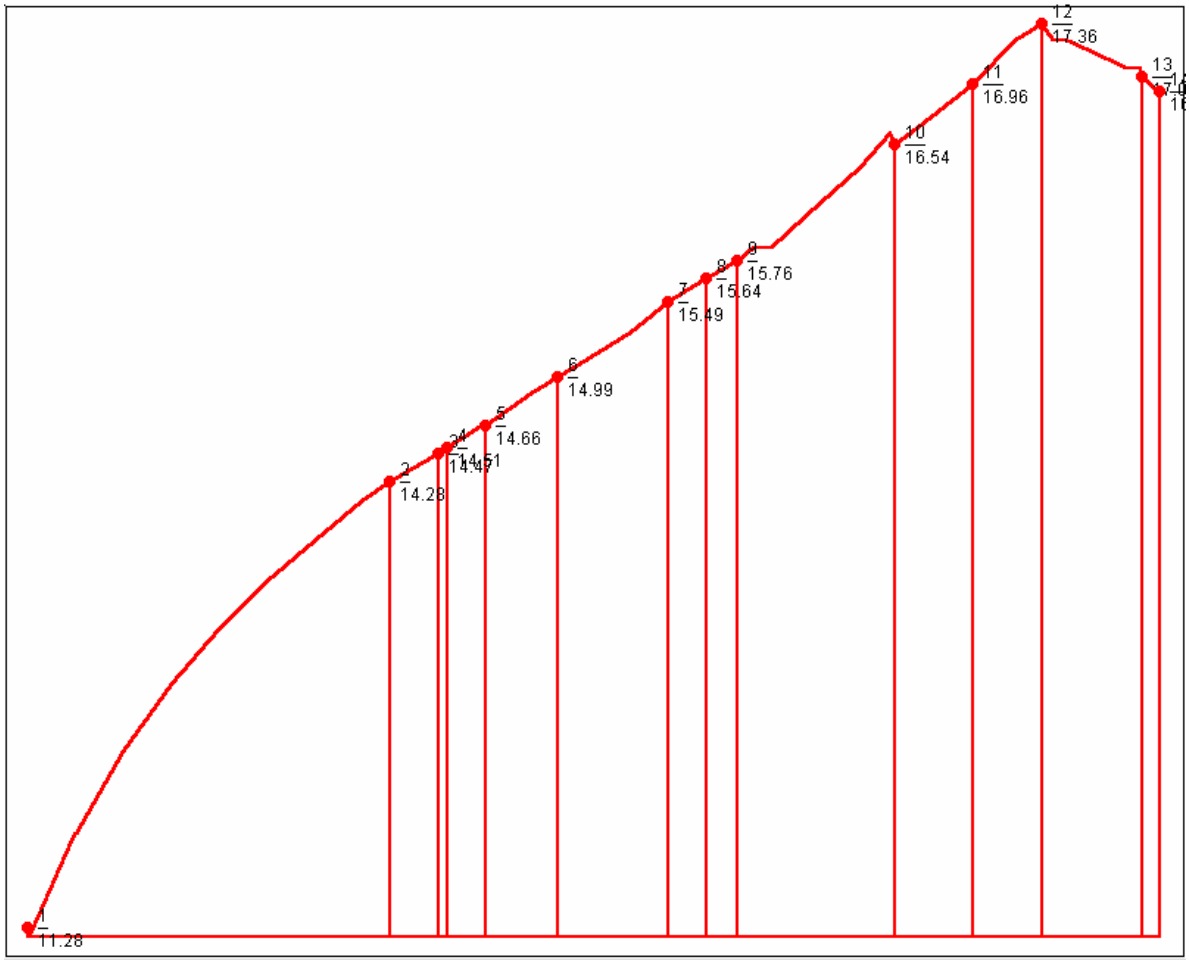

Figure 74: Distributed ice load from the weight of ice for a conductor, 10 mm in diameter on the profile of the route of "Fastov – Novokievskaya" 110 kW (recurrence period of 50 years, for open exposure, 10 m height), N/m

To level the discrepancy, the use was made of smoothing technique [107] by which the mean value of the random field of an investigated parameter is determined, for any point of the locality, by smoothing the ordinates according to the formula:

$$M = \frac{\sum_{i=1}^{N} Q_i c_i p_i}{\sum_{i=1}^{N} c_i p_i} \qquad (74)$$

where N – is the number of weather stations, Q_i – is the ordinate of the field equal to the value of investigated parameter for the i-th weather station, c_i – is the weighting function of smoothing, p_i – is the weighting function of accuracy which, in most cases, is described as:

$$p_i = \sqrt{n_i} \qquad (75)$$

where n_i – is the volume of data sampling for the i-th weather station.

The weighting function of smoothing is found by the formula:

$$c_i = exp\left(\frac{-d_i}{a}\right) \qquad (76)$$

where a – is the constant determining the measure of smoothing, d_i – is the distance from the point, for which the expectation is calculated, to the i-th weather station.

This procedure was made for all Ukrainian weather stations (without mountainous stations). Figure 75 shows the results obtained after the smoothing operation for example on Fig. 73.

Figure 76 shows the resulting icing load on the OHTL “Fastov – Novokievskaya” line route.

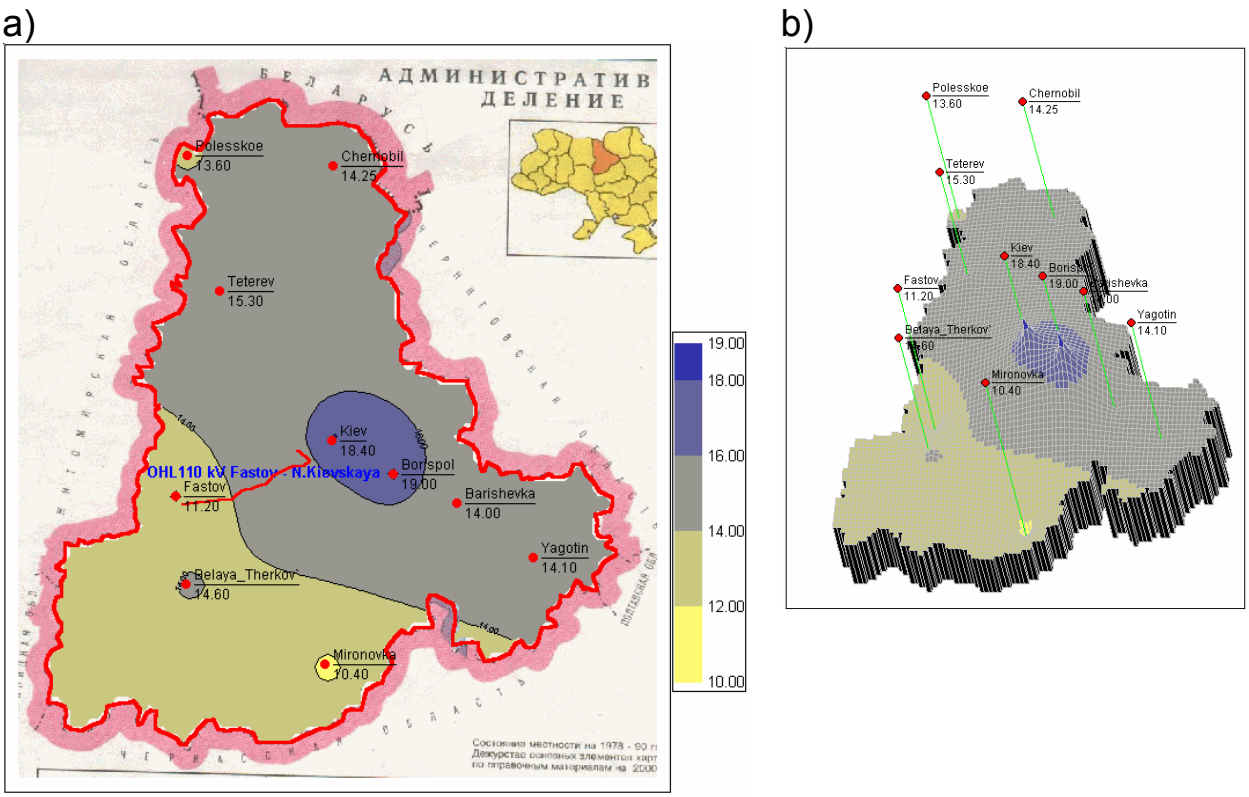

Figure 75: Map of Kiev region zoning by smoothing ice load on 1 meter conductor with 10 mm diameter, located on 10 m height above ground level, for return period 50 years, N/m
a) icing map; b) three-dimensional view

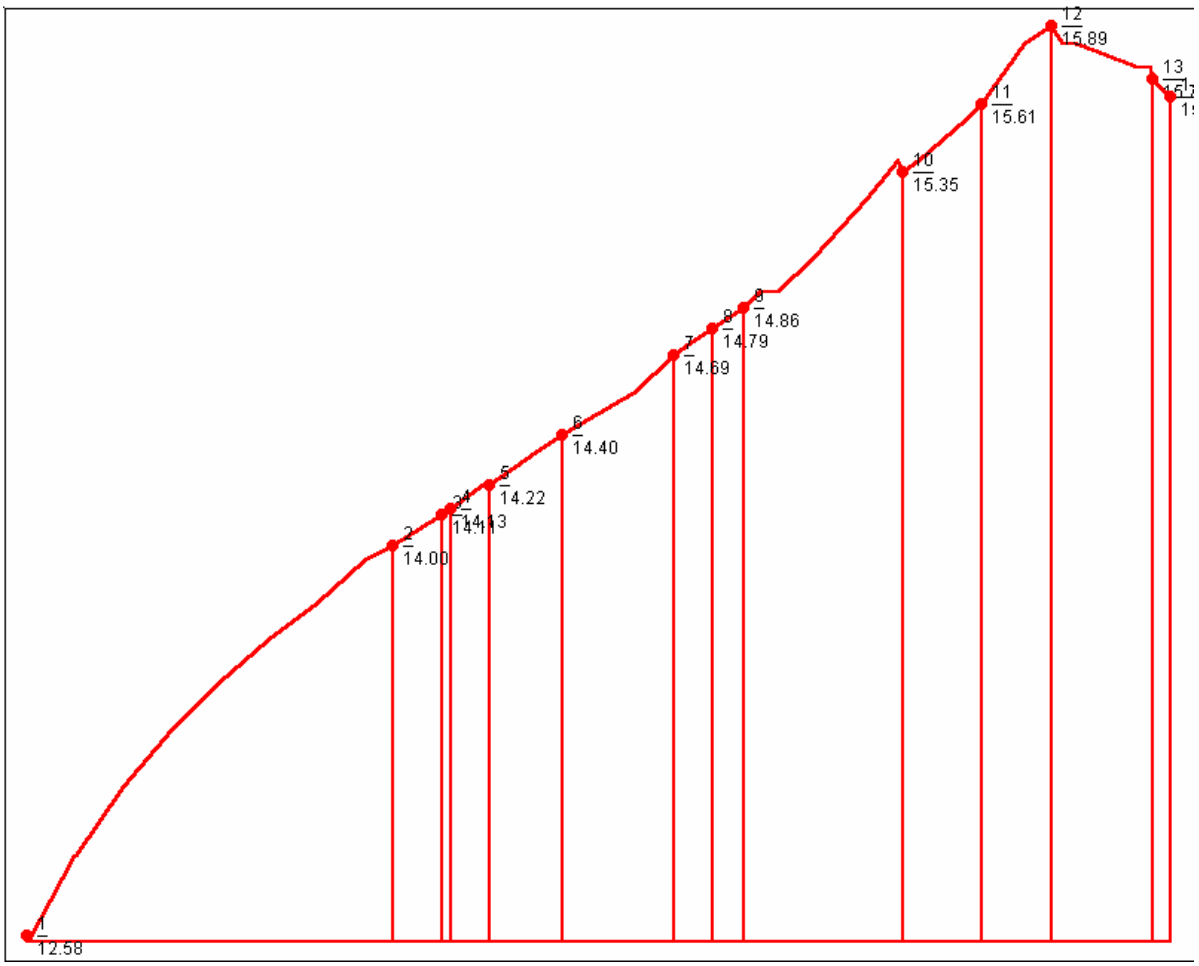

Figure 76: Distributed ice load from the weight of ice for a conductor, 10 mm in diameter on the profile of the route of "Fastov – Novokievskaya" 110 kW (recurrence period of 50 years, for open exposure, 10 m height), N/m